Holes in glued laminated timber beams

The influence of the cylindrical anisotropy of wood on the stress distribution of unreinforced and reinforced holes

Hermsen, Tomas M.

Award date:
2023

Holes in glued laminated timber beams

The influence of the cylindrical anisotropy of wood on the stress distribution of unreinforced and reinforced holes

Master thesis

T.M. Hermsen

Eindhoven University of Technology
Department of the Built Environment
Structural Engineering and Design

Final version

August 25th, 2023

Title	Holes in glued laminated timber beams
Subtitle	The influence of the cylindrical anisotropy of wood on the stress distribution of unreinforced and reinforced holes
Version	Final version
Date	August 25th, 2023
Location	Eindhoven, The Netherlands
Author	T.M. (Tomas) Hermsen
Student number	1631675
E-mail	t.m.hermsen@student.tue.nl
Department	The Built Environment
Master	Architecture, Building and Planning
Master track	Structural Engineering and Design
Chair	Innovative Structural Design
Graduation Committee	Ir. A.P.H.W. (Arjan) Habraken *Assistant Professor Innovative Structural Design*
	Dr. Ir. S.P.G. (Faas) Moonen *Associate Professor Innovative Structural Design*
	Ir. G.J.C. (Gert-Jan) Rozemeijer *Director Lüning Ingenieurs in houtconstructies*

Preface

During my semester abroad in Stockholm, I had the opportunity to explore the field of timber structures through a course called "Design of Timber-Based Hybrid Structures" at KTH, lectured by R. Crocetti. During this time, I was first introduced to the topic of holes in glulam beams. During a meeting to explore the different graduation topics available by Arjan Habraken, one particular topic captured my interest, holes in glulam beams. Eventually, this topic became the theme of my graduation project.

I want to thank the members of my graduation committee for their guidance throughout the graduation project. In specific ir. A.P.H.W. (Arjan) Habraken, Dr. Ir. S.P.G. (Faas) Moonen and ir. G.J.C. (Gert-Jan) Rozemeijer for their expertise and insightful feedback. Moreover, I also want to thank Ir. R. Crocetti for introducing me to the topic of holes in glulam beams and sparking my interest in timber structures, and Ir. C. Tapia for sharing his Python scripts of glulam beams with internal reinforcement, which proved immensely helpful in automating the numerical processes. Finally, I want to thank my family and friends, who have always supported me.

Tomas Hermsen,

Eindhoven, August 2023

Abstract

The presence of holes in a glulam beam induces stress concentrations in the vicinity of the hole due to the redistribution of the shear and bending stresses leads that can no longer be transferred through the weakened cross-section. This redistribution leads to the development of tensile stresses perp. to the grain. Combined with increased shear stresses, these tensile stresses perp. to the grain promote crack initiation. The failure mechanism involves crack propagation at two diagonally opposed quadrants. Literature demonstrated that cracks initiate near the mid-width of the cross-section due to pronounced stress peaks resulting from the cylindrical anisotropy of wood.

Timber is commonly regarded as an orthotropic material or even further simplified to a transversely isotropic material. Thus, only a distinction is made between the parallel and perp. to the grain direction. The difference between the radial and tangential direction is neglected, and a smeared average is assumed for the perp. to the grain direction. However, the difference between the stiffness in the radial and tangential direction, low rolling shear stiffness and cylindrical orientation of the annual rings in the laminations lead to the pronounced stress peaks near mid-width. Therefore, considering the cylindrical anisotropy of wood leads to a more accurate approximation of the actual stress distribution in the vicinity of a hole.

The cylindrical anisotropy of wood is compared against the commonly assumed orthotropic behaviour. Three different lay-up configurations were considered. A glulam beam with a circular hole placed along the neutral axis of the beam served as the base configuration for the unreinforced situation. When considering the cylindrical anisotropy of wood, the resulting stress distribution becomes inhomogeneous along the width, with pronounced stress peaks near mid-width that are 1,5 to 2 times greater than the orthotropic case. Shear stresses show a similar inhomogeneous distribution but with less pronounced stress peaks. Additionally, the fictive tensile force obtained magnitudes 16% to 30% lower than the orthotropic case.

The influence of reinforcements was also examined. Three scenarios were considered: a single rod, two rods along each other and plywood panels. The rods were placed at an angle of 45°. The analysis revealed that a single rod was the most effective in reducing the tensile stresses perp. to the grain, shear stresses and fictive tensile force, followed by the scenario of two rods. The plywood panels were the least effective.

The damaged state was also assessed. It was observed that rods gradually take a more significant portion of the tensile stresses as the crack approaches the rod and eventually can halt the crack propagation. Contrary, the panels were less effective and appeared to be not able to halt but to slow down the crack propagation.

This thesis revealed that reinforcements, specifically a single rod placed at the mid-width of the cross-section, are generally more effective than external reinforcements. The maximum dimensions for the hole height h_h recommended in the design standards contradict the findings of this thesis. The design standard allows for larger holes when external reinforcements are applied. However, based on the

reductions achieved by the reinforcements, it appears to be safer to enlarge internally reinforced holes rather than externally reinforced holes.

Table of contents

List of Figures

List of tables

1

INTRODUCTION

1.1 Problem definition

Introducing holes in glued laminated timber (glulam) beams is a frequent necessity in practice. They create a path for plumbing, electrical and other service-relevant infrastructure if these cannot be placed under or around the beam for architectural, aesthetical, or other reasons. The introduction of the hole disrupts the stress flow in the beam and leads to the redistribution of shear, and bending stresses around the hole. This redistribution generates tensile stresses perp. to the grain and increased shear stresses in the vicinity of the hole, which were not present before the introduction of the hole. Especially the tensile stresses perp. to the grain are of concern since the strength of timber in this direction is relatively low. Therefore, the stress concentrations can reduce the load-bearing capacity of the beam significantly.

The failure mechanism of unreinforced and reinforced holes is well known. It involves crack propagation in the direction along the grain in two diagonally opposed quadrants starting at the location where the tensile stresses perp. to the grain reaches its maximum. The first crack usually appears in the upper right quadrant (towards mid-span), followed by the lower left quadrant (towards support). The cracks propagate until a sudden global brittle failure occurs, usually at the left bottom quadrant of the hole. It was identified that the tensile stresses perp. to grain are the primary reason for crack initiation [1].

The design of holes according to design standards revolves around calculating a fictive tensile force composed of two additive components: a shear and moment component, each representing the respective part of the stresses that must be redistributed around the hole [2]. The force must be resisted by either the volume-dependent fictive tensile resistance of the glulam or by reinforcements. The concept of reinforcements is to increase the tensile strength perp. to the grain locally in the regions where cracks are expected to occur. Therefore, reinforcements can increase the load-bearing capacity and prevent or even halt the propagation of cracks. There are two types of reinforcements: internal and external reinforcements. Generally, internal reinforcements are preferred since they are concealed in the glulam and are easier to install at a relatively low cost.

Literature [3] [4] [5] reported that cracks always initiated near the mid-width of the cross-section, regardless of whether the hole was reinforced or not. This behaviour was attributed to the cylindrical

anisotropy of wood [3], which leads to an inhomogeneous stress and strain distribution along the cross-sectional width with a pronounced stress peak near the mid-width. The inhomogeneous stress and strain distribution along the width at the face of the hole were also verified experimentally [6]. These observations underscore the importance of considering the cylindrical anisotropy of wood to accurately approximate the stress distribution in the vicinity of an unreinforced and reinforced hole [7].

Timber is a highly anisotropic material bound to a conical shape with varying material properties in different directions. Timber is commonly assumed to be an orthotropic material with three principal directions: longitudinal, radial and tangential. The longitudinal direction exhibits the highest stiffness, approximately 10-15 times greater than the radial direction, while the radial direction is approximately 1,5 to 2 times stiffer than the tangential direction for most softwoods [8]. Therefore, most structural applications simplify timber to a two-dimensional transverse isotropic material. Thus, only making a distinction between the parallel and perp. to the grain direction and assuming plane stress in de width direction. This simplification is justified because the stiffness in the longitudinal direction is far greater than in the radial and tangential directions, the two perp. to the grain directions. The stiffness in the perp. direction is taken as the smeared average of the radial and tangential stiffness [9]. Nonetheless, these simplifications lead to an inadequate approximation for applications where the stresses perp. to the grain govern the design [10], such as holes in glulam beams.

The cylindrical anisotropic model results in a more accurate approximation but is more complex than the usual orthotropic or transverse isotropic approximation commonly used for most structural applications. The laminations possess a cylindrical orientation arising from the annual addition of new material in the radial direction. Therefore, to implement the cylindrical anisotropy of wood in a numerical model, the cylindrical orientations of the individual laminations in relation to the tree stem they were sawn from need to be defined. Furthermore, the difference between the radial and tangential stiffness and the low rolling shear stiffness contribute to the inhomogeneous stress distribution. Noteworthy, the cylindrical anisotropy of wood does not affect the stresses parallel to the grain [9].

1.2 Objective

So far, only Tapia [11] investigated the influence of the cylindrical anisotropic model to glulam beams with holes numerically. However, the cylindrical anisotropic model was omitted for the remainder of his thesis due to the dependency of the pith orientations in a glulam cross-section. All other literature regarding holes in glulam is based on orthotropic or transverse isotropic behaviour underscoring the relevance of assessing the influence of the cylindrical anisotropy on the structural behaviour of holes in glulam beams.

Therefore, this thesis aims to study the influence of the cylindrical anisotropy of wood on the stress distribution of a glulam beam containing a circular hole through a numerical study. The study will analyse the influence of cylindrical anisotropy on the stress distribution in the vicinity of an unreinforced and reinforced hole, comparing it with the orthotropic reference case to highlight any significant discrepancies between the two models. Therefore, the main research question is as follows:

"What is the influence of the cylindrical anisotropy of wood on the stress distribution of a glulam beam with an unreinforced and reinforced hole?"

To address this research question, several sub-question will be answered:

- How does the cylindrical anisotropy of wood affect the stress distribution in the vicinity of an unreinforced hole?
- How does the cylindrical anisotropy of wood affect the stress distribution in the vicinity of a reinforced hole?
- What happens when stationary cracks are regarded to the stresses considering the cylindrical anisotropy of wood?

1.3 Limitations

The primary objective of this thesis is to gain a better understanding of the cylindrical anisotropy of wood on the stress distribution in the vicinity of a hole. It is important to acknowledge that this represents only one aspect of a structurally safe design: the loading aspect. However, to determine if a glulam member with a hole is structurally safe, the ultimate resistance of the member has to be determined as well. This resistance aspect, however, is not regarded in this thesis.

1.4 Thesis outline

- Chapter 2 presents an extensive overview of the structural behaviour of a glulam beam with a hole. The stress distribution in the vicinity of a hole is discussed first, followed by crack development. Subsequently, the treatment of the design of a glulam beam with a hole according to the design standards is discussed. Lastly, the influence of reinforcements on structural behaviour is discussed.
- Chapter 3 focuses specifically on the cylindrical anisotropy of wood. It discusses the origin of the annual rings, the assumptions of the material model and the constitutive relationship. Lastly, the application of the material model to a glulam beam with a hole is discussed based on available literature.
- Chapter 4 centres around the second generation of Eurocode 5. This chapter delves into the rules and regulations outlined in this standard.
- Chapter 5 discusses the numerical models employed in this thesis and the post-processing of these models.
- Chapter 6 discusses the effects of the cylindrical anisotropy on the stress distribution in a glulam beam with an unreinforced circular hole.
- Chapter 7 investigates the potential of reinforcements to mitigate stress concentrations near a circular hole in a glulam beam. It explores different reinforcement strategies and evaluates their effectiveness in reducing stress concentrations and the fictive tensile force.
- Chapter 8 examines the influence of stationary cracks on stress distribution in the unreinforced and reinforced state.
- Chapter 9 answers the research question introduced in this chapter. The chapter presents the findings and conclusions of the study and offers recommendations for further research on this topic.

2

STRUCTURAL BEHAVIOUR OF A GLULAM BEAM WITH A HOLE

It is well known that holes reduce the load-bearing capacity of a glulam member considerably. The introduction of a hole in a glulam member introduces a geometric discontinuity which disturbs the stress flow in the weakened member, as shown in Figure 2-1. As a result, the stress components need to be redistributed around the hole. This redistribution causes additional stresses in the direction perp. to the grain, and increased shear stresses at the periphery, which were absent in the unweakened cross-section. Especially the tensile stresses perp. to the grain are important since this is the weakest direction of timber. The magnitude of these additional stresses depends on factors such as the size shape and shape of the hole and the ratio of the internal forces. These additional stresses can initiate cracks, leading to the global brittle failure of the beam. The failure mechanism is well known and involves the propagation of cracks in the direction parallel to the grain along the beam axis [12]. The cracks start from two zones located at diagonally opposed corners, where high tensile stresses perp. to the grain are present.

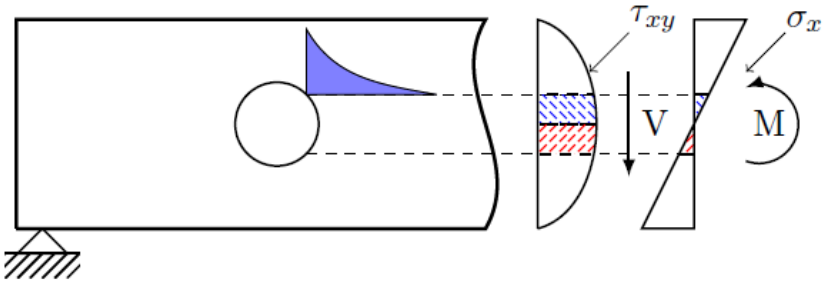

***Figure 2-1**: Part of the shear and bending stresses that must be redistributed around the hole [11].*

2.1 Stress distribution in the vicinity of the hole

Introducing a hole induces stress concentrations, particularly in the form of tensile stresses perp. to the grain and increased shear stresses along the periphery of the hole, which promote crack initiation. This section describes these stress concentrations to better understand the structural behaviour of a glulam beam with a hole.

2.1.1 Tensile stresses perp. to the grain

The introduction of a hole leads to the redistribution of the shear and bending stresses resulting in tensile stresses perp. to the grain at distinct locations at the periphery of the hole. It was shown that the tensile stresses perp. to the grain were the primary reason for crack initiation by evaluating a quadratic failure criterion [1]. The exact location of the tensile stresses depends on the type of loading considered. Typically, holes in glulam beams experience a combination of shear and moment action and in some rare occasions to pure moment loading.

Figure 2-2 (a) depicts the stresses perp. to the grain resulting from pure moment loading. Tensile stresses perp. to the grain occur at three distinct regions, forming a symmetric pattern around a vertical axis that passes the middle of the hole [11]. Tensile stresses are found in the upper left and right quadrants and at the centre of the bottom of the hole. Conversely, compressive stresses arise at the two bottom corners and the top of the hole. The angle φ indicates where the largest value of the tensile stresses arise along the periphery of the hole, and consequently, cracks are likely to initiate. For the situation where a hole is loaded by a pure moment, the maximum tensile stress can be found at an angle of 30° [12].

Pure shear is not possible due to the fundamental relationship V = M. However, the "pure" shear case can be obtained by subtracting the results of the pure moment case from the combined shear and moment case [12]. Figure 2-2 (b) depicts the stresses perp. to the grain for the "pure" shear case. The figure shows that the tensile stresses occur in the upper right and lower left quadrants of the hole and are identical. Compressive stresses occur at the two remaining quadrants. The stress pattern is symmetric along a diagonal axis. Contrary to the pure moment case, the angle φ at which the tensile stresses reach a maximum is higher and occurs at an angle of 50° (+ 180°). Comparing Figure 2-2 (a) and (b), it becomes evident that the tensile stresses arising from the "pure" shear case are the most prominent.

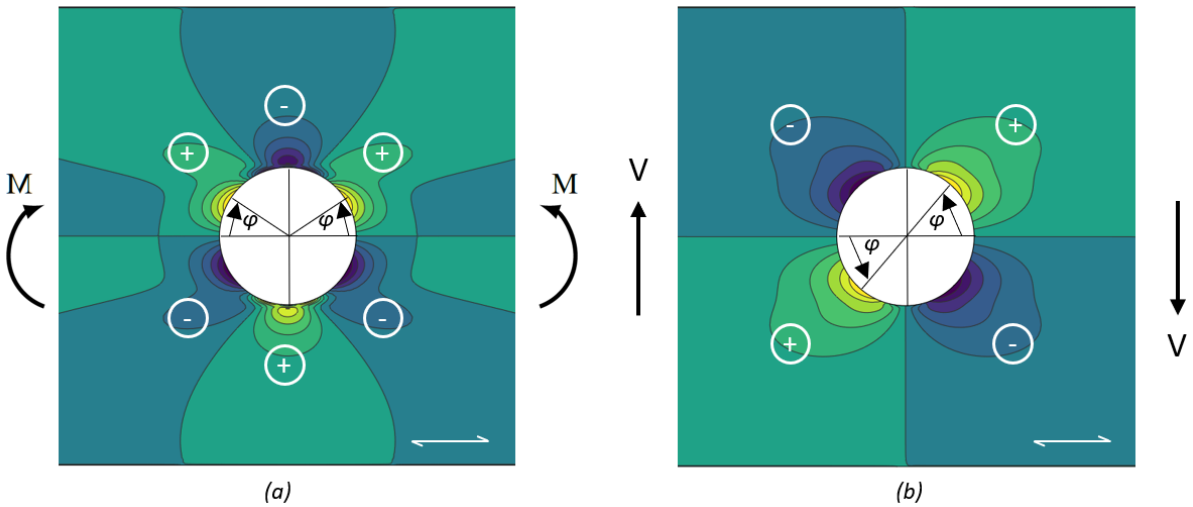

Figure 2-2: *Distribution of the stresses perp. to the grain for a circular hole loaded by pure moment (a) and "pure" shear action (b). The plus signs indicate tension stresses, and the negative signs compression stresses.*

The distribution of the stresses perp. to the grain for the combined shear and moment case is obtained by superimposing the stresses of the pure moment and "pure" shear case. The superimposing of the

two cases shows that the upper right quadrant is decisive since the tensile regions of the pure moment and "pure" shear action are additive. The bending moment is also slightly higher at this side of the hole. Contrary, the tensile stresses in the lower left quadrant are superposed with the compressive stresses from the pure moment case and are thus reduced. As a result, anti-symmetrical stress distribution in the vicinity of the hole occurs, as is depicted in Figure 2-3. This anti-symmetrical pattern becomes more pronounced for a greater M/V ratio [12]. Compressive stresses perp. to the grain occur at the remaining two quadrants of the hole. However, these compressive stresses do not govern the design because timber has lower resistance to tensile stresses perp. to the grain. The angle φ is within the range of 40° (+ 180°) ≤ φ ≤ 60° (+ 180)°. Depending on the M/V ratio, the angle φ comes closer to 40° (small M/V ratio) or 60° (large M/V ratio). The angle of the upper right quadrant is generally smaller than the lower left quadrant.

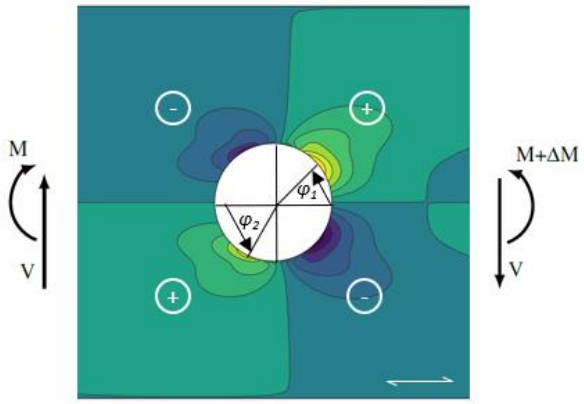

Figure 2-3: *Distribution of the stresses perp. to the grain for the combined shear and moment case.*

In addition, square and rectangular shapes are commonly applied geometries alongside circular holes. These geometries show similar patterns for the stresses perp. to the grain [13]. Figure 2-4 depicts the distribution of the stresses perp. to the grain in the vicinity of a square and a rectangular hole with an aspect ratio of 1:2,5. The location of the maximum tensile stress perp. to the grain arises at the corner radius.

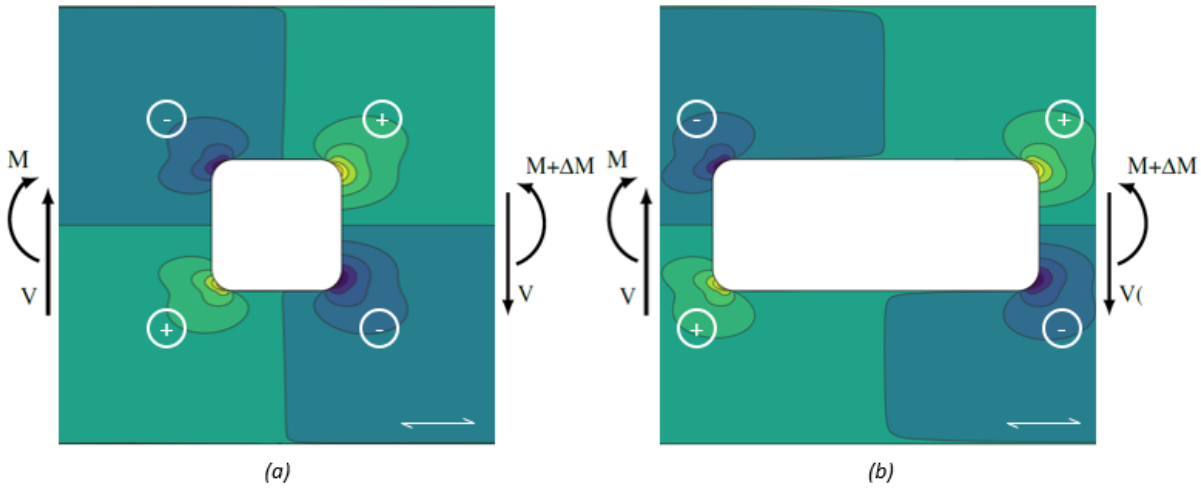

Figure 2-4: *Distribution of the stresses perp. to the grain in the vicinity of a square hole (a) and rectangular hole with an aspect ratio of 1:2.5 (b) loaded by a combined moment and shear action.*

The hole geometry determines the magnitude of the tensile stresses perp. to the grain. The corner radius is an essential parameter for square and rectangular holes. A smaller corner radius increases the magnitude of the tensile stress perp. to the grain. The tensile stress concentrations in square and

rectangular holes are more pronounced than in circular holes, primarily attributed to the smaller corner radius inherent in rectangular holes relative to circular holes. Furthermore, the aspect ratio of rectangular holes significantly impact the tensile stresses perp. to the grain.

So far, only holes positioned along the neutral axis of the beam have been discussed. However, it also happens that holes are arranged with an eccentricity *e* relative to the neutral axis of the beam. This eccentricity affects the stresses in the perp. to the grain direction. As a result, the redistribution of the portion of the shear stresses decreases for an eccentric-positioned hole. Contrary, the proportion of the bending stresses increases significantly due to the eccentricity. [14]. Figure 2-5 depicts the influence of the eccentricity on the portion of the shear and bending stresses that must find an alternative path. As the eccentricity increases, the proportion of bending stresses that require redistribution around the hole becomes more substantial. Therefore, the M/V ratio substantially influences eccentrically positioned holes, with a greater M/V ratio resulting in higher stresses perp. to the grain.

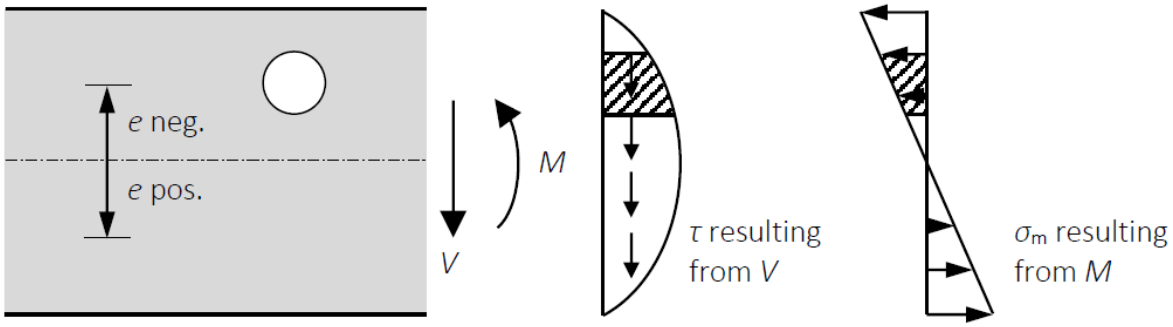

***Figure 2-5**: The parts of the shear and bending stresses must find an alternative path around the hole [14].*

Not only does the eccentricity affects the parts of the shear and bending stresses that must find an alternative path, but it also affects the angle φ and, thus, the location along the periphery of the hole where the maximum tensile stress perp. to the grain occurs. The angle φ increases slightly to 50° to 60° for a circular hole with a positive eccentricity. This change occurs due to the moment component of the tensile stresses. In contrast, the angle becomes smaller for a negative eccentricity, approximately 30° to 35° [5]. Both diagonally opposed quadrants can become decisive, contrary to a hole placed along the neutral axis of the beam [5]. Figure 2-6 illustrates the distribution of the stresses perp. to the grain in the case of a circular hole with a negative (a) and positive eccentricity (b) positioned in a shear-dominant region.

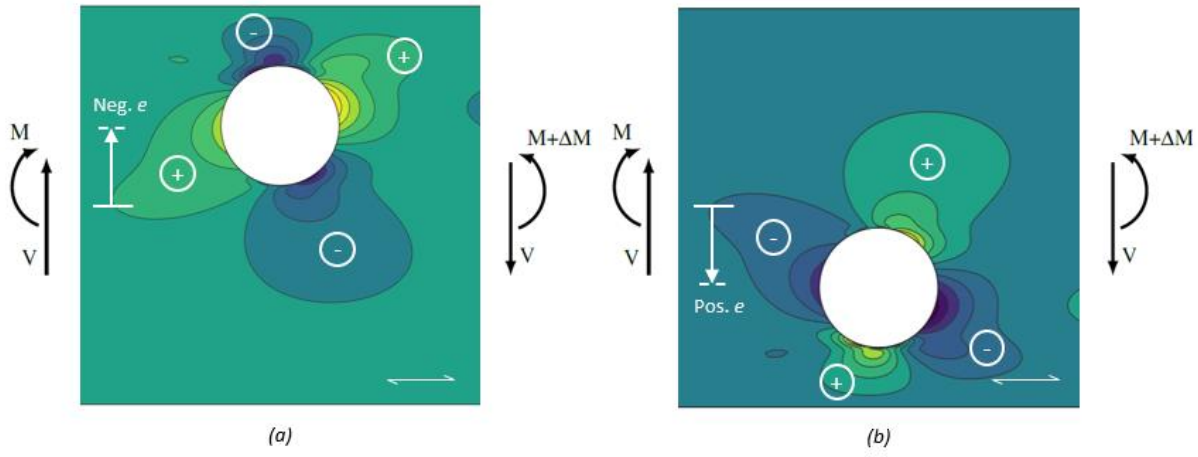

***Figure 2-6:** The distribution of the stresses perp. to the grain for a circular hole placed with a negative (a) and a positive (b) eccentricity subjected to combined shear and moment action.*

2.1.2 Shear stress concentrations

Linear elastic fracture mechanics (LEFM) classifies fracture behaviour into three distinct failure modes: the first mode, mode I, is characterized by tensile stresses, and modes II and III are characterized by shear stresses [11]. Mode II concerns in-plane deformation, while Mode III relates to out-of-plane deformation. Mode III is not expected to occur due to the in-plane loading of the beam. Therefore, modes I and II are the only modes of relevance for a glulam beam with a hole. The previous paragraph discussed the tensile stresses perp. to the grain responsible for mode I. This paragraph aims to address the stresses responsible for mode II, the shear stress concentrations that arise due to the presence of a hole.

The shear stresses near the hole significantly deviate significantly from the distribution according to beam theory [15]. Figure 2-7 displays the distribution of shear stresses in a beam with a circular hole (a) and square hole (b) along four different sections along the span of the beam exemplarily. The shear stresses at τ_4 are conform to beam theory, whereas the shear stresses at τ_1, τ_2 and τ_3 deviate due to the influence of the hole. The closer the considered section is to the hole, the greater the deviation from beam theory becomes. Instead of exhibiting a parabolic distribution over the height, shear stresses form peaks near the edges of the holes, as they must find alternative paths through the beam. Pronounced peaks are observed at the corners of the holes, with the maximum shear stress occurring at τ_2. In the case of a circular hole, the peak of shear stresses along the vertical path occurs roughly at an angle φ of 45°, while this happens in the corner radius for the square hole.

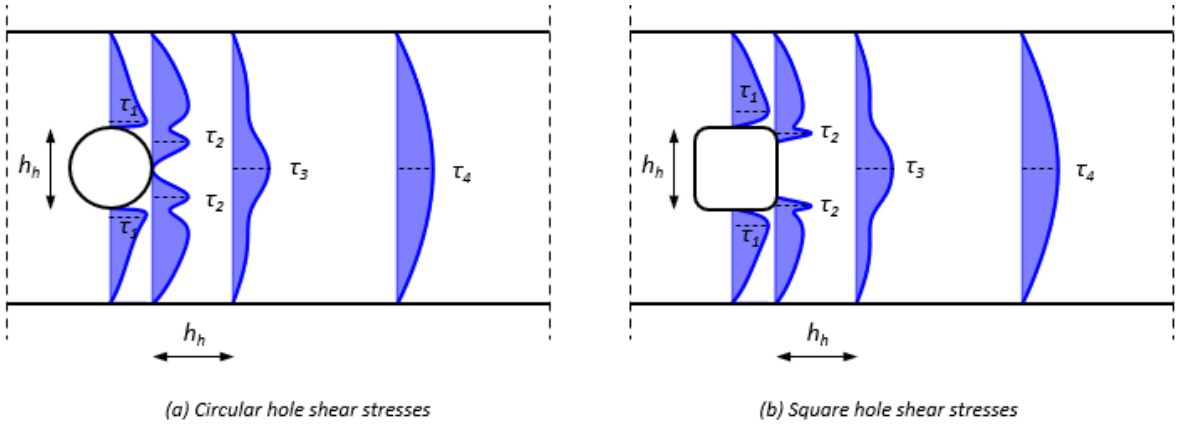

Figure 2-7: *Distribution of the shear stresses in a beam with a hole.*

Similar to the tensile stresses perp. to the grain, the shear stresses also increase in the vicinity of the hole, although the stress distribution pattern is different. Figure 2-8 depicts the shear stress distribution for a circular (a) and a square hole (b). The patterns are qualitatively similar for both hole geometries, yet the stress peaks for the square hole are notably higher in the corners due to the less favourable geometry resulting from the small corner radius.

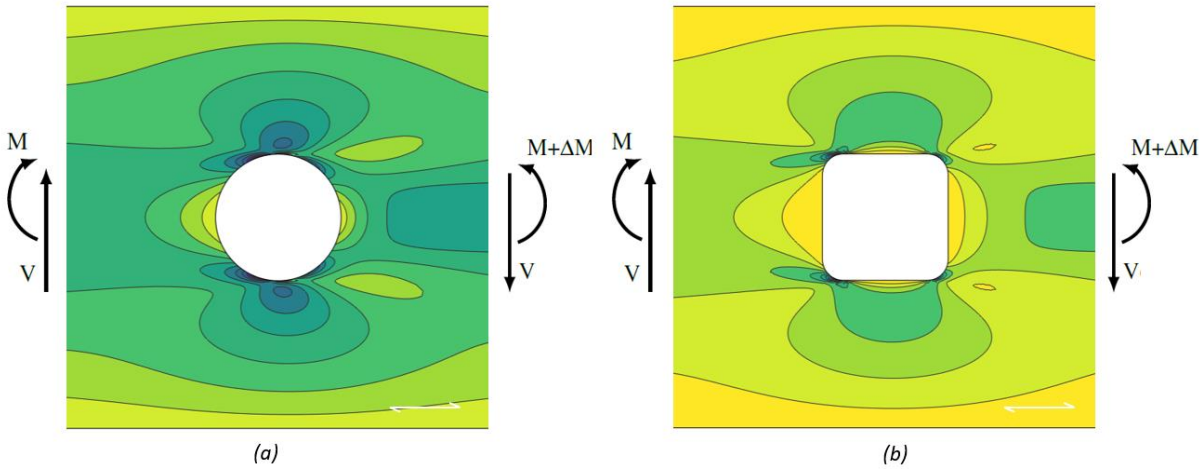

Figure 2-8: *The shear stresses in the vicinity of a circular hole (a) and square hole (b).*

2.2 Failure behaviour

Section 2.1 discussed the stresses that cause crack initiation and propagation. The next step is to describe the failure mechanism of a glulam beam with a hole. The literature has extensively described the failure behaviour for unreinforced and reinforced holes. The global failure behaviour is described first, followed by a detailed description of the crack initiation.

2.2.1 Global failure behaviour

The global failure mechanism is primarily characterized by tensile stresses perp. to the grain. However, it is worth noting that failure occurs due to the combined interaction of bending stresses and stresses perp in situations with a high M/V ratio (almost pure moment loading). to the grain at the periphery of the hole [16]. Cracks start to initiate along the periphery of the hole where the tensile stresses perp. to the grain attain their maximum. The crack plane orientations are dependent on the specific load combination regarded. Similar to the stresses perp. to the gain, a different pattern is observed between a hole loaded by a pure moment and those experiencing combined shear and moment actions. Figure 2-9 (a) represents the crack planes corresponding to the load combination of a combined shear and moment action in the case of a circular hole. Figure 2-9 (b) shows that the cracks propagate from a similar angle φ in experimental tests as described in section 2.1.1. Quadrants subjected to compressive stresses are not prone to cracking/failure since failure in the quadrants loaded in tension occurs considerably earlier.

Experimental investigations [3] conducted on circular holes have shown that the first crack initiations primarily occurred at the upper right quadrant of the hole. The crack at the upper right quadrant occurred in the range of 40° (+180°) ≤ φ ≤ 60° (+180°). The difference between loads at which cracks started to initiate depended on the M/V ratio. Aicher & Höfflin [3] observed that for a small M/V ratio (M/V = 1,5h), the initial cracks appeared at a relatively low load difference between the two quadrants. Conversely, in cases with larger M/V ratios (M/V = 5h), the initial crack tended to initiate significantly earlier in the upper right quadrant compared to the lower left quadrant.

Furthermore, an increase in the relative hole size h_h/h resulted in a decrease in the load-bearing capacity, as is to be expected [3]. Contrary to crack initiation, the ultimate failure of the beam occurred when the crack plane, situated in the bending tension region closer to the support (lower left quadrant), propagated until it reached the end of the beam at the support [17].

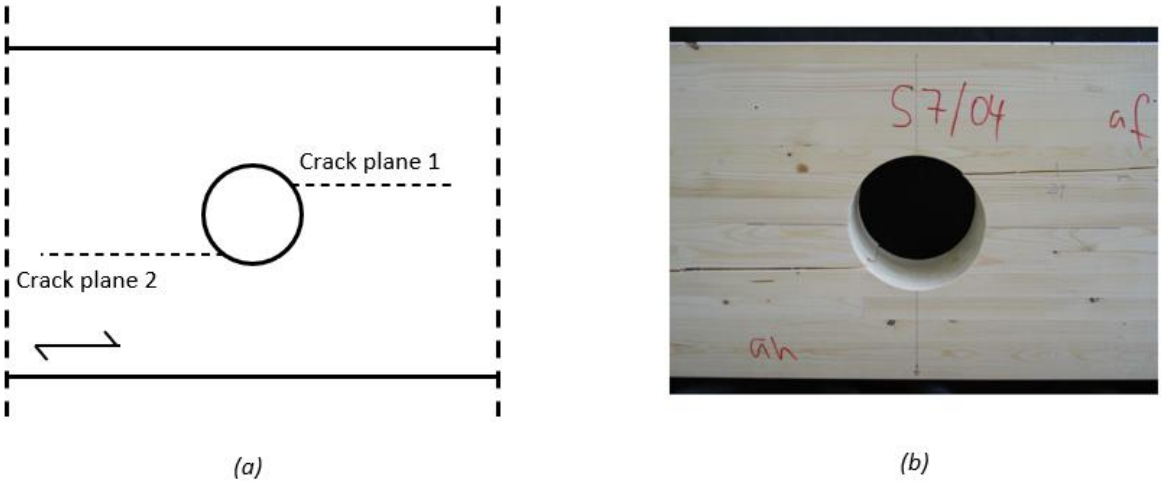

Figure 2-9: *Definition of the crack planes for a circular hole (a). (b) Picture of two propagated cracks at the upper and lower region observed in an experimental test of a circular hole from the test series of Aicher & Höfflin [3]. The picture was taken from [11].*

Analogously to circular holes, square holes showed similar crack development, with cracks initiating at the right side of the hole within the corner radius [4]. Danzer et al. [5] conducted a study on circular holes arranged with an eccentricity in relation to the neutral axis of the beam. They found that the eccentricity had a marginal influence on larger holes (0,35*h*). However, smaller holes (0,25*h*) exhibited a more pronounced effect of the eccentricity.

2.2.2 Crack stages

Four distinct crack stages can characterise the crack development. The first stage involves crack initiation occurring near the mid-width of the cross-section, which results from the cylindrical anisotropy of wood [7]. In the second stage, the crack initiated in the middle extended towards the edges of the cross-section. The third stage marks the development of the crack along the complete cross-sectional width, leading to a transition from localised to global damage. In the final crack stage, the crack propagates along the longitudinal direction of the beam length until reaching the point of ultimate failure. The ultimate failure manifests as the crack propagates unstably towards the left end of the beam [3]. Figure 2-10 represents the four stages of crack development.

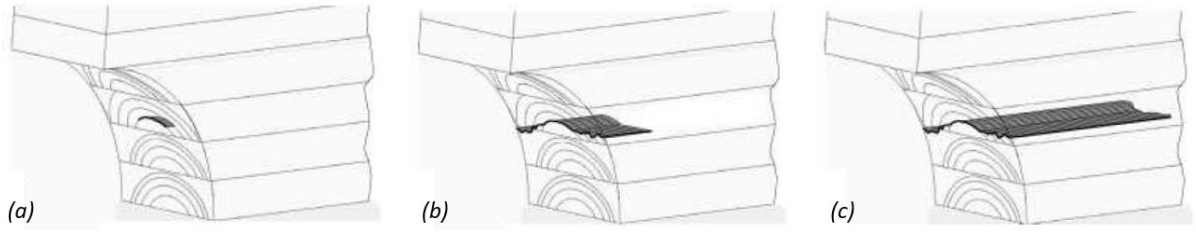

Figure 2-10: *Schematical representation of the crack stages along crack plane 1, adopted from [7]. (a) Crack stage 1 represents Crack initiation near mid-width. (b) crack stage 3 represents a fully developed crack along the cross-sectional width. (c) Crack stage 4 represents the crack at global failure.*

2.2.3 Crack initiation

A consistent observation in all tested specimens was that the first cracks initiated at the mid-width of the cross-section. This phenomenon can be attributed to the cylindrical anisotropy of wood, which induces an inhomogeneous distribution of the stresses along the cross-sectional width [3]. The main characteristic of this inhomogeneous stress distribution is the pronounced stress peak occurring near the mid-width of the cross-section [10]. Figure 2-11 (a) illustrates an exemplary representation of this

inhomogeneous stress distribution along crack plane 1 in the upper right quadrant of the hole. These prominent stress peaks arise due to the annual rings in the laminations, each possessing a cylindrical orientation. The crack development starts with a tangential crack aligning with the curvature of the annual rings. This inhomogeneity of the stresses and strains was verified through experimental tests by Aicher & Höfflin [18] through strategic placement of strain gauges across the cross-sectional width. They tested two configurations defined by their applied load combinations: pure moment action and the combined shear and moment action. They placed strain gauges along the periphery of the hole, explicitly targeting the locations where the maximum tensile stresses perp. to the grain were expected to reach their peak. A comparison of the experimentally verified non-uniform strain distribution with a three-dimensional cylindrical anisotropic model revealed a good agreement, as shown in Figure 2-11 (b) for the combined shear and moment action. The figure shows a good agreement between the strain distribution of the three-dimensional model (solid line) and the measured strain distribution in the strain gauges (square dots).

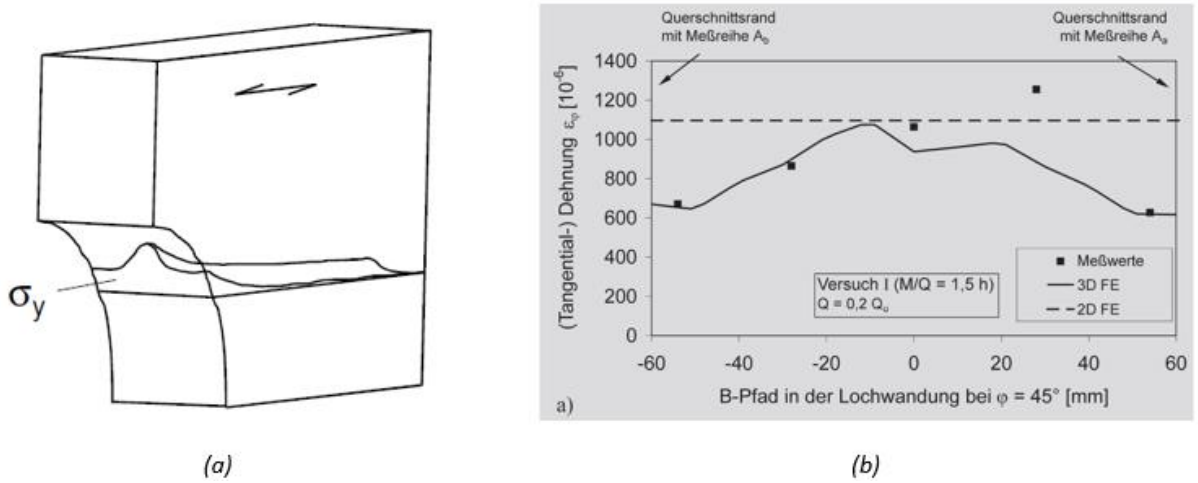

Figure 2-11: *(a) Exemplary illustration of the inhomogeneous stress distribution along the cross-sectional width at a plane where the maximum tensile stresses perp. to the grain occur [3]. (b) Experimental and numerical strain distribution along the cross-sectional width at the angle of φ = 45° [6].*

Figure 2-12 shows the damage evolution along crack plane 2 of a specimen with a square hole, which was part of the test series from [4]. The left image displays the initiation of the crack, which originates near the mid-width, as discussed earlier, and follows the trajectory of the annual rings while propagating tangentially. The middle image represents the third crack stage, with the crack fully extended to the outer edges of the glulam cross-section. Initially propagating tangentially, the crack eventually transitions to the radial direction at a specific point. A noteworthy feature of the crack is its non-uniform shape, deviating from the simplified assumption of straight crack development across the width typically associated with an orthotropic representation. Once started, the crack propagated along the direction aligned with the annual rings until it switched to the radial direction perp. to them. The location of this switch follows from a minimum in the stiffness perp. to the grain. However, this will be discussed in the next chapter.

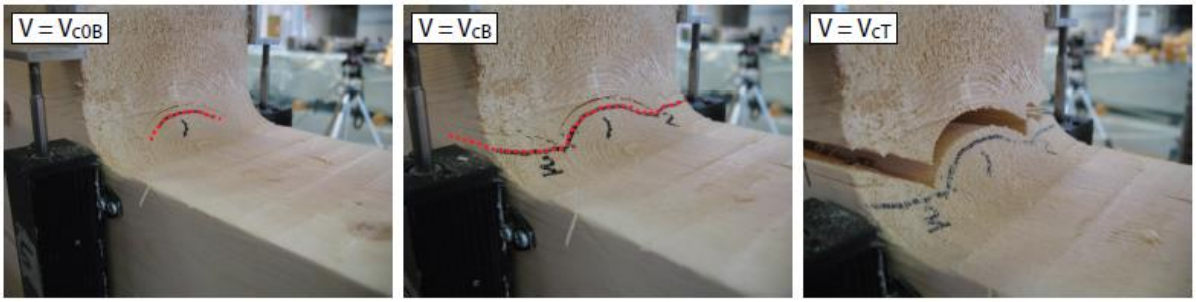

Figure 2-12: *Crack development observed in a square hole at crack plane 2 [4].*

2.2.4 Crack loads

The crack stages are distinguished based on a corresponding shear force that mark their initiation. These shear forces mark the beginning of the respective crack stage.

- The shear force at crack initiation ($V_{c,\ init}$) denotes the shear force at which the first observed crack emerges. Due to the asymmetric nature of the cracks, two specific loads are recorded for each hole, corresponding to the initial cracks at the upper right and lower left regions.
- The shear force at a crack along the total glulam width ($V_{c,\ width}$) represents the shear force at which the crack has fully propagated across the entire width of the cross-section. Again, two loads are documented for this stage, reflecting the complete development of cracks along the width.
- The ultimate failure shear force (V_u) corresponds to the shear force at which the beam experiences global failure. Unlike the previous crack stages, only one load is reported for the ultimate load.

The crack loads exhibit a prominent scatter in the results. This prominent scatter may arise due to two primary factors: the cylindrical anisotropy of wood and the volume effect, also known as the size effect.

2.2.5 Size effect

The observed phenomenon of the size effect further influenced the load-bearing capacity. The height of the beam did not exhibit a linear increase in the failure shear force; instead, an increase in beam height resulted in a lower observed ultimate failure shear force [3]. This lower ultimate failure shear force suggests larger beams have lower strength than smaller ones. The "Weibull weakest link theory", a stochastic phenomenon, explains this behaviour. According to this theory, the probability of encountering a severe defect such as knots and resin pockets, which can lead to failure in a beam, increases with an increase in the volume of the beam [19]. This volume effect is also present in other applications, such as curved beams, where tensile stresses perp. to the grain govern the design.

2.3 Design of holes according to design standards

Having established the stress distribution in the vicinity of the hole and the associated failure mechanism, the next step is to look at how the design standards treat the design of a glulam beam with a hole. Something remarkable is immediately noticeable here: the current version of Eurocode 5 [20] does not contain any rules or regulations for the design of holes in glulam beams. However, the national annexes of Germany [21] and Austria [22] dedicated a section to the design of holes. The approach presented in these national annexes is based on a classic strength of materials approach and revolves around calculating a fictive tensile force $F_{t,90}$. This force represents the integral of the stresses perp. to the grain $\sigma_{t,90}$ along a horizontal path. This horizontal path starts along the periphery where

the tensile stress perp. to the grain $\sigma_{t,90}$ reaches its maximum. The tensile stresses perp. to the grain along this horizontal path will decrease over a distance $x_{t,90}$ from the hole until they reach zero. Figure 2-13 defines this fictive tensile force for a circular hole.

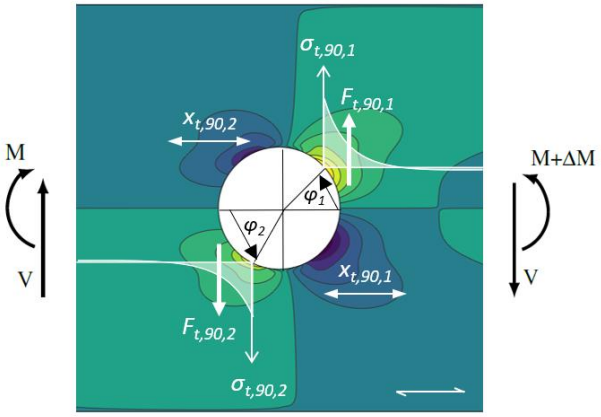

***Figure 2-13**: Definition of the fictive tensile force $F_{t,90}$.*

Kolb & Epple [23] showed that the fictive tensile force comprises two additive components; a shear component $F_{t,90,V}$ following from the redistribution of the shear stresses and a moment component $F_{t,90,M}$ following from the redistribution of the bending stresses [2]. The shear component originates from an analytical equilibrium consideration and conforms sensible half of the integral of the parabolically distributed shear stresses along the full hole depth [24], while the moment component is an empirical relation based on the observed load capacity losses in experimental tests for holes loaded by pure moment action [25]. It was, however, shown that the moment component needs amendments [12] since the formula is partly over-conservative [2]. A revised formula for the moment component was derived and implemented in the second generation of Eurocode 5. However, this will be discussed in §4.2.

Figure 2-14 shows the schematic representation of the simplified fictive tensile force $F_{t,90}$ used by the national annexes. A simplified triangular stress distribution is adopted instead of the actual non-linear stress distribution. The maximum tensile stress equals the tensile strength in the direction perp. to the grain $f_{t,90}$. The length $\ell_{t,90}$ defines the distance over which the tensile stresses reach a value of zero.

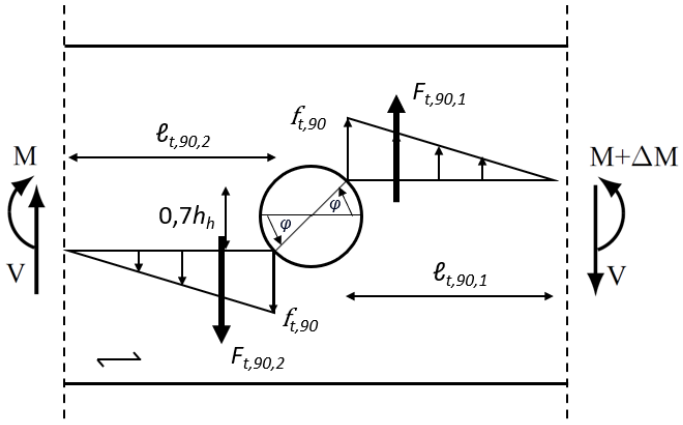

***Figure 2-14:** Schematic representation of the fictive tensile force assumed by the design standards.*

However, the resistance of the member is also important. The resistance should be greater than the applied action on the member in order to guarantee a safe design. Therefore, the fictive tensile force must be resisted by a fictive tensile resistance. This fictive tensile resistance depends on a volume-dependent tensile strength perp. to the grain. The fictive resistance determines whether the glulam

beam with a hole has sufficient resistance against the fictive tensile force or that additional measures, such as reinforcements, are necessary.

Additionally, to this fictive tensile force, the Austrian national annex [22] also states that the shear stress concentrations near the hole need to be verified. This formula is based on the work of Blass & Bejtka [15]. A stress concentration factor was derived through a multiple regression analysis over the results of 2.000 FEM simulations of rectangular holes with a constant shear force and a hole geometry within the range of $0{,}1 \leq \ell_h/h \leq 1{,}0$ and $0{,}1 \leq h_h/h \leq 0{,}4$. The stress concentration factor is multiplied by the shear stress of the net cross-section, resulting in the shear stress at the edge of the hole. These values must be lower than the shear strength of the timber. However, research [26] demonstrated that this formula yields conservative values for larger corner radii and partially far too low values for small corner radii.

2.4 Reinforcements

When the fictive tensile force discussed in the previous paragraph is greater than the resistance that the glulam beam can offer, additional measurements must be taken. These additional measurements can be done by reducing the hole size or changing the position to a more favourable location. However, this is not always possible. Therefore, reinforcements can be applied. In general, there are two types of reinforcements: internal and external. The goal of the reinforcements is to increase the tensile resistance perp. to the grain locally in the regions where cracks are expected to occur to achieve ductile failures [27]. Thus, the reinforcements can increase the load-bearing capacity of a glulam beam with a hole, halt crack propagation and prevent brittle failure. Reinforcements need to be designed for the full fictive tensile force. Thus, neglecting the contribution of the glulam, which equals a fully cracked cross-section [26]. However, research [26] [28] indicated that the internal and external reinforcements share this force with the glulam in the undamaged state.

2.4.1 Internal reinforcements

Blass & Bejtka [15] were the first to study the influence of internal reinforcements in the form of screws on the load-bearing capacity of rectangular and circular holes. Their test program included rectangular holes reinforced by screws arranged vertically and at an angle of 45° as well as circular holes reinforced with vertically placed screws. The load-bearing capacity of rectangular holes increased by approximately 40% for vertically placed screws, while the screws placed at a 45° angle substantially increased the load-bearing capacity by 97%. However, circular holes showed a less significant increase of only 14% in load-bearing capacity. The notable discrepancy between the load-bearing capacities of vertically placed screws for circular and rectangular holes stems from the vertical screw in a rectangular hole being positioned closer to the edge of the hole and, thus, the stress peak.

Höfflin [1] conducted experimental tests on glulam beams with holes, employing seven test series with various vertically installed reinforcement configurations. These experimental tests revealed that using one or two self-tapping screws with a similar diameter (d = 12 mm) along the cross-sectional width did not result in a significant difference. The crack initiation load and the load at the crack along the total width were almost identical for both test series. Conversely, comparing one and two glued-in threaded rods with the same diameter (d = 12 mm), a 25% higher crack initiation load was observed for the two-rod configuration. Notably, the crack initiation load for the single rod fell even below the tested unreinforced reference beam. This series probably had some material weakening and indicated that internal reinforcements do not always prevent crack initiation [11]. However, considering ultimate loads, installing two internal reinforcements led to higher values before failure. As soon as the crack starts to propagate, the reinforcements start to bear more load gradually. Installing two screws increased the ultimate failure load V_u and thus delayed the ultimate failure of the beam (8).

Danzer et al. [5] tested eccentrically placed circular holes reinforced by inclined screws, observing a 40% increase in the crack initiation load [5]. Contrary, vertically installed screws achieved only an

increase of 5% to 20% [1]. Furthermore, using self-tapping screws at a 30° angle resulted in a remarkable increase of up to 98% in the ultimate failure load V_u.

In addition to experimental tests, numerical studies were conducted to examine the stress distribution in the vicinity of a hole. Aicher [17] was the first to perform a numerical study on circular holes reinforced by vertically installed rods. The study revealed that a vertically placed rod did not significantly decrease the tensile stresses perp. to the grain (5-14%) and was ineffective in reducing the shear stresses in the vicinity of the hole (5-14%).

Tapia & Aicher [28] investigated the influence of the angle of inclination on reducing the stresses in the vicinity of a circular hole. Through a 3D finite element analysis, the study demonstrated that an inclined rod was more effective than a vertically placed rod in reducing tensile stresses perp. to the grain, achieving a reduction of 28% to 40%. Moreover, the inclined rod reduced shear stresses by 30% to 40%, a substantial improvement over the vertically placed rod. This increase can be attributed to increased beam stiffness near the hole region, reducing shear stresses along the crack plane [15]. The study analysed the redistribution of stresses in the damaged state caused by a horizontal crack along crack planes 1 and 2. The presence of a vertical rod reduced the stresses perp. to the grain, although a small peak remained at the crack tip. The inclined rod further decreased the stresses perp. to the grain, while the shear stresses remained relatively unchanged in the region preceding the reinforcement, regardless of the crack length. This indicates that once the crack has expanded beyond the reinforcement, the shear stresses are solely responsible for crack propagation.

Danzer et al. [14] obtained similar results for eccentrically placed circular holes. A numerical analysis indicated that inclined screws outperformed vertical screws. For holes with a positive eccentricity (placed in the bending compression zone), an angle of 30° is better. An angle of 45° proved better for holes with negative eccentricity (located in the bending tensile zone) regarding tensile stresses perp. to the grain. An angle of 45° reduced the shear stresses significantly for all eccentricities [5].

2.4.2 External reinforcements

External reinforcements provide an alternative method for reinforcing holes. Panels made of plywood or laminated veneer lumber (LVL) are (screw-) glued to the beam to increase the load-bearing capacity.

Aicher & Tapia [29] investigated the effectiveness of external reinforcements, particularly plywood panels made of spruce and birch with a thickness of 21 mm and varying dimensions. Experimental tests conducted on holes reinforced by plywood panels revealed that the crack development is similar to that of unreinforced holes (4). Like the unreinforced holes, cracks initiate at the mid-width of the cross-section. However, the tests demonstrated that the plywood panels significantly increased the crack initiation load. The plywood panels made it even possible to achieve the total characteristic shear capacity of a beam without a hole. Generally, birch plywood panels outperformed those made of spruce.

Aicher [26] performed a numerical study to examine the influence of different parameters, including the plywood panel's thickness, dimensions, and stiffness, on the percentage of the fictive tensile force $F_{t,90}$ taken by the panel. The parameter study revealed that the panels maximally took half of the tensile force. Additionally, the width of the panel had a less pronounced effect than initially anticipated, resulting in a marginal increase of 20-25% when doubled. Surprisingly, the impact of the modulus of elasticity of the panel, E_y (orientated perp. to the span of the beam), on the fictive tensile force was found to be smaller than expected, considering the corresponding increase in stiffness. Furthermore, increasing the panel thickness reduced the tensile force by 20-25%.

2.5 Discussion

This chapter discussed the structural behaviour of unreinforced and reinforced holes. The initiation of cracks occurred at two diagonally opposed quadrants due to stress concentrations at the periphery of

the hole, but the right upper quadrant is generally the decisive quadrant. Tensile stresses perp. to the grain play a significant role in crack initiation, while the shear stresses contribute to a lesser extent. In both unreinforced and reinforced specimens, crack initiation started at the mid-width of the cross-section due to the cylindrical anisotropy of wood. This cylindrical anisotropy induces an inhomogeneous stress distribution along the cross-sectional width, leading to pronounced stress peaks near the mid-width. The cracks further propagate to the outer edges of the cross-section, whereafter, the crack develops in the longitudinal direction until brittle global failure of the specimen is reached.

The observation of crack initiation at the mid-width of the cross-section in both unreinforced and reinforced configurations makes this study particularly intriguing, as it seeks to investigate the development of this stress peak and the factors influencing it. The study also aims to explore reinforcement methods to reduce these stress peaks and identify the most effective reinforcement type. Furthermore, considering that design standards assess a glulam beam with a hole based on the fictive tensile force, $F_{t,90}$, it is essential to examine the influence of the cylindrical anisotropy of wood on this force. Additionally, the fictive tensile force serves as a valuable indicator of the effectiveness of the reinforcements, as it represents the tensile stresses perp. to the grain along the crack plane. By comparing this force in both unreinforced and reinforced situations, it becomes possible to assess the reduction achieved by the reinforcements. To gain a comprehensive understanding of the cylindrical anisotropic model, the following chapter will delve into the concept of this material model.

3

CYLINDRICAL ANISOTROPY OF WOOD

Timber is a highly anisotropic material bound to a conical shape with varying material properties in different directions. Timber is commonly considered an orthotropic material with three distinct directions: longitudinal, radial, and tangential. Timber is often simplified to a two-dimensional transversely isotropic material, assuming plane stress in the width direction, for structural applications. Due to the relatively small difference between the radial and tangential directions, only a distinction is made between parallel and perp. to the grain directions. The stiffness in the perp. to the grain direction is taken as the smeared average of the radial and tangential stiffness [9].

The assumptions do not accurately predict stresses in applications involving tensile stresses perp. to the grain, such as glulam beams with holes. Neglecting the cylindrical orientation of the annual rings and the orthotropy in the radial-tangential (RT) plane influences the stresses only minor in the parallel to the grain direction. However, substantial differences arise in the perp. direction. Thus, a 3-dimensional model considering the cylindrical orientation of the annual rings and the orthotropy in the RT-plane is necessary to accurately estimate the stresses in the direction perp. to the grain.

The previous chapter discussed the structural behaviour of holes in glulam beams, revealing the initiation of cracks at the mid-width of the cross-section due to the cylindrical anisotropy of wood. This chapter discusses the cylindrical anisotropy of wood in detail, including its origin, representation within a glulam cross-section, and constitutive relation. Lastly, the application of the cylindrical anisotropic model to existing applications in the literature involving a glulam beam with a hole is discussed.

3.1 Cylindrical anisotropy of wood and glulam

3.1.1 Origin annual rings

A tree grows in two directions: longitudinally and radially. The former is the primary growth direction and occurs vertically along the length direction of the tree stem, whereas the latter is the secondary direction of growth and occurs over a year, resulting in the formation of concentric rings known as annual rings. During the growing season from spring to autumn in the Northern Hemisphere, the radial growth process is driven by cell division within the cambium, an extremely thin layer between the

wood and bark. The annual rings become visible in a transverse cross-section of a tree stem. These annual rings can be further classified into earlywood and latewood.

During spring, the formation of earlywood occurs, characterized by the development of a thin-walled cell layer. The primary function of earlywood is transporting water and nutrition up and down the tree. This cell layer exhibits a low density and strength, originating from the thin cell walls. Due to these thin-walled cells in the radial direction, the shear stiffness is very low [30]. In contrast, latewood forms during the summer when there is a reduced need for water and nutrition transportation, and the emphasis shifts towards prioritizing strength. Latewood cells have thicker walls, a compact arrangement, and a darker colour than earlywood. Figure 3-1 depicts an example of the annual ring structure. The right picture clearly illustrates the compact cell layers of latewood. The density, strength, and stiffness of the cell walls increase as they thicken. Furthermore, the latewood layer is thinner than the earlywood layer. The average density of earlywood in Norway spruce is 300 kg/m^3, while the density of latewood is around 1000 kg/m^3 [30].

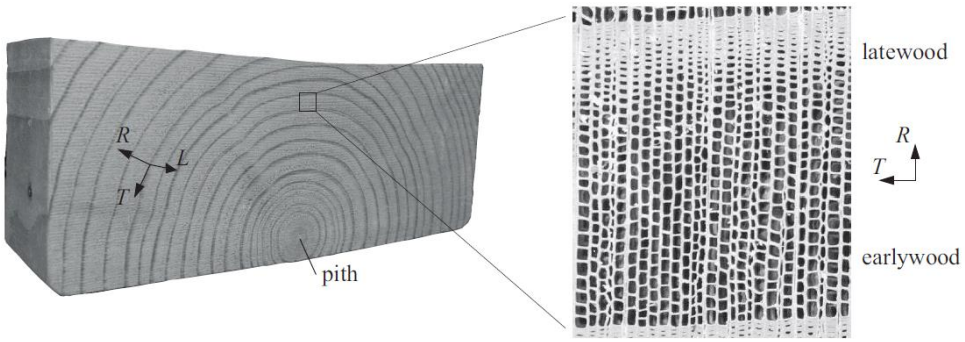

Figure 3-1: *Growth ring pattern and cell structure of early- and latewood [31].*

3.1.2 Simplifications

The mechanical properties of wood in the plane perp. to the stem are influenced by the yearly addition of new wood in the radial direction. Additionally, mechanical behaviour significantly differs between the longitudinal direction and the plane perpendicular to it. A common approach to simplify the stem of a tree is to approximate it as a conical geometry that exhibits anisotropic properties [10]. This approximation considers the gradual decrease in diameter along the stem axis from top to bottom. However, incorporating the diameter variation would complicate the anisotropy of wood. Thus, for simplicity, the conical shape is further simplified to a cylindrical shape [10]. This cylindrical representation is more accessible to implement in modern Finite Elements programs.

In this simplified cylindrical model, three principal material directions are defined: the longitudinal axis (L) parallel to the tree trunk, the radial direction (R) perpendicular to the annual rings, and the tangential direction (T) along the annual rings. The radial and tangential directions are at a plane perpendicular to the longitudinal direction. Although the presence of earlywood and latewood introduces variations in mechanical properties along the radial direction, these periodic inhomogeneities are neglected at the macro scale, treating the wood as a quasi-homogeneous continuum [10]. Additionally, this material behaviour does not consider growth irregularities such as knots and resin pockets [30].

3.1.3 Individual lamination

The next step is reducing the tree trunk to individual laminations. The laminations have a rectangular cross-section sawn parallel to the pith of the stem. The sawing disrupts the cylindrical orientation within the tree trunk. The orientation to the pith defines the local coordinate system of an individual lamination. It strongly depends on the employed sawing pattern and the specific location within the tree trunk. The pith marks the centre of the local cylindrical coordinate system in the laminations. Two

additional parameters, *d,* and *e*, define the local coordinate system. The parameter *d* represents the distance from the pith to the bottom face of the lamination, while *e* denotes the eccentricity of the pith from the mid-width of the lamination. Figure 3-2 depicts the just-described concept.

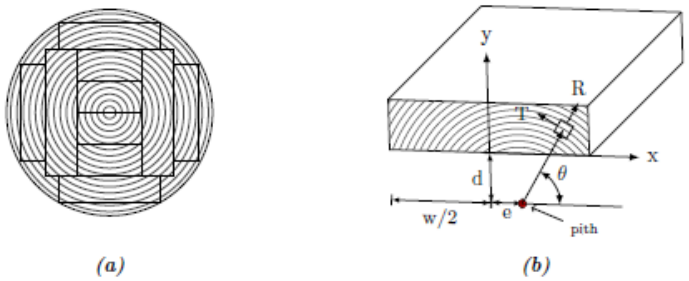

Figure 3-2: *(a) Shows an example of a possible sawing pattern. (b) Illustrates the local coordinate system and its parameters in a single lamination [11].*

3.1.4 Glulam cross-section

The manufacturing process of a glulam cross-section involves stacking laminations, each possessing its own cylindrical coordinate system. As each lamination is obtained from a distinct position within the tree trunk, it possesses its own unique cylindrical coordinate system. Thus, to accurately model a glulam cross-section, it is necessary to specify the orientation of each lamination relative to the pith from the stem it was sawn. Specifying every individual orientation is tedious since every lamination will have a unique orientation. Therefore, the literature uses more systematic patterns to describe all the pith orientations in a glulam cross-section.

Two coordinate systems must be distinguished to analyze tensile stresses perp. to the grain. Firstly, the local cylindrical coordinate systems are associated with the individual laminations. Secondly, the global Cartesian coordinate system describes the geometry of the glulam cross-section and the application of boundary conditions.

3.2 Constitutive relation

Hooke's law can express the constitutive relations for a three-dimensional linear-elastic orthotropic continuum. Considering the local material coordinate system with the three principal material directions defined by the longitudinal *L*, radial *R,* and tangential *T*, the constitutive relation within the linear elastic regime is given as:

$$\varepsilon = S\sigma \tag{3.1}$$

Where ε is the strain vector, and σ is the stress vector given by equation (3.2) and (3.3):

$$\varepsilon = [\varepsilon_{LL} \quad \varepsilon_{RR} \quad \varepsilon_{TT} \quad \Upsilon_{RT} \quad \Upsilon_{LT} \quad \Upsilon_{LR}]^T \tag{3.2}$$

$$\sigma = [\sigma_{LL} \quad \sigma_{RR} \quad \sigma_{TT} \quad \tau_{RT} \quad \tau_{LT} \quad \tau_{LR}]^T \tag{3.3}$$

Expanding the compliance matrix [S] results in equation (3.4):

$$S = \begin{bmatrix} \frac{1}{E_{LL}} & \frac{-\upsilon_{RL}}{E_{RR}} & \frac{-\upsilon_{TL}}{E_{TT}} & 0 & 0 & 0 \\ \frac{-\upsilon_{LR}}{E_{LL}} & \frac{1}{E_{RR}} & \frac{-\upsilon_{TR}}{E_{TT}} & 0 & 0 & 0 \\ \frac{-\upsilon_{LT}}{E_{LL}} & \frac{-\upsilon_{RT}}{E_{RR}} & \frac{1}{E_{TT}} & 0 & 0 & 0 \\ 0 & 0 & 0 & \frac{1}{G_{RT}} & 0 & 0 \\ 0 & 0 & 0 & 0 & \frac{1}{G_{LT}} & 0 \\ 0 & 0 & 0 & 0 & 0 & \frac{1}{G_{LR}} \end{bmatrix} \quad (3.4)$$

The compliance matrix [S] consists of nine independent engineering constants. The subscripts *L*, *R*, and *T* refer to the three principal material directions of wood. The nine engineering constants consist of three moduli of elasticity E_{ii}, three moduli of shear $G_{ij,}$ and the six Poisson's ratios v_{ij}. The first subscript refers to the direction of the applied stress, and the second is the direction of the lateral deformation. The relationship between the Poisson's ratios and the moduli of elasticity, due to the symmetry of the compliance matrix [C], is shown in equation (3.5):

$$v_{ij} = \frac{E_{ii}}{E_{jj}} v_{ji}, (i, j = L, R, T, i \neq j) \quad (3.5)$$

A transformation matrix [T] can convert from the local cylindrical coordinate system to the global Cartesian coordinate system. Therefore, the compliance matrix of the global coordinate system is related to the cylindrical coordinate system by the following relation:

$$\bar{S} = T\, S\, T^{-1} \quad (3.6)$$

Equation (3.7) depicts the transformation matrix.

$$T = \begin{bmatrix} 1 & 0 & 0 & 0 & 0 & 0 \\ 0 & c^2 & s^2 & -2sc & 0 & 0 \\ 0 & s^2 & c^2 & 2sc & 0 & 0 \\ 0 & sc & -sc & c^2 - s^2 & 0 & 0 \\ 0 & 0 & 0 & 0 & -s & c \\ 0 & 0 & 0 & 0 & c & s \end{bmatrix} \quad (3.7)$$

Where c = cos *α*, s = sin *α*, and *α* is the rotation angle. Figure 3-3 illustrates the relationship between the cylindrical, the Cartesian coordinate system and the angle *α.* The angle of rotation *α* of a specific cross-sectional point with coordinates (*x, y*) is influenced by the sawing pattern of the lamination. The following equation can determine the angle α:

$$\alpha = tan^{-1}\left(\frac{(y+d)}{x - \left(e + \frac{W}{2}\right)}\right) \quad (3.8)$$

Equation (3.9) can be used to obtain the stresses perp. to the grain at any given point:

$$\sigma_{yy} = sin^2\ \cdot \sigma_{\mathrm{RR}} + \cos^2 \alpha \cdot \sigma_{\mathrm{TT}} + 2 \sin \alpha \cos \alpha \cdot \sigma_{\mathrm{RT}} \quad (3.9)$$

Furthermore, the stiffness perp. to the grain at any point can be obtained by equation (3.10):

$$E_{yy} = \left(sin^4 \alpha \cdot \frac{1}{E_{\mathrm{RR}}} + \sin^2 \alpha \cos^2 \alpha \cdot \left(\frac{1}{G_{RT}} - \frac{2\nu_{RT}}{E_{TT}}\right) + \cos^4 \alpha \cdot \frac{1}{E_{\mathrm{TT}}}\right)^{-1} \quad (3.10)$$

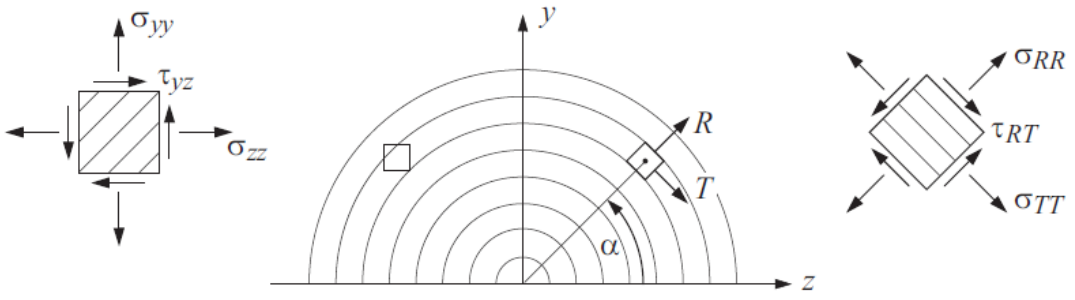

Figure 3-3: *Schematic overview of the different stress components for the cylindrical and Cartesian coordinate system [31].*

Figure 3-4 exemplarily depicts the influence of the angle α on the global stiffness perpendicular to the grain E_{yy}. The figure reveals that a minimum global stiffness perpendicular to the grain occurs at an angle of 45°, originating from the low rolling shear stiffness [31]. A maximum is obtained at an angle of 90° the global stiffness is aligned to the radial direction of the annual rings at this angle. The global stiffness is equal to the tangential stiffness at an angle of 0°.

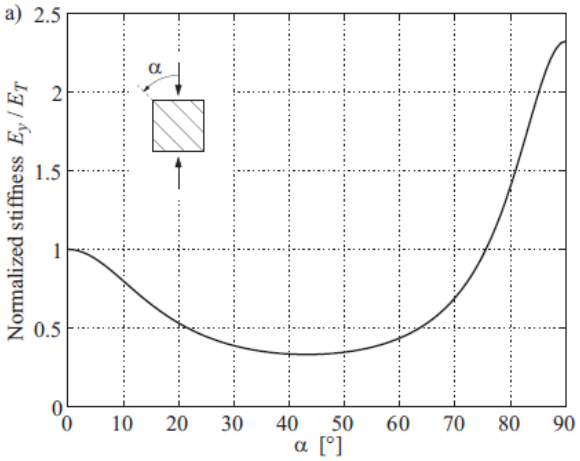

Figure 3-4*: Influence of the local orientation of the stiffness in the direction perpendicular to the grain [31].*

The most important effect of the transformation matrix [T] is the shear and normal strain coupling effect. This coupling means normal and shear compliances are no longer uncoupled as in loading in the local cylindrical orientation [9]. This results in off-axis shear strain ε_{xy} besides the strains ε_x and ε_y. The global stiffness is, therefore, dependent on the shear stiffness of the local cylindrical configuration, as illustrated by the middle term of equation (3.10). This complex shear coupling effect and the low shear stiffness in the RT-plane contribute to the inhomogeneous stress distribution [8].

3.3 Glulam beam with a hole

Tapia [11] performed a numerical analysis to quantify the tensile stresses perp. to the grain along a plane starting from the location of the maximum tensile stress along the periphery of the hole. Figure 3-5 compares the result of the numerical analysis with an orthotropic reference case. The previous version of EN 14080 [32] served as the basis for the elastic properties of the orthotropic model. In this version, the modulus of elasticity perpendicular to the grain direction was determined to be 460 N/mm^2. However, the current version specifies a revised value of 300 N/mm^2. The elastic properties

of the cylindrical anisotropic model are based on the stiffness ratios in the equation utilized by Aicher & Dill-Langer [10] and applied to the elastic properties of GL32h of DIN EN 14080 [32]. From the figure, it becomes apparent that all the piths aligned, although the specific lay-up configuration was not explicitly mentioned. The presence of a distinct stress peak at the mid-width of the cross-section provides support for this observation. The observed stress peak is approximately 2,5 times higher than the orthotropic reference model. Furthermore, the analysis revealed that the fictive tensile force $F_{t,90}$ was 14% and 20% higher than the orthotropic model for beams with a cross-sectional width of 100 and 260 mm, respectively.

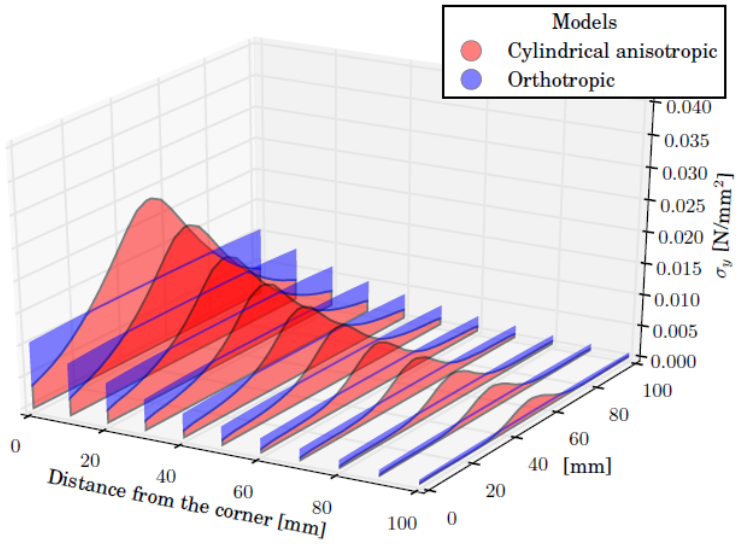

Figure 3-5: *Comparison of the tensile stresses perp. to the grain along a horizontal path at the location of maximum tensile stresses along the periphery of the hole for the orthotropic (blue) and cylindrical anisotropic models [11].*

Tapia [11] also investigates a hole reinforced by a vertically placed steel rod. Figure 3-6 compares the tensile stresses perp. to the grain and shear stresses for the unreinforced and reinforced cases for a 120 mm wide beam reinforced by a rod with a diameter of 12 mm. The figure reveals a reduction of 23,4% for the fictive tensile force. Furthermore, the figure shows that a vertically placed rod does not significantly affect the shear stresses when considering the cylindrical anisotropy of wood. This lack of reduction aligns with the observations regarding vertically placed rods in section 2.4.1.

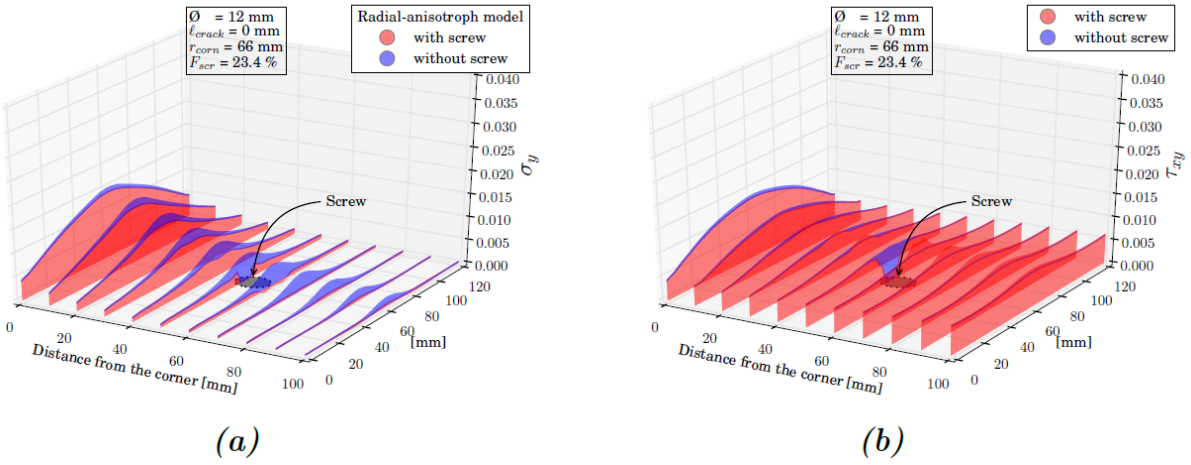

Figure 3-6: *Comparison of the tensile and shear stresses along a horizontal path for the reinforced and unreinforced cases [11].*

Because the cylindrical anisotropic representation is highly dependent on the lay-up of each lamination in the region of interest, the cylindrical anisotropic behaviour was omitted, and the orthotropic model was used for the remainder of the research.

3.4 Discussion

This chapter discussed the cylindrical anisotropy of wood. The cylindrical anisotropy of wood has a pronounced influence on the stress distribution perp. to the grain direction of timber. The commonly assumed orthotropic behaviour of timber is inadequate for situations involving tensile stresses perp. to the grain occur, as it provides only an average value of these stresses across the width. A three-dimensional representation that considers the cylindrical anisotropy of wood is necessary to approximate the inhomogeneous stress distribution near the hole.

Contrary to the orthotropic model, the cylindrical anisotropic model is more extensive and thus needs additional parameters for a correct implementation in a numerical analysis. Important are the individual pith orientations of the laminations. Each lamination in a glulam cross-section possesses a unique pith orientation following from the different sawing patterns.

The remainder of this thesis focuses on the influence of the cylindrical anisotropy of wood on the structural behaviour of a beam with a circular hole. However, before moving on, the second generation of Eurocode 5 will be discussed.

4

DESIGN OF HOLES ACC. FUTURE VERSION EUROCODE 5

Chapter 2 provided a comprehensive analysis of the structural behaviour of holes, including the brittle failure mechanism, stress distribution in the vicinity of a hole, the concept of the fictive tensile force, and the influence of reinforcements. The chapter revealed that the current version of Eurocode 5 [20] provides no detailing rules or formulas for assessing holes in glulam beams. However, the implementation of holes is enabled only through non-contradictory information given in the National Annexes to Eurocode 5 of Germany [21] and Austria [22]. Therefore, with the introduction of a new generation of Eurocodes, the European standardization committee responsible for Eurocode 5, CEN/TC 250/SC 5, decided to form a Working Group 7 "Reinforcement", to close the gap between recent developments and practical needs [33]. This working group is responsible for developing reinforcement guidelines for timber structures, including reinforcements for holes in glulam beams. The development of the new version was still under development at the time of writing this thesis. The consolidated draft was made available for comment at the end of 2021. This chapter is based on section "8.3 Additional rules for members with special geometries" of this consolidated draft [34].

4.1 Basic concepts

Holes larger than or equal to 50 mm or 0.1*h* should be checked for stress concentration effects. However, holes should not be placed in unreinforced zones in members where stresses perp. to the grain are already present due to geometry or loading, e.g., curved or tapered beams. An exception is made if a more detailed analysis is performed, but how to do this is not mentioned.

Circular and rectangular holes are permitted, but circular holes are preferred and should ideally be positioned along the neutral axis of the member. It should be noted that the design standard allows only eccentric placement for circular holes. Shear-dominated regions are preferred over moment-dominated regions for hole placement. Additionally, the influence of service installations on local timber moisture content should be considered.

Rectangular holes up to 0,2*h* and circular holes up to 0,2*h* or 0,3*h* (depending on the eccentricity) are permissible. The length of rectangular holes is limited by $\ell_h/h_h \leq 2{,}5$ and $\ell_h \leq 0{,}5h$. Furthermore, rectangular holes should be rounded to minimize the stress concentrations. The corner radius, *r,* should have a minimum value of 20 if h_h is less than or equal to 200 mm and a minimum corner radius of 40 mm if h_h is greater than 200 mm. The distance from the support to the nearest edge of the hole, $\ell_{A,}$ should be greater than 0,5*h* for both hole shapes, and the distance from the end of the beam to the closest edge of the hole ℓ_v should be greater than *h*. Individual holes should be spaced at least 300 mm or 1,5*h* apart, except for circular holes where the minimum distance equals the hole diameter. Table 4-1 represents a summary of the minimum and maximum dimensions.

Table 4-1: *Minimum and maximum dimensions of unreinforced holes [34].*

Minimum distances				**Maximum dimensions**		
End	Spacing	Support	Edges	Rectangular		Circular
$\ell_v \geq h$	Individual hole: $\ell_z \geq 1{,}5h$	$\ell_A \geq h/2$	$h_{ru} \geq 0{,}15h$ at least 1 lamination	$\ell_h/h_h \leq 2{,}5$	$h_h \leq 0{,}2h$	For $e \leq \pm 0{,}1h$: $d \leq 0{,}3h$
	Group of circular holes: $\ell_z \geq d$		$h_{rl} \geq 0{,}2h$ at least 1,5 laminations	$\ell_h \leq 0{,}5h$		For $e \geq \pm 0{,}1h$: $d \leq 0{,}2h$

4.2 Fictive tensile force

The calculation of the fictive tensile force is dependent on the position of the hole relative to the neutral axis. Different formulas must be applied for holes placed along the neutral axis of the beam and those placed with eccentricity. However, for both cases, the following check should be satisfied:

$$\frac{\frac{F_{t,90,V}}{\ell_{t,90,V}} + \frac{F_{t,90,M}}{\ell_{t,90,M}}}{0{,}5 \cdot b \cdot k_{vol} \cdot k_{space} \cdot f_{t,90}} \leq 1{,}0 \tag{4.1}$$

The numerator represents the fictive tensile force, which is again composed of a shear and moment component and individual integration lengths $\ell_{t,90}$. However, these are determined differently for the two cases and will be discussed further on. The denominator represents the fictive tensile resistance. The fictive tensile resistance comprises the width *b,* a volume factor k_{vol}, a reduction factor for a group of holes and the tensile strength $f_{t,90}$ of the timber. The factor 0,5 originates from the simplified triangular stress distribution as shown in Figure 2-14. The volume effect can be determined with the following equation:

$$k_{vol} = \left(\frac{V_{ref}}{0{,}25 \cdot b \cdot d_{hole}^2}\right)^{0{,}2} \; with \; V_{ref} = 0{,}01 \; m^3 \tag{4.2}$$

It is allowed to place up to 3 circular holes at a closer distance parallel to the grain of each other, but the fictive resistance must be reduced with a space factor k_{space}:

$$k_{space} = min\begin{cases} 1 \\ 1 - 0{,}2 \cdot \dfrac{1{,}5h - \ell_z}{1{,}5h} \\ 1 - 0{,}4 \cdot \dfrac{5d - \ell_z}{5d} \end{cases} \tag{4.3}$$

4.2.1 Hole placed along the neutral axis of the beam

For the case of a hole placed along the neutral axis of the beam, the shear component and the integration length of the shear component can be calculated with equations (4.4) and (4.5):

$$F_{t,90.\mathrm{V,Ed}} = \frac{V \cdot 0{,}7 \cdot d_{hole}}{4 \cdot h} \cdot \left[3 - \left(\frac{0{,}7 \cdot d_{hole}}{h}\right)^2\right] \cdot k_{diam} \tag{4.4}$$

$$\ell_{t,90,V} = 1{,}3\, d_{hole} \tag{4.5}$$

Here, d_{hole} is the applicable diameter of the hole, which is equal to the diameter in the case of circular holes and $k_{shape}\, h_h$ in the case of rectangular holes. The factor, $k_{shape,}$ accounts for the effect of the shape of a rectangular hole. This factor can be determined with the equation below:

$$k_{shape} = 1{,}25 + 0{,}3\frac{\ell_h}{h_h}\left[4\frac{V_d h}{M_d} - 3\left(\frac{V_d h}{M_d}\right)^2\right] \tag{4.6}$$

The factor k_{diam} accounts for the stress distribution and the location of crack initiation and can be calculated with the equation below:

$$k_{diam} = 1{,}1 + 1{,}3\left[\frac{d_{hole}}{h} - \left(\frac{d_{hole}}{h}\right)^2\right] \tag{4.7}$$

The moment component and integration length for a hole placed along the neutral axis of the beam can be calculated with the equations:

$$F_{t,90.\mathrm{M,Ed}} = 0{,}09 \cdot \frac{M_d}{h} \cdot \left(\frac{d_{hole}}{h}\right)^2 \tag{4.8}$$

$$\ell_{t,90,M} = 0{,}8\, d_{hole} \tag{4.9}$$

4.2.2 Circular hole placed with an eccentricity

It is also allowed to place circular holes with an eccentricity to the neutral axis of the beam. However, the formulas for the shear and moment components are slightly different. It was shown in section 2.1 that a hole placed with an eccentricity is subjected to different ratios of the shear and bending stresses that need to be redistributed around the hole compared to a hole placed along the neutral axis of the beam.

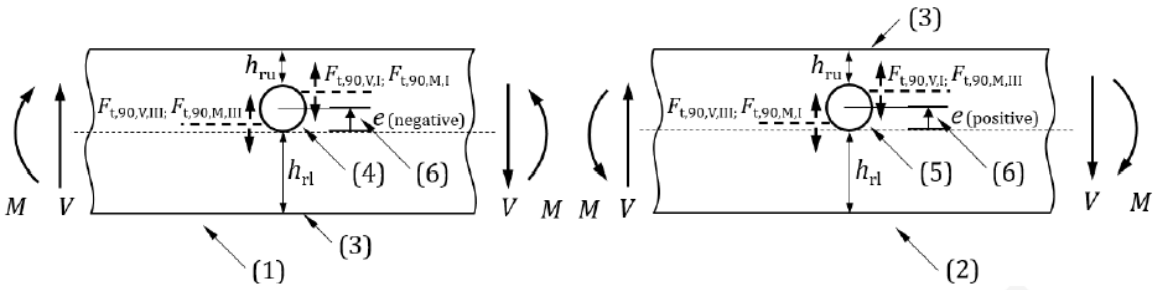

Figure 4-1: *The different force components that need to be checked depending on the direction of the bending moment [34].*

The following set of relevant forces for the two considered quadrants should be used:

For positive bending moments:

$$\begin{matrix} F_{t,90.\mathrm{V,I}} + F_{t,90.\mathrm{M,I}} \\ F_{t,90.\mathrm{V,III}} + F_{t,90.\mathrm{M,III}} \end{matrix} \tag{4.10}$$

For negative bending moments:

$$\begin{matrix} F_{t,90.\mathrm{V,I}} + F_{t,90.\mathrm{M,III}} \\ F_{t,90.\mathrm{V,III}} + F_{t,90.\mathrm{M,I}} \end{matrix} \tag{4.11}$$

The shear component in the case of eccentrically placed circular holes can be determined with the equation below:

$$F_{t,90.\mathrm{V,I/III,Ed}} = \frac{V \cdot 0{,}7 \cdot h_d}{4 \cdot h} \cdot \left[3 - \left(\frac{0{,}7 \cdot h_d}{h}\right)^2\right] \cdot k_{ec,I/III} \tag{4.12}$$

The integration length $\ell_{t,90,V}$ is equal to the integration length of the shear component for centrally placed holes. The formula is almost identical to the centrally placed holes. However, an additional parameter for the eccentricity, $k_{ec,I/III}$ is added. This parameter can be determined with the equations (4.13) and (4.14):

$$k_{ecc,I} = 0{,}1 + \frac{d}{h} + 4{,}5 \cdot \frac{h_{ru}}{h} - 5{,}0 \cdot \left(\frac{h_{ru}}{h}\right)^2 \tag{4.13}$$

$$k_{ecc,III} = 0{,}1 + \frac{d}{h} + 4{,}5 \cdot \frac{h_{rl}}{h} - 5{,}0 \cdot \left(\frac{h_{rl}}{h}\right)^2 \tag{4.14}$$

The moment component in the case of eccentrically placed circular holes depends on the considered quadrant and can be determined with the equations below:

$$F_{t,90,M,I} = M_d \cdot \frac{d}{h^3} \cdot max \begin{cases} -0{,}62 \cdot (e - 0{,}13 \cdot d) \\ -0{,}2 \cdot (e - 0{,}45 \cdot d) \\ -0{,}3 \cdot (e - 0{,}08 \cdot d) \end{cases} \tag{4.15}$$

$$F_{t,90,M,III} = M_d \cdot \frac{d}{h^3} \cdot 0{,}22 \cdot (e + 0{,}19 \cdot d) \tag{4.16}$$

The determination of the integration lengths for the moment component differs in the case of a hole placed along the neutral axis of the beam.

$$\ell_{t,90,M} = \ell_{t,90,M,I} = 0{,}8 \cdot h_d \cdot \left(1 - \frac{e}{d}\right) \; with \; 0{,}6d \; \leq \; \ell_{t,90,M,I} \; \leq 1{,}0d \tag{4.17}$$

$$\ell_{t,90,M} = \ell_{t,90,M,III} = 0{,}4 \cdot d \tag{4.18}$$

4.3 Increased shear stresses at the hole

Besides the fictive tensile force, the increased shear stresses at the periphery of the hole need to be checked. The increased shear stresses at the hole must be verified against the design shear strength $f_{v,d}$. This verification is shown in the equation below:

$$\tau_{max,d} = k_\tau \cdot \frac{1{,}5 \cdot V_d}{b \cdot (h - h_d)} \leq f_{v,d} \tag{4.19}$$

The factor k_t takes the increased shear stresses into account. This factor can be calculated with the equation below:

$$k_\tau = k_{rad} \cdot \left(1 + \frac{\ell_h}{h}\right) \cdot \left(\frac{h_h}{h}\right)^{0{,}2} \tag{4.20}$$

The factor k_{rad} is a factor to account for the effect of the corner radius on the shear stress and may be taken as 1,8 without further verification in the case of glued laminated timber.

4.4 Reinforced holes

Suppose the beam cannot provide enough resistance by itself. In that case, it becomes necessary to apply reinforcements to increase the load-bearing capacity and prevent the uncontrolled propagation of cracks within the regions exposed to tensile stresses perp. to the grain. The reinforcements can be classified into two types:

1) Internal reinforcements:
   - Fully threaded screws.
   - Screwed-in threaded rods with wood thread.
   - bonded-in threaded or ribbed steel rods
2) External reinforcements:
   - Glued-on plywood boards.
   - Glued-on laminated veneer lumber.
   - Glued-on laminations made from either structural timber, plywood, or laminated veneer lumber.
   - Pressed-in punched metal plate fasteners.

The minimum and maximum dimensions are more favourable when reinforcements are applied, as seen in Table 4-2.

The denominator of equation (4.1) is replaced by the resistance of the reinforcements $F_{t,90,Rd}$. It is assumed that the glulam does not contribute to the tensile resistance; thus, the reinforcements take the total force. The approach to determine this resistance is based on the type of reinforcement.

Table 4-2: *Minimum and maximum dimensions for reinforced holes [34].*

<table>
<tr><th colspan="4">Minimum distances</th><th colspan="3">Maximum dimensions</th></tr>
<tr><td>End</td><td>Spacing</td><td>Support</td><td>Edges</td><td colspan="2">Rectangular</td><td>Circular</td></tr>
<tr><td rowspan="2">$\ell_v \geq h$</td><td>Individual hole:
$\ell_z \geq h$</td><td rowspan="2">$\ell_A \geq h/2$</td><td>$h_{ru} \geq 0{,}15h$
at least 1 lamination</td><td>$\ell_h/h_h \leq 2{,}5$</td><td rowspan="2">$h_h \leq 0{,}3h$[1]
$h_h \leq 0{,}4h$[2]</td><td rowspan="2">$d \leq 0{,}3h$[1]
$d \leq 0{,}4h$[2]</td></tr>
<tr><td>Group of circular holes:
$\ell_z \geq d$</td><td>$h_{rl} \geq 0{,}2h$
at least 1,5 laminations</td><td>$\ell_h \leq h$</td></tr>
</table>

[1] Internally reinforced holes

[2] Externally reinforced holes

4.4.1 Internal reinforcements

The checks that need to be performed for internal reinforcements depend on whether fully threaded screws or glued-in steel rods are used. The fully threaded screws need to be checked for a minimum value of either the withdrawal capacity $F_{w,k}$ or tensile capacity $F_{t,d}$ of the fully threaded screw:

$$F_{t,90.,\mathrm{Rd}} = n_r \cdot min\begin{Bmatrix} F_{w,k} \\ F_{t,d} \end{Bmatrix} \tag{4.21}$$

The parameter n_r represents the number of reinforcing elements. Only one row of internal reinforcements can be considered.

Two checks need to be performed when glued-in steel rods are used. The tensile strength $F_{t,d}$ of the glued-in rod and the bond line resistance $F_{b,d}$. The minimum value of these two checks is governing as is shown in the equation below:

$$F_{t,90.,\mathrm{Rd}} = n_r \cdot min\begin{Bmatrix} F_{t,d} \\ F_{b,d} \end{Bmatrix} \tag{4.22}$$

Lastly, the effective anchorage length, $\ell_{r,}$ can be determined with the equation below:

$$\ell_r = \begin{cases} h_{rl} \; or \; h_{ru} & for \; rectangular \; holes \\ h_{rl} + 0{,}15h_h \; or \; h_{ru} + 0{,}15h_h & for \; circular \; holes \end{cases} \tag{4.23}$$

Internal reinforcements should be limited to locations in the member subjected to a low shear force. Furthermore, the increased shear stresses at the hole should be checked, as described in section 4.3. If this check is not satisfied, internal reinforcements should not be used.

The internal reinforcements need to comply with some minimum values. The distance between the edge of the hole to the centre of the internal reinforcement, $a_{3,c,}$ should be 2,5d. The distance from the edge of the beam to the centre of the internal reinforcement, $a_{4,c,}$ should have a minimum spacing of 2,5d. Furthermore, the centre-to-centre distance between two rods, a_2, must be 4d minimal.

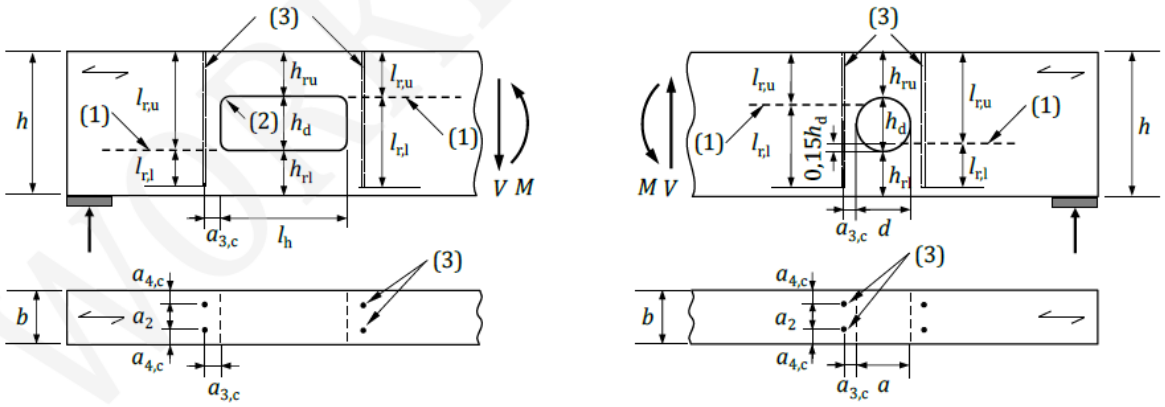

Figure 4-2: *Minimum and maximum spacing of internal reinforcements [34].*

4.4.2 External reinforcements

The external reinforcements need to be checked for a minimum value of either the design shear stress in the glue line or the tensile stress in the reinforcement. These two checks are shown in the equation below:

$$F_{t,90.,\mathrm{Rd}} = n_r \cdot min\left\{\begin{matrix} f_{b2,d} \cdot \ell_r \cdot b_r \\ \frac{f_{t,d}}{k_k} \cdot b_r \cdot t_r \end{matrix}\right\} \tag{4.24}$$

The parameter n_r represents the number of reinforcing elements. This is equal to two in the case of external reinforcements. Without further verification, the design glue-line strength, $f_{b2,d}$, may be taken as 0,75 N/mm^2. The design strength of the plate $f_{t,d}$. t_r and b_r describe the panel thickness and width, respectively. The factor k_k considers the characteristics of the non-uniform distribution of stresses and concentration of stresses at the panel edge facing the peak stresses in the timber member [33]. Without further notification, the value of k_k may be taken equal to 2,0 in glulam beams with rectangular cross-sections. Lastly, the relevant height of the plane reinforcement can be determined with the equation below:

$$\ell_r = \begin{cases} h_{rp} & for\ rectangular\ holes \\ h_{rp} + 0{,}15h_h & for\ circular\ holes \end{cases} \tag{4.25}$$

The external reinforcements need to comply with some minimum and maximum values. The first limitation is regarding the width of the plane, b_r, which should fall in between the range 0,25 $\ell_h \leq b_r \leq$ 0,6 $\ell_{t,90}$. The length of the panel under perpendicular to the grain stresses $\ell_{t,90}$ is equal to 0,5 (h_h + h). The last limitation is regarding the height of the panel; respectively, below and above the hole should have a maximum of either 80 mm or 0,25 ℓ_h. Figure 4-3 shows the representation of the geometric parameters of the panel.

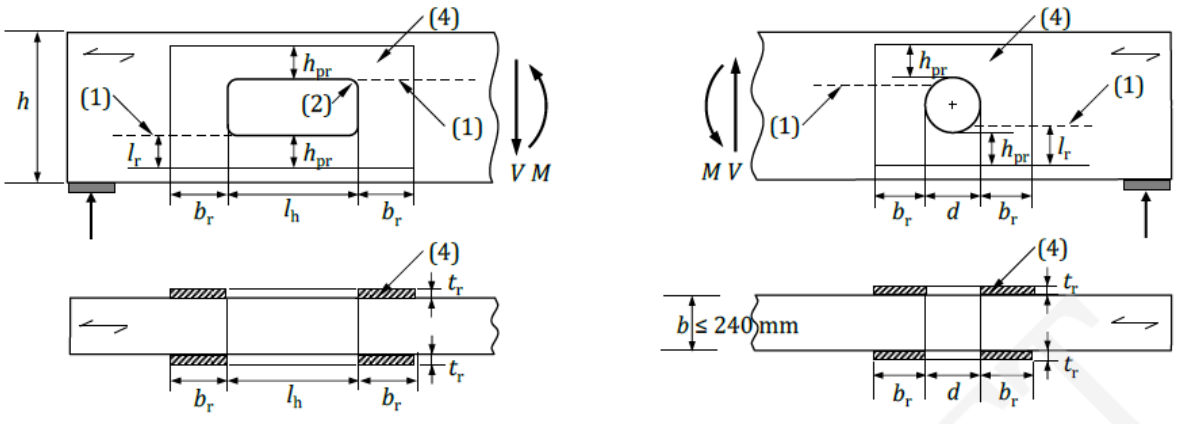

Figure 4-3: *Representation of the geometric parameters of external reinforcements [34].*

4.5 Discussion

The future version of Eurocode 5 introduces detailing rules and checks for assessing the structural capacity of a glulam beam with a hole. The design approach revolves around calculating a fictive tensile force, which needs to be resisted by the fictive resistance of the unreinforced glulam. When reinforcements are applied, the reinforcements must resist the total force. However, the design standard does not provide specific guidelines for reducing the pronounced stress peaks near the mid-width of the cross-section.

5

METHODOLOGY

This chapter presents the description of the numerical models to compare the orthotropic model employed for most structural applications with the more accurate representation considering the cylindrical anisotropy of wood. Four cases were examined: one orthotropic and three cylindrical anisotropic cases with three varying lay-up patterns. The Finite Element software Abaqus v2019 [35] was used, along with its scripting interface, to create and analyse the stress distribution in the vicinity of a hole. Multiple models were created to analyse the stress distribution in the vicinity of a hole.

Python scripting, employing the Object-Oriented Programming (OOP) approach, was utilized to parameterize the models, accelerate the modelling process, and facilitate the post-processing of results. The adoption of the OOP approach led to the creation of reusable and robust scripts. First, the models for the unreinforced situation were created. Due to the differences between the orthotropic and cylindrical anisotropic behaviour, different scripts were written. These scripts were extended to incorporate the application of reinforcements, particularly external reinforcements.

5.1 Studied configuration

5.1.1 Unreinforced situation

It was chosen to focus on a circular hole placed along the neutral axis of the beam with a relative hole height of 0,3*h*, resulting in a hole height h_h of 120 mm. This hole height complies with the upper limit for the hole height of an internally reinforced hole according to the second generation of Eurocode 5 [34], as discussed in the previous chapter. Figure 5-1 depicts the considered glulam beam and hole configuration. The beam has a height of h = 400 mm, a width of w = 120 mm and a total length of 1.925 mm representing a medium-sized beam. The effective span between the two supports is 3.600 mm (9*h*). The beam is loaded by two point loads placed at a distance of 1.600 mm (4*h*) from the supports with a distance of 400 mm between the point loads. A circular hole is placed along the neutral axis of the beam at a distance of 2*h* from the left support and the point load. This results in an M/V ratio of 2*h* at the centre of the hole.

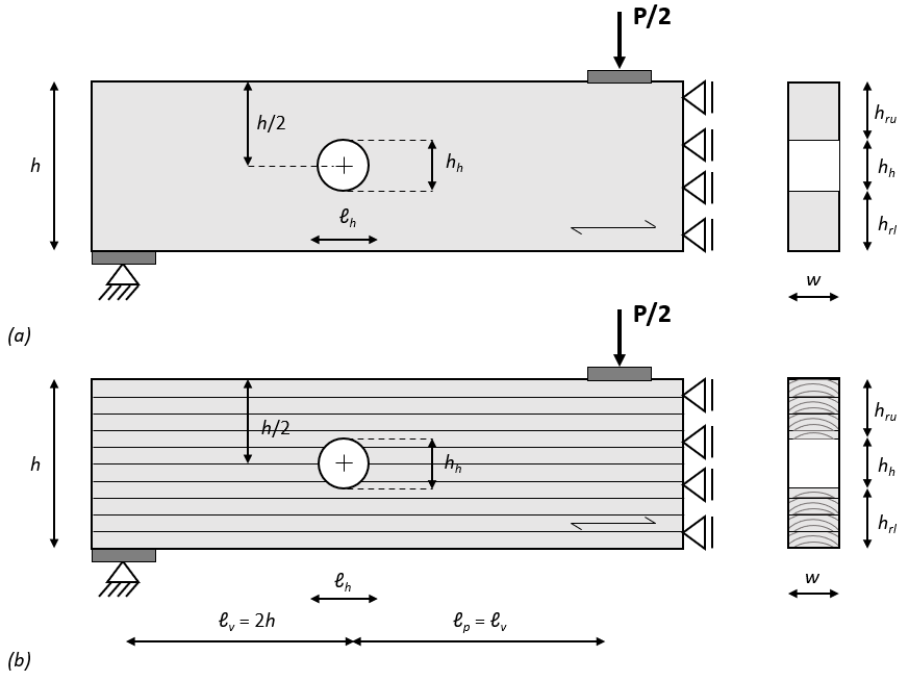

***Figure 5-1**: The studied configuration; (a) orthotropic model (b) cylindrical anisotropic models.*

The dimensions previously discussed provide sufficient information to create the orthotropic model. However, the cylindrical anisotropic model requires additional parameters related to the orientation of the laminations. These parameters include the thickness of individual laminations and the orientation of the pith within each lamination. A thickness of 40 mm was chosen for the laminations, resulting in 10 laminations for a beam with a height of 400 mm. This lamination thickness seems to be the standard thickness for most glulam manufacturers in west-Europe.

Moreover, it is essential to define the orientation of each lamination to the cross-section from which it was sawn. It is important to note that the orientation of the pith and annual rings are not part of the strength grading of the laminations nor the production process of a glulam cross-section. Given the arbitrary nature of these orientations, simplifications are necessary to study the influence of the annual rings consistently. This study adopts the same lay-up configurations as Aicher & Dill-Langer (12). However, the patterns were adjusted to a lamination thickness of 40 mm. Figure 5-2 depicts the three studied lay-ups.

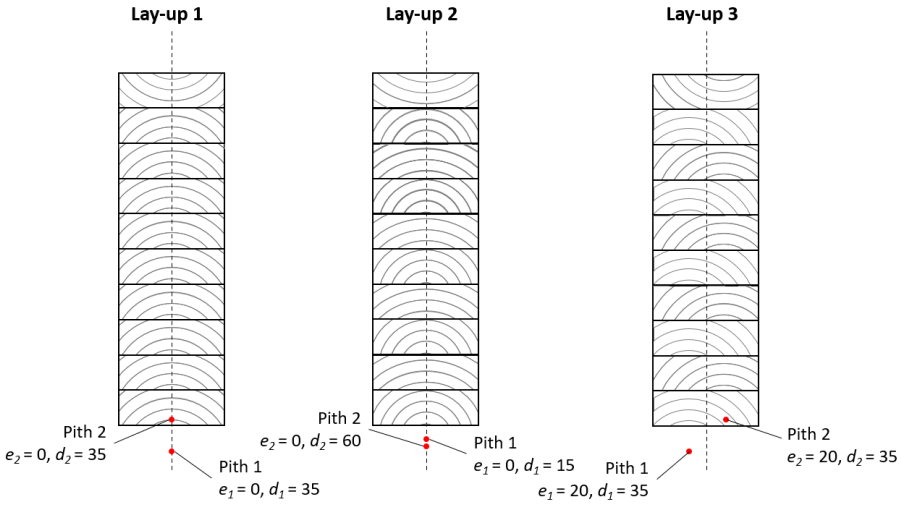

***Figure 5-2:** The three different employed lay-ups.*

5.1.2 Reinforced situation

Three reinforcement scenarios were examined: a single rod placed at the mid-width, two rods positioned along each other, and a plywood panel glued to both sides of the glulam beam. Each scenario is described in detail below.

The first and second scenarios examine rods installed at an inclination angle β of 45°. This angle was the most effective for reducing tensile stresses perp. to the grain and shear stresses in circular holes positioned along the neutral axis [28]. The first scenario employs rods with a diameter of d = 14 mm, while the second one employs a diameter of d = 10 mm. The rod diameters were explicitly chosen such that the total area of the rods is equal in both scenarios, enabling a consistent comparison. The rods are rotated around a point at a distance of $a_{3,c}$ = 2,5d from the theoretical location of the maximum tensile stresses perp. to the grain along the periphery of the hole. This theoretical location corresponds to an angle φ of 45° (+180°) and a distance of 25 mm and 35 mm away from the periphery of the hole for one and two rods, respectively. The distance from the outer edges of the glulam to the rod was equal to a_4 = 2,5d in the case where two rods are present at each crack plane. Furthermore, the effective anchorage length ℓ_r is 200 mm. All the geometric parameters adhere to the requirements outlined in the second generation of Eurocode 5 [34]. Figure 5-3 illustrates the above-described parameters for the two scenarios.

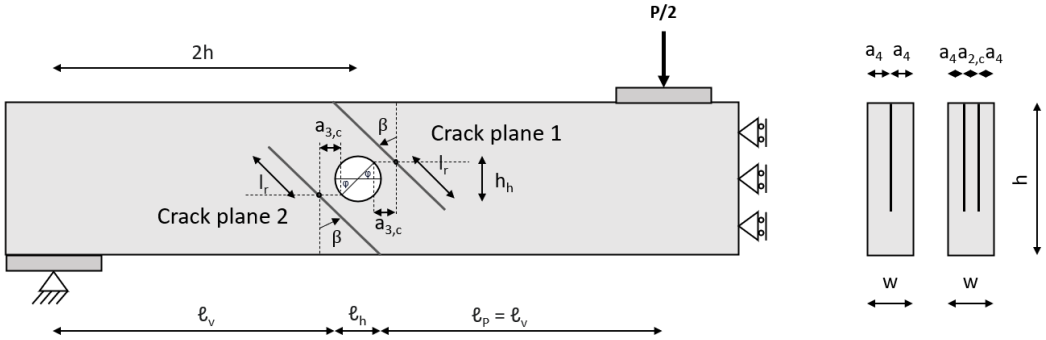

Figure 5-3: *The first and second scenarios with rods employed at an angle of 45°.*

The third and final scenario involved an externally reinforced hole, where plywood panels made of birch are glued to the outer edges of the cross-section. These plywood panels had a thickness t_r of 24 mm. This thickness equals a panel thickness vs beam width ratio $2t_r/w$ of 0,4. The dimensions h_{pr} and b_r are 80 mm resulting in a panel with a length and width of 280 mm. All the listed geometric parameters comply with the requirements outlined in the second generation of Eurocode 5 [34]. Figure 5-4 illustrates the above-described parameters for the third scenario.

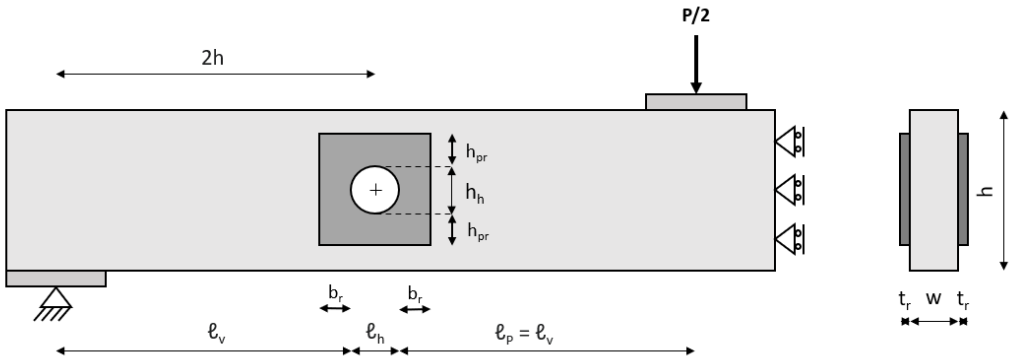

Figure 5-4: *The third scenario with a plywood panel glued to both sides of the glulam.*

5.2 Material properties

The glulam strength class GL24h was chosen for the orthotropic model because it appears to be the standard strength class for most glulam manufacturers in West Europe. Table 5-1 presents the constitutive properties of the glulam, which are based on NEN-EN 14080 [36]. The Poison ratios were taken from [37].

Table 5-1: *Material properties for glulam strength class GL24h according to NEN-EN 14080 [38].*

Strength class	Ref	E_x	E_y	E_z	G_{xy}	G_{xz}	G_{yz}	v_{xy}	v_{xz}	v_{yz}
		(N/mm^2)			(N/mm^2)			(-)		
GL24h	[38]	11.500	300	300	650	650	65	0,02	0,02	0,3

The constitutive properties of the cylindrical anisotropic model are different compared to the orthotropic model since no distinction is made between the radial and tangential directions. It is precisely this difference that causes the pronounced stress peaks. Therefore, the constitutive properties from NEN-EN 14080 [38] are inappropriate. The stiffness ratios in equation (5.1) obtained good agreements between numerical simulations and experimental test results [19].

$$E_L : E_R : E_T : G_{RL} : G_{TL} : G_{RT} = 1 : 10{,}8 : 0{,}67 : 0{,}67 : 0{,}67 : 0{,}042 \quad (5.1)$$

Therefore, these stiffness ratios were also applied in this thesis. Table 5-2 presents the constitutive properties of these stiffness ratios applied to GL24h. Again, the Poison ratios were taken from [37].

Table 5-2: *Material properties for the glulam according to stiffness ratios proposed by [10].*

Material	Ref	E_L	E_R	E_T	G_{LR}	G_{LT}	G_{RT}	v_{LR}	v_{LT}	v_{RT}
		(N/mm^2)			(N/mm^2)			(-)		
Glulam	[10]	11.500	1.065	715	715	715	45	0,02	0,02	0,3

The Young's modulus *E* for steel rods was taken as 210.000 N/mm^2, and the Poison ratio *v* as 0,3. Table 5-3 presents the constitutive properties of the panel based on plywood made of birch. The constitutive properties are based on [26], [29].

Table 5-3: *Material properties for birch plywood according to [26], [29].*

Material	E_x	E_y	E_z	G_{xy}	G_{xz}	G_{yz}	v_{xy}	v_{xz}	v_{yz}
	(N/mm^2)			(N/mm^2)			(-)		
Plywood (birch)	9.100	8.400	370	620	620	50	0,04	0,4	0,4

5.3 Description of numerical models

5.3.1 Unreinforced orthotropic model

The unreinforced orthotropic model consists of glulam and rigid plate parts. The glulam part is modelled as a 3D solid deformable part using linear continuum elements with reduced integration (C3D8R). To reduce computational effort, symmetry conditions were applied. Specifically, symmetry was employed in the YZ-plane at the mid-span of the beam, dividing the total length of the beam in

half. Additionally, symmetry was employed in the XY plane at the mid-width of the cross-section, resulting in a division of the cross-section into two halves. Implementing these symmetry conditions significantly reduced the total number of elements and the computation time.

The glulam part was discretized using elements with a width of 4 mm along the cross-sectional width. Along the periphery of the hole, the elements had a size of 2 mm. The element size increased to 5 mm in a region extending 250 mm on both sides of the hole. Beyond this region, the element size gradually increased, reaching a size of 20 mm at both ends of the beam. Figure 5-5 (a) shows the meshing for the unreinforced orthotropic model. The elastic properties presented in Table 5-1 were applied to the glulam part, with the material directions aligning the global Cartesian coordinate system of the model.

Rigid elements of type R3D4 were employed to model the support and load plate with the following dimensions: 250x40x120 mm^3 (*l x h x b*). A reference point was positioned near the centre of the support plate to apply the boundary condition. Another reference point was placed at the centre of the load plate to introduce the point load. The point load for the quarter beam was 2.500 N. The support and load plate were connected with tie constraints to each other

5.3.2 Unreinforced cylindrical anisotropic model

The unreinforced cylindrical anisotropic model also consists of glulam and rigid plate parts. However, the glulam part needs additional modifications to accurately represent the cylindrical anisotropy of wood. Firstly, the glulam part had to be partitioned into multiple cells corresponding to the individual laminations. Secondly, the local cylindrical coordinate systems for each lamination had to be modelled. Subsequently, the elastic properties specified in Table 5-2 were assigned to the individual laminations. Due to the asymmetric nature of lay-up 3, the symmetry along the XY plane could not be applied, and thus, the full width had to be modelled. Furthermore, wedge elements were employed to achieve a finer mesh in specific cells, as shown in Figure 5-5 (b).

Like the orthotropic model, the cylindrical anisotropic model employed elements with a width of 4 mm along the cross-sectional width. Also, the periphery of the hole was discretized with elements of a size of 2 mm. The four laminations passing through the hole were discretized with 20 elements along the height of the lamination, while the laminations farther away from the hole were discretized with 10 and 5 elements along the height, respectively. Similar to the orthotropic model, the elements were finer near the hole along the *x*-direction with a size of 5 mm, increasing to 20 mm at the ends of the beam. Figure 5-5 (b) illustrates the meshing for the unreinforced cylindrical anisotropic model.

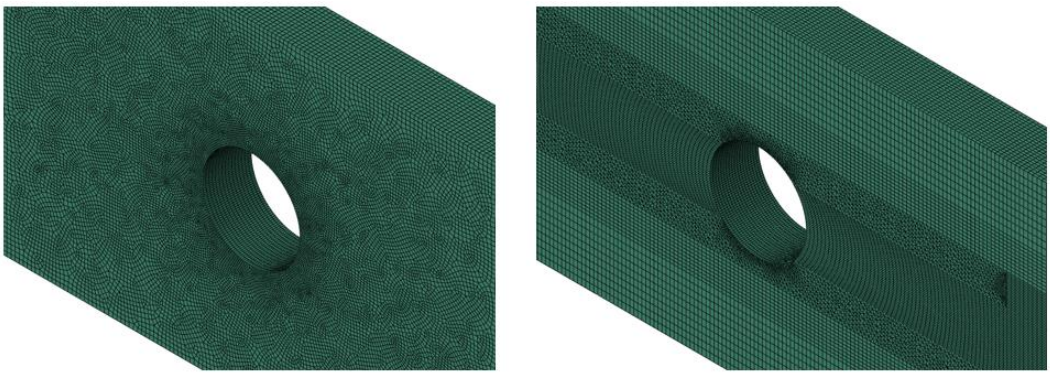

(a) Orthotropic *(b) Cylindrical anisotropic*

Figure 5-5: *Example of the meshing for the unreinforced orthotropic (a) and cylindrical anisotropic model (b).*

5.3.3 Internal reinforced models

The unreinforced model described in the previous section was extended for the application of internal rods. The creation of the model was based on the replication repository (34) for the numerical study conducted on internally reinforced holes by Tapia & Aicher (5).

To represent the rods, continuum linear elements with reduced integration (C3D8R) were employed. The discretization of the rods was performed with elements of a size of 3 mm. So-called "*tie constraints*" were used to connect the respective surface pairs in contact with the rods and glulam beam. The elements at the periphery of the hole had a size of 2 mm, which increased to a size of 3 mm in proximity to the rods. The remaining meshing of the glulam was done similarly to the unreinforced models. Figure 5-6 depicts the discretization of the internally reinforced orthotropic model.

Contrary to the other models, particularly the cylindrical anisotropic models, which were constructed “manually“. The meshing of the glulam part becomes too complex to parametrize within reasonable time and effort. However, a drawback of this approach is that performing a parameter study becomes a lot more complicated and time-consuming.

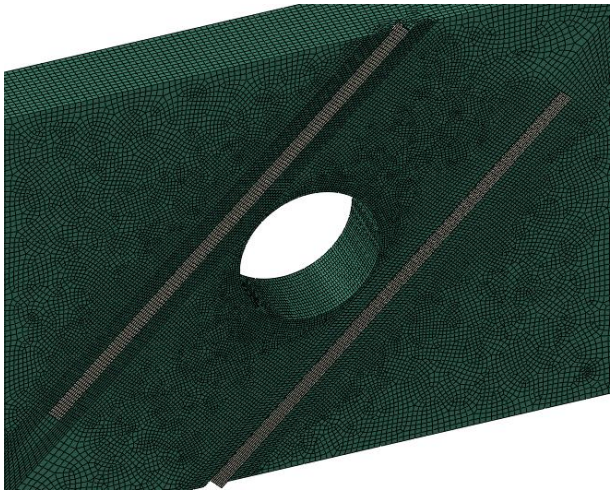

Figure 5-6: *Example of the meshing for the internal reinforced orthotropic model.*

5.3.4 External reinforced models

The previously described unreinforced models were extended with a panel for the case where external reinforcements are used. Continuum linear elements with reduced integration (C3D8R) were employed. Eight elements in the width direction discretised the width of the panel. The elements are 2 mm at the periphery of the hole and gradually increase to 5 mm at the outer edges of the panel. Figure 5-7 presents the meshing of the panel for the orthotropic model, although the mesh of the panel is similar to the cylindrical anisotropic model. So-called "*tie constraints*" were used to establish the connection between the respective surface pairs in contact with the panel and glulam beam. The constitutive properties presented in Table 5-3 were assigned to the plywood panel. The strong axis (E_x) is oriented perpendicular to the longitudinal axis of the beam, utilising the strong direction along the tensile stresses perp. to the grain.

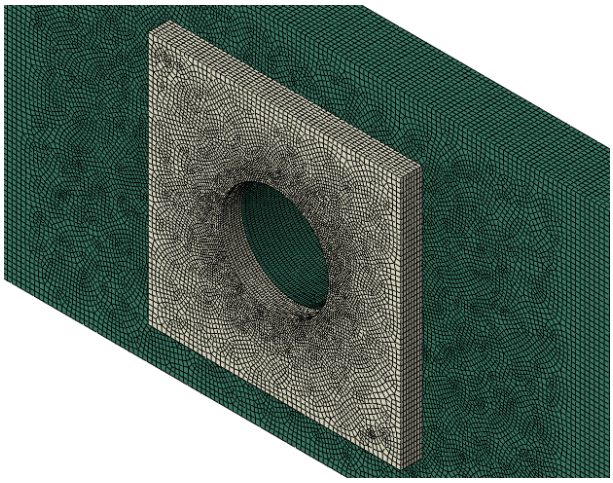

Figure 5-7: *Example of the meshing for the external reinforced orthotropic model.*

5.4 Extension for the damaged state

The Extended Finite Element Method (XFEM) was employed to model a stationary crack parallel to the grain direction of the beam to evaluate the impact of the different crack stages on the stress redistribution in the glulam at the region of the highest tensile stress. At the location of the crack, an unmeshed surface was placed, cutting all the enriched elements it intersected, depicted in Figure 5-8. Because only a stationary crack was considered, neither crack extension nor fracture mechanics were considered, and all crack stages were subjected to the same load. However, an increasing crack is commonly related to an increasing load.

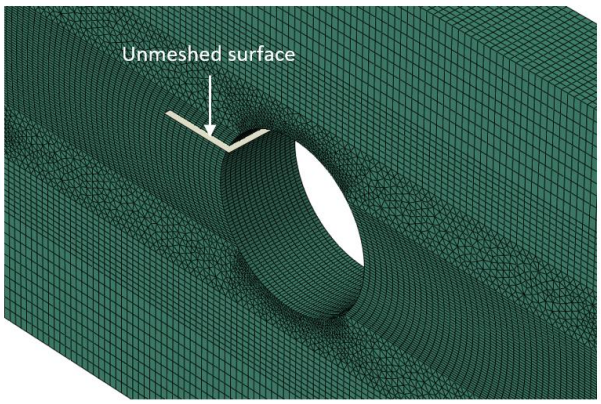

Figure 5-8: *The application of XFEM to the unreinforced cylindrical anisotropic model for crack stage 3.*

Some simplifications had to be made due to the complex geometry of the cracks observed in the literature. Because the cracks are modelled as a flat surface, no curvature analogous to the growth rings is considered, as discussed in section 2.2.3. Furthermore, the crack surfaces are rounded based on the research of Danielsson & Gustafsson [37]. They showed through a numerical model considering the facture behaviour employing cohesive elements that the cracks showed a rounded crack surface.

Three distinct crack stages are defined between crack initiation and the extension of the crack to the outer edges of the glulam. The cracks are placed where the tensile stresses perp. to the grain are the largest. The characteristics of the three considered crack stages are:

- Stage 1: Crack width 40 mm, crack depth 20 mm.
- Stage 2: Crack width 80 mm, crack depth 40 mm.
- Stage 3: Crack width 120 mm, crack depth 60 mm.

It should be mentioned to the reader that the curved crack surface induces an incomplete severance at certain elements, owing to the partial intersection of the crack surface with the element. Consequently, a pixelated crack shape is formed along the perimeter of the crack surface, which can be seen in the figures in the following chapters.

5.5 Post-processing

The Python scripts were extended with a function responsible for post-processing to obtain the necessary results from the models. The fictive tensile force $F_{t,90}$ is calculated, and the maximum tensile stress perp. to the grain $\sigma_{y,\,max}$ along the cross-sectional width is located. The fictive tensile force gives a good indication of the effectiveness of the reinforcements in reducing the tensile stresses perp. to the grain. Furthermore, some additional data for creating different figures were extracted from the model.

5.5.1 Fictive tensile force

The first step of the function is determining where the tensile stresses perp. to the grain reach their maximum. This is done by creating a path along the perimeter of the hole. The maximum of the tensile stresses perp. to the grain is located along this path. The coordinates of the point are saved and used to create a horizontal path at each z-position where element nodes are present. This horizontal path lasts $2h_h$ and extends away from the hole. Along this path, the stresses perp. to the grain are integrated with the composite trapezoidal rule until they reach a value of zero. The result is then multiplied by the width of an element if it is located between two elements and half the width if the path is located at the edges of the cross-section. Finally, the values obtained along each path are added to get the total fictive tensile force. This value is the final value of the fictive tensile force when the entire cross-section is modelled (lay-up 3), or it is multiplied by two when only half of the cross-section is modelled (the other three cases). The results of this calculation are saved to a text file. A schematic representation of this procedure is shown in Figure 5-9.

5.5.2 Maximum tensile stress along the width

The maximum tensile stress perp. to the grain $\sigma_{y,\,max}$ along the cross-sectional width is another important result obtained by the numerical models. A single path is created along the width of the beam based on the coordinates of the location of the maximum tensile stress along the perimeter of the hole. The data along this path is saved in a NumPy array. Finally, the maximum value of the tensile stresses perp. to the grain is located and saved to a text file. Figure 5-9 also shows this procedure.

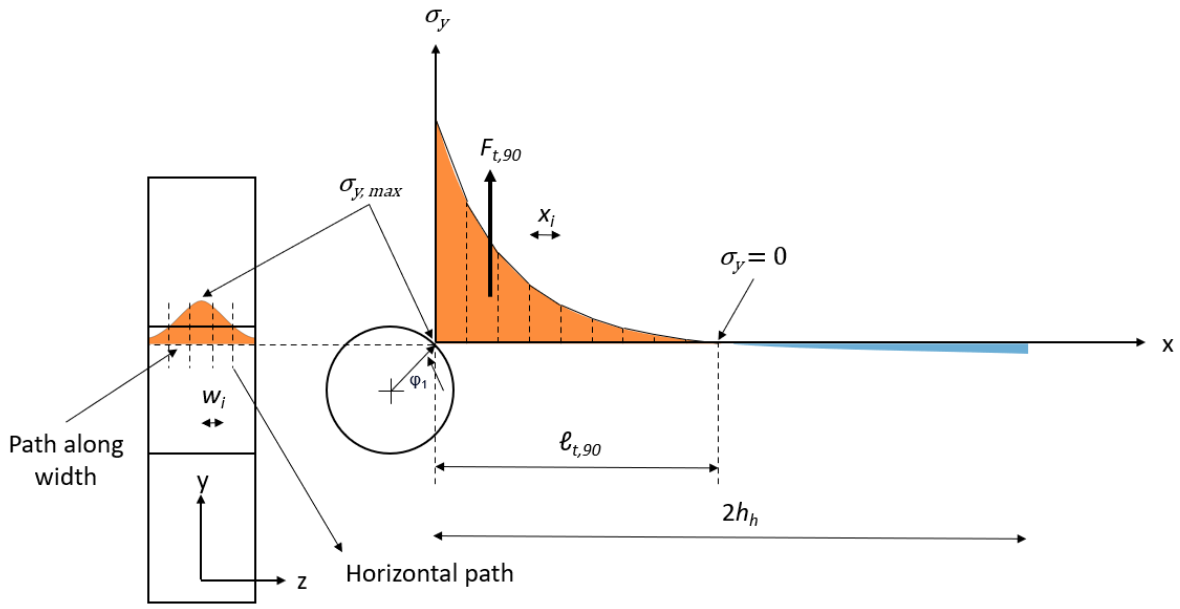

Figure 5-9: *Schematic representation of the fictive tensile force $F_{t,90}$ calculation and obtaining the maximum tensile stress perp. to the grain along the cross-sectional width $\sigma_{y,max}$.*

6

UNREINFORCED HOLES

It is generally known that holes reduce the load-bearing capacity of a glulam beam considerably. The introduction of the hole leads to tensile stresses perp. to the grain and increased shear stresses. These stresses can initiate cracks leading to a sudden brittle failure.

This chapter evaluates the influence of the cylindrical anisotropy of wood on the stresses in the vicinity of a hole. The tensile stresses perp. to the grain, shear stresses and fictive tensile force are regarded along a horizontal plane where crack initiation is most likely to occur. The three cylindrical anisotropic cases are compared to the orthotropic reference case.

6.1 Stress distribution

This section will present the stress distribution for the configuration discussed in section 5.1 with a circular hole with a diameter of 0.3*h*. The orthotropic and cylindrical anisotropic cases will be compared for the upper right quadrant of the hole, as cracks are expected to initiate here first. The results were processed after running the scripts for the respective unreinforced models. First, the stresses perp. to the grain along the periphery of the hole are discussed.

6.1.1 Tensile stresses perp. to the grain

Figure 6-1 illustrates the stresses perp. to the grain σ_y along the perimeter of the hole. The positive values indicate tension, and the negative values indicate compression. Section 2.1.1 revealed that for holes arranged along the neutral axis of the beam, the maximum tensile stress occurs at an angle of approximately 45°. This angle holds for the orthotropic case; however, this angle is slightly lower for the cylindrical anisotropic cases, with a maximum of around 30°. The difference between the angles is less pronounced at the lower left quadrant of the hole, where the stress peaks seem to be located at the interface of two adjacent laminations, as indicated by the small jumps of the tensile stresses.

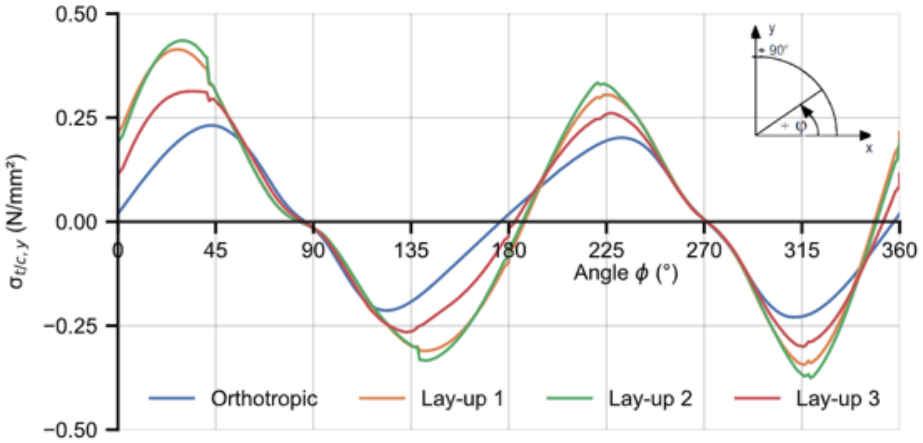

Figure 6-1: *The stresses perp. to the grain along the periphery of the hole.*

Figure 6-2 depicts the tensile stresses perp. to the grain along the width of the cross-section at the height of the location of the maximum tensile stress for the four cases. For the three cylindrical anisotropic cases, an inhomogeneous stress distribution is found along the width, with pronounced stress peaks near the middle of the cross-sectional width, similar to what was reported for a glulam cross-section subjected to uniaxial tensile stress [10]. In the orthotropic case, however, the stresses stay nearly constant along the width. Lay-up 2, with a jumping pith distance *d*, has the most prominent stress peak, with a value of 1,9 times greater than the orthotropic reference case. The stress peak in Lay-up 1 is slightly lower (1,8). The stress peak is a factor of 1,5 higher compared to the orthotropic reference casein case of lay-up 3, with a periodically varying eccentricity *e*. The peak occurs at an offset similar to the eccentricity of the pith from the cross-sectional mid-width.

An eccentricity of the pith positively influences the magnitude of the tensile stress peak. The exact magnitudes of the stress peaks are shown in Table 6-1. These results hold for the middle of the cross-section. However, significantly lower values are observed when one looks at the edges of the cross-section ($z = \pm 60$ mm). There, significantly lower values are observed for the cylindrical anisotropic cases compared to the orthotropic reference case.

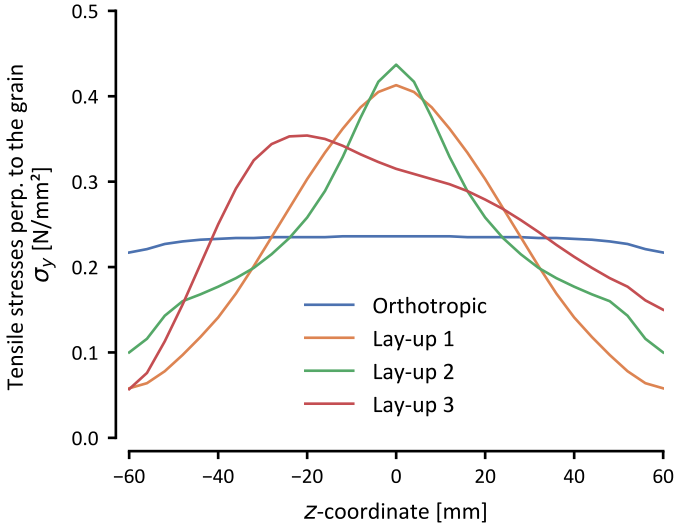

Figure 6-2: *Tensile stresses perp. to the grain along the width at the location where the tensile stresses reach their maximum along the periphery of the hole.*

Table 6-1: *Magnitude of the tensile stress peaks $\sigma_{y,\,max}$.*

	Orthotropic	Lay-up 1	Lay-up 2	Lay-up 3
	(N/mm²)			
$\sigma_{y,\,max}$	0,236	0,413	0,437	0,354

Figure 6-3 shows the tensile stresses along a horizontal path beginning at the edge where the tensile stresses perp. to the grain reach its maximum. Again, the four cases are shown. The orthotropic case represents a path at z = 0 mm (mid-width), while the three cylindrical anisotropic cases are plotted over a path at z = 0 mm and at z = ±60 mm (outer edges). Tensile stresses along the path at mid-width for lay-ups 1 and 2 remain higher than for the orthotropic reference case, requiring a somewhat longer distance to achieve a value of zero. The tensile stresses for lay-up 3 are slightly above the orthotropic case since they are plotted at mid-width, and as discussed, the stress peaks occur at a distance of 20 mm away from mid-width. The paths at the outer edges remain under the orthotropic case. The short distance before reaching a value of zero is noteworthy. This distance is roughly half the distance of the orthotropic reference case at the outer edges of the glulam.

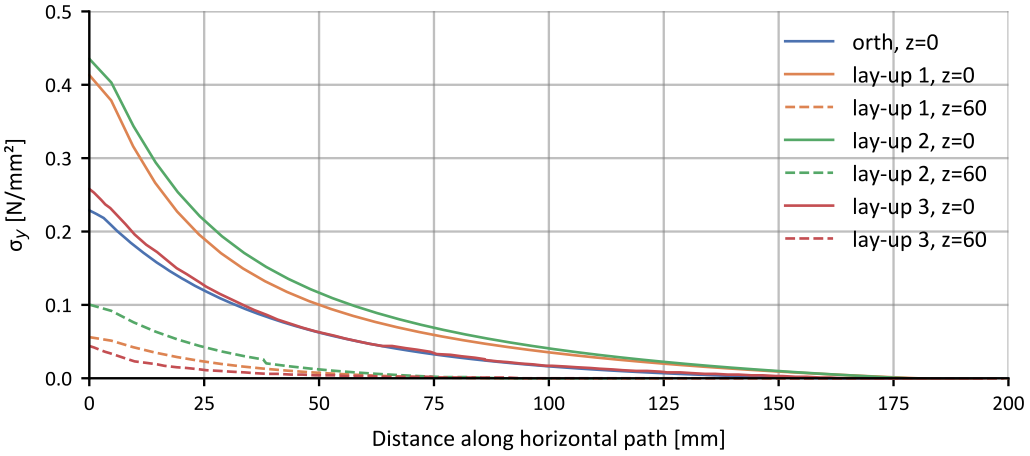

Figure 6-3: *Tensile stresses perp. to the grain along a horizontal path at z=0 and z=60.*

Figure 6-4 presents the tensile stresses perp. to the grain along a horizontal plane (crack plane 1) where the tensile stresses reach their maximum. As expected, the tensile stresses perp. to the grain remains almost constant along the cross-sectional width for the orthotropic model. However, if the cylindrical anisotropy of wood is considered, the stress distribution deviates considerably from the orthotropic reference model. An inhomogeneous stress distribution is observed with pronounced stress peaks near mid-width. The figure shows that the tensile stresses are concentrated at the edge of the hole in the middle region of the cross-section and are remarkably lower at the outer edges. In contrast, the orthotropic reference model distributes tensile stresses more evenly.

As explained above, the concentration of the stresses is responsible for the observed behaviour in the experimental tests. In all tested specimens, cracks initiated near the mid-width of the cross-section, highlighting the need to reduce this prominent stress peak. An internal reinforcement placed in the middle of the cross-sectional width seems to be the most suitable choice. By doing so, the reinforcement is strategically positioned at the location where the majority of tensile stresses perp. to the grain concentrate. However, the influence of reinforcements will be discussed in the next chapter.

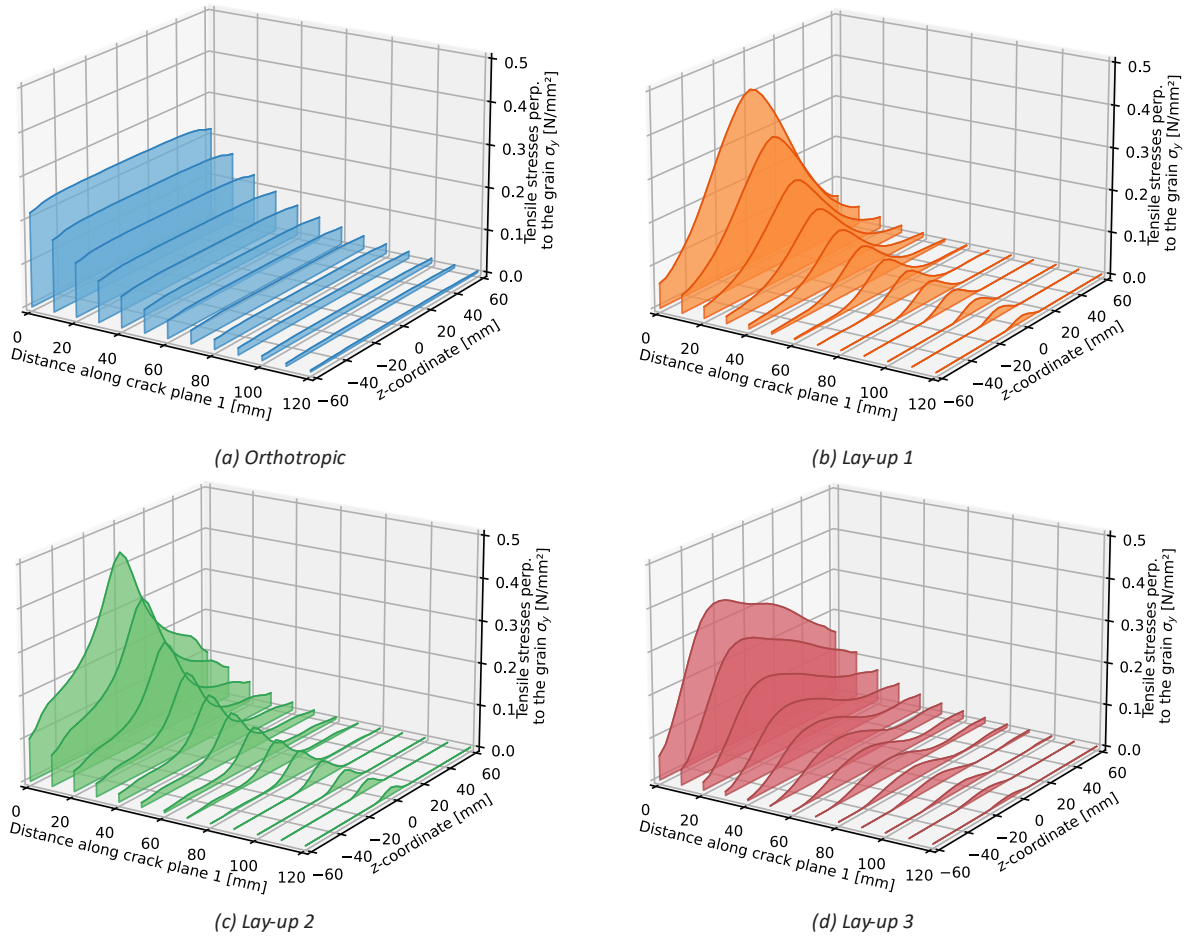

(a) Orthotropic

(b) Lay-up 1

(c) Lay-up 2

(d) Lay-up 3

Figure 6-4: *The tensile stresses perp. to the grain along crack plane 1 at the same height as the maximum tensile stress at the periphery of the hole for the unreinforced situation.*

The concept of the fictive tensile force $F_{t,90}$ was introduced in section 2.3. This force is an important concept in the design of holes since it determines whether the glulam has enough resistance against this force or if reinforcements must be applied to ensure structural integrity. The magnitude of the fictive tensile force is equal to the volume of the tensile stresses perp. to the grain along crack plane 1, as is depicted in Figure 6-4. It was discussed that slightly higher values were obtained for the fictive tensile force when the cylindrical anisotropy of wood is considered [11]. However, that study was performed with different constitutive properties. Since it is such an essential concept, the influence of the cylindrical anisotropy of wood for this specific configuration is investigated.

Table 6-2 presents the fictive tensile force for the four cases, following the procedure outlined in section 5.5.1. The fictive tensile force, according to the future version of Eurocode 5 [34], is added for reference. A detailed calculation of this force is added in 9.2Appendix A. The results indicate that the cylindrical anisotropy of wood has a positive effect on the magnitude of the fictive tensile force, resulting in forces that are approximately 15% to 30% lower compared to the orthotropic case and 27% to 39% lower compared to the second generation of Eurocode 5. Furthermore, it is observed that the value of the force obtained using [34] is greater than the values for the four cases but closer to the orthotropic case. This observation aligns with the expectations, as the formulas described in [34] are based on the assumption of orthotropic material behaviour.

Table 6-2: *Fictive tensile force for the orthotropic and three cylindrical anisotropic cases.*

	Orthotropic	Lay-up 1	Lay-up 2	Lay-up 3	EC 5 [34]
			(N)		
$F_{t,90}$	996	699	735	836	1.152

6.1.2 Shear stresses

Section 2.1.2 discussed the importance of the shear stresses on crack propagation. Figure 6-5 represents the shear stresses along crack plane 1 for the four considered cases. Similar to the tensile stresses perp. to the grain, an inhomogeneous distribution of the shear stresses is observed at the periphery of the hole. However, contrary to the tensile stresses, this inhomogeneous stress distribution becomes less prominent at a certain distance from the periphery of the hole. Noteworthy is that the magnitude of the shear stress peaks for the cylindrical anisotropic cases is relatively similar to the orthotropic reference case. At the same time, they are significantly lower at the outer edges. The shear stresses along a horizontal path at mid-width (z = 0) show that the shear stresses for the cylindrical anisotropic cases remain somewhat constant. In contrast, the shear stresses increase if one looks at a horizontal path at the outer edges (z = ±60). The opposite can be said for the orthotropic reference case, where the shear stresses are more significant at the face of the hole and decrease over a distance away from the hole. The findings from these investigations suggest that the cylindrical anisotropy of wood provides a more advantageous representation of the shear stresses compared to the conventional orthotropic model commonly applied.

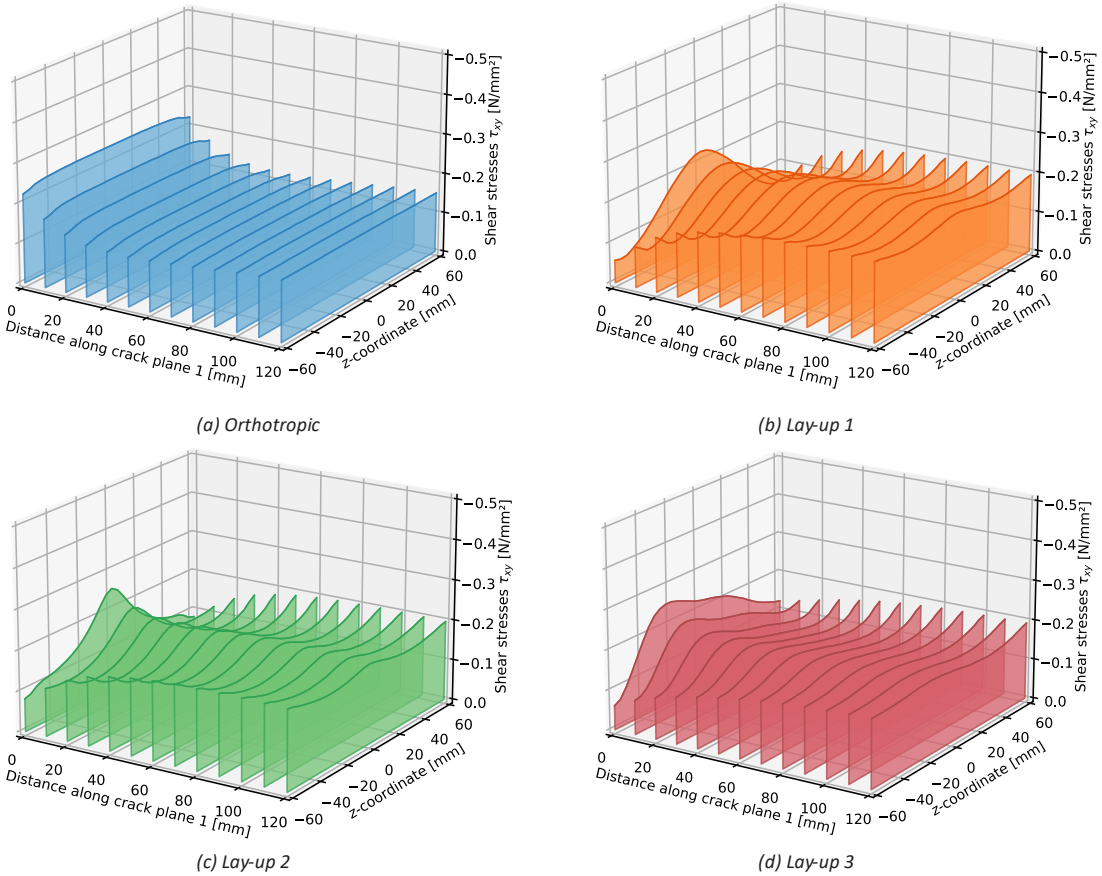

(a) Orthotropic *(b) Lay-up 1*

(c) Lay-up 2 *(d) Lay-up 3*

Figure 6-5: *The shear stresses along crack plane 1 at the same height as the maximum tensile stress at the periphery of the hole for the unreinforced situation.*

The literature showed that increasing the width of the cross-section results in more prominent stress peaks when a cross-section is loaded by uniaxial tensile stress [10]. This observation raises the question of whether the same behaviour can be observed in a beam with a hole loaded in a combined shear and moment action. To investigate this, the width of the beam was varied within the range of 80 to 240 mm, with increments of 40 mm. The selected range complies with the practical dimensions commonly encountered in practice.

Figure 6-6 presents the results of this parameter study. The ratio between the orthotropic and cylindrical anisotropic cases for the maximum tensile stress perp. to the grain, and the fictive tensile force are plotted along the y-axis. Remarkably, it can be observed that for all three considered lay-ups, an increase in width does not result in a more significant stress peak or an increase in the magnitude of the fictive tensile force. These findings indicate that contrary to the behaviour observed in uniaxial tensile stress situations, the width of the beam does not have a significant impact on stress concentration or the fictive tensile force in the case of a beam with a hole subjected to combined shear and moment loading.

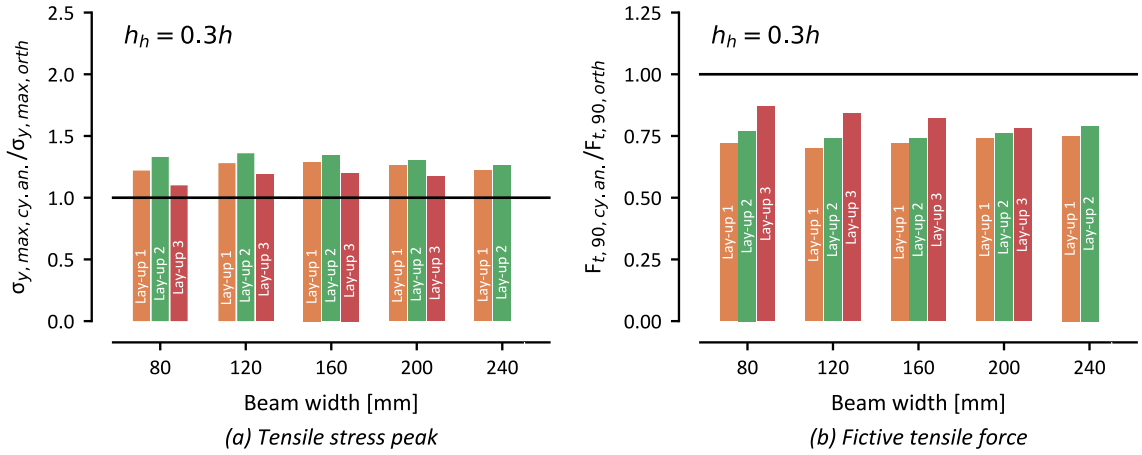

Figure 6-6: *Influence of the beam width on the maximum tensile stress perp. to the grain $\sigma_{y,max}$ and the fictive tensile force $F_{t,90}$.*

6.2 Discussion

This chapter investigated the stress distribution of an unreinforced circular hole with a relative hole height of 0,3*h* placed along the neutral axis of the beam. Four cases were studied: an orthotropic reference model and three cylindrical anisotropic models with three distinct lay-ups with different systematic patterns of the pith orientations.

It was found that the three cylindrical anisotropic models lead to an inhomogeneous stress distribution along the width of the cross-section with pronounced stress peaks near the mid-width. Specifically, the tensile stresses perp. to the grain are negatively affected and reach values of 1,5 to 1,9 times greater than those obtained from an orthotropic model. Contrarily, the stresses at the outer edges of the cross-section are notably lower. A similar pattern was observed for the shear stresses, although the peak experienced less significant differences in magnitude compared to the orthotropic model. Additionally, it was quantified that the cylindrical anisotropy positively influences the fictive tensile force, resulting in values of 15% to 30% lower compared to the orthotropic case. It became evident that a periodically varying eccentricity has a positive effect. Furthermore, it was observed that an increasing beam width does not increase the stress peak, contrary to what was observed for a glulam cross-section subjected to uniaxial tension [10].

Based on these observations, two statements can be made. From a design standard point of view, the cylindrical anisotropy of wood does not necessarily need to be considered since lower values of the

fictive tensile force are obtained, meaning that the orthotropic model is on the conservative side. On the other hand, the cylindrical anisotropy of wood is a reasonable explanation for the observed crack initiation near the mid-width of the cross-section and thus cannot be neglected. The majority of the tensile stresses perp. to the grain are situated near the mid-width of the cross-section close to the periphery of the hole. Therefore, considering the cylindrical anisotropy of wood is inevitable if one wants to prevent crack initiation and increase the load-bearing capacity of a glulam beam with a hole.

The next step is to investigate the possibilities of reducing these pronounced stress peaks by employing reinforcements. However, already some statements can be made regarding the choice for the type of reinforcement. The analysis of the unreinforced holes has revealed that a substantial portion of the tensile stresses perp. to the grain is concentrated near the mid-width of the cross-section close to the face of the hole. Consequently, placing a rod at this location is expected to be highly effective in reducing these stress concentrations. On the other hand, employing panels glued to the edges of the beam seems less efficient since they are situated further away from most of the stress concentration. These initial findings indicate that a rod placed near the mid-width of the cross-section would likely yield more favourable reductions than glued-on panels. Therefore, a comprehensive investigation and analysis will be conducted in the next chapter to investigate whether these statements are true.

7

REINFORCED HOLES

The previous chapter showed that the cylindrical anisotropy of wood leads to an inhomogeneous stress distribution along the cross-sectional width with pronounced stress peaks near mid-width up to two times the maximum of the orthotropic reference case. These pronounced stress peaks near the mid-width reasonably explain the behaviour observed in the tests where the cracks always appeared near the middle of the cross-section. The shear stresses showed an inhomogeneous distribution as well. However, the peaks were similar to the maximum of the orthotropic reference case.

This chapter examines the influences of internal and external reinforcements on the stress distribution in the vicinity of a circular hole. The reinforcements aim to increase the tensile resistance locally at the locations where cracks are expected to occur and thus increase the load-bearing capacity of a glulam beam with a hole. Three distinct scenarios are investigated: The first two regards internal reinforcements. A single rod and the applications of two rods in a single row are studied. The last scenario studies the effect of a plywood panel made from birch. Additionally, the impact of these reinforcements on the stress distribution at various stages of crack development is explored. The discussion begins with an examination of internal reinforcements, followed by an evaluation of external reinforcements.

7.1 Internal reinforcements

7.1.1 Stress distribution

After submitting the jobs for the respective models, the results were processed. First, the tensile stresses perp. to the grain along the width of the cross-section at the height of the location of the maximum tensile stress are discussed. These tensile stresses along the width for both scenarios are presented in Figure 7-1 for the four considered cases. The solid line represents the unreinforced situation and the reinforced situation by the dashed line.

First, the scenario where a single rod is installed will be discussed. The stiffness of the rod is higher in relation to the glulam, mitigating the stresses in the glulam to the rod. A pronounced reduction of the stress peak at the mid-width of the cross-section is observed for all four cases. However, this reduction

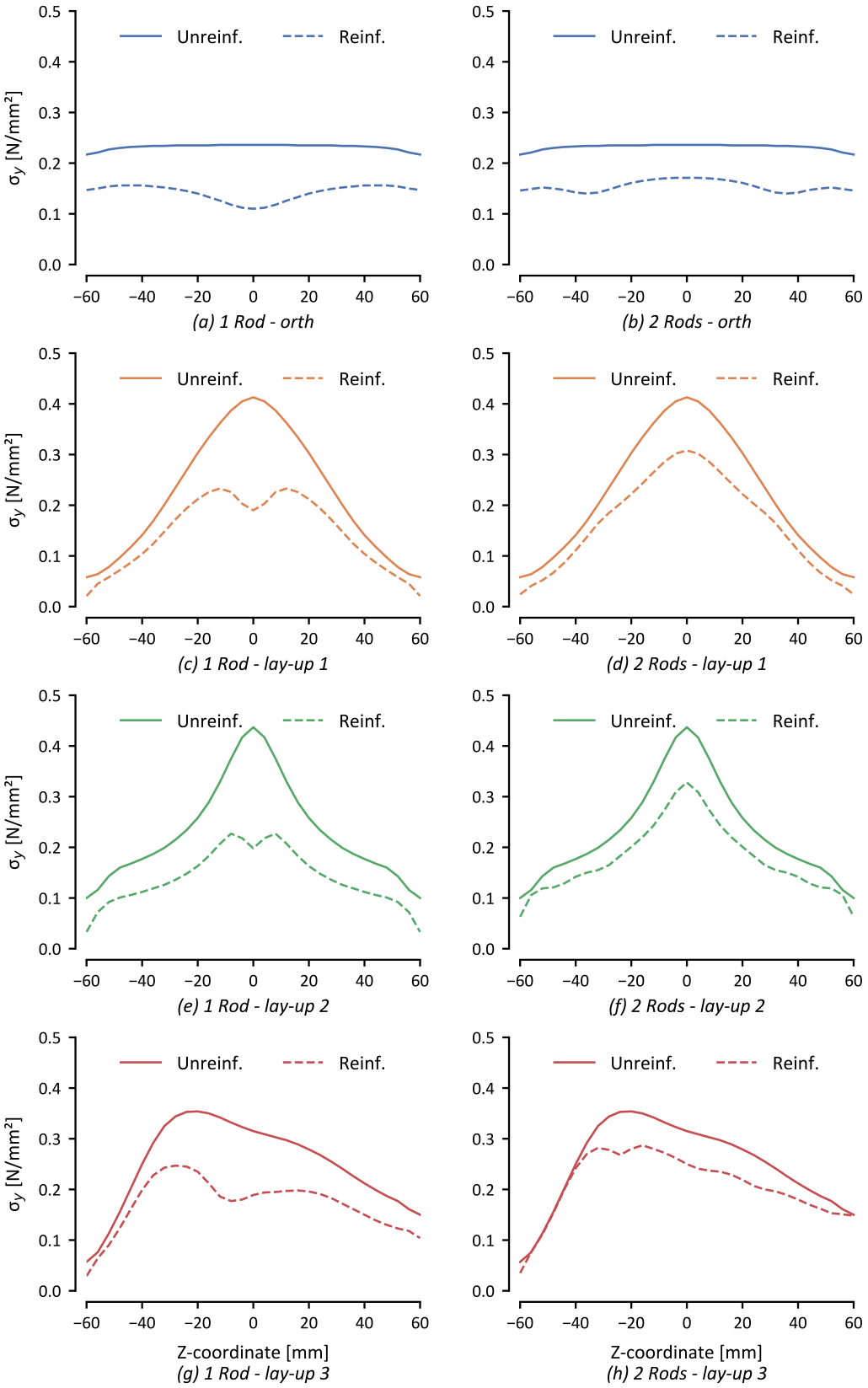

Figure 7-1: *Tensile stresses perp. to the grain along the width for the unreinforced and reinforced situations.*

differs slightly between the four cases. A more pronounced reduction is obtained for lay-ups 1 and 2, with reductions of 44% and 46%, respectively. The reductions for lay-up 3 and the orthotropic case are

less pronounced and are 30% and 34%, respectively. This difference arises from the placement of the rod not being exactly at the maximum tensile stress along the width, as is the case for lay-ups 1 and 2. Thus, a periodically varying eccentricity negatively affects the reduction of the stress peak, and the orthotropic case underestimates the reduction if the piths are perfectly aligned. However, it is questionable if this ever occurs in practice.

Next, the scenario with two rods placed in a single row along the width is discussed. A pronounced reduction is observed, however less pronounced as for the scenario where 1 rod is installed, especially for the cylindrical anisotropic models. The difference between the reductions for lay-ups 1 and 2 with a centrically placed pith and lay-up 3 with a periodically varying eccentricity of the pith converges, thus meaning that a periodically varying eccentricity is less detrimental in the case of two rods. However, it appears that the orthotropic model slightly overestimates the reduction for the scenario with two rods.

Table 7-1 presents the maximum tensile stress along the cross-section width for the unreinforced and reinforced situations for the four considered cases. The reductions achieved by the reinforcements are presented as well.

Table 7-1: *Reduction of the stress peak $\sigma_{y,\,max}$ along the width at the face of the hole.*

	Orthotropic		Lay-up 1		Lay-up 2		Lay-up 3	
	(N/mm^2)							
$\sigma_{y,\,max,\,unreinf.}$	0,236		0,413		0,437		0,345	
$\sigma_{y,\,max,\,reinf.}$	1 rod	2 rods	1 rod	2 rods	1 rod	2 rods	1 rod	2 rods
	0,156	0,171	0,233	0,308	0,227	0,328	0,247	0,287
Reduction	33,9%	27,5%	43,6%	25,4%	48,1%	24,9%	30,2%	18,9%

Figure 7-2 presents the influence of a single rod on the stresses perp. to the grain along crack plane 1. The red area indicates the stresses perp. to the grain in the reinforced state, while the yellow area represents the reduction of the stresses obtained by the rod. It becomes evident that there is a pronounced reduction of the maximum stresses perp. to the grain at the edge of the hole for the three cylindrical anisotropic cases. The reduction becomes even more pronounced in the region preceding the rod, as is to be expected. Almost no tensile stresses remain for this region. Thus, the rod has taken all the tensile stresses present in this region which were there prior to installing the rods. Overall, the reduction is mainly concentrated near the middle of the cross-section. The tensile stresses are also significantly reduced for the orthotropic case. However, contrary to the three cylindrical anisotropic cases, some tensile stresses remain in the region preceding the rod. Moreover, the position of the rod can easily be derived from the figure by the dips of the tensile stresses along the middle of the cross-section ($z = 0$).

The tensile stresses perp. to the grain along crack plane 1 for the scenario where two rods are present, are shown in Figure 7-3. A rather significant reduction of the tensile stresses is observed. However, as one might have noticed, the reduction is less pronounced when only one rod is employed. The three cylindrical anisotropic cases showed a more significant reduction than the orthotropic case for one rod. The opposite is observed for the scenario with two rods where the orthotropic case achieves a more significant reduction. Another noteworthy difference is that some tensile stresses remain in the region preceding the rod. This was not the case for the three cylindrical anisotropic cases when one rod was present.

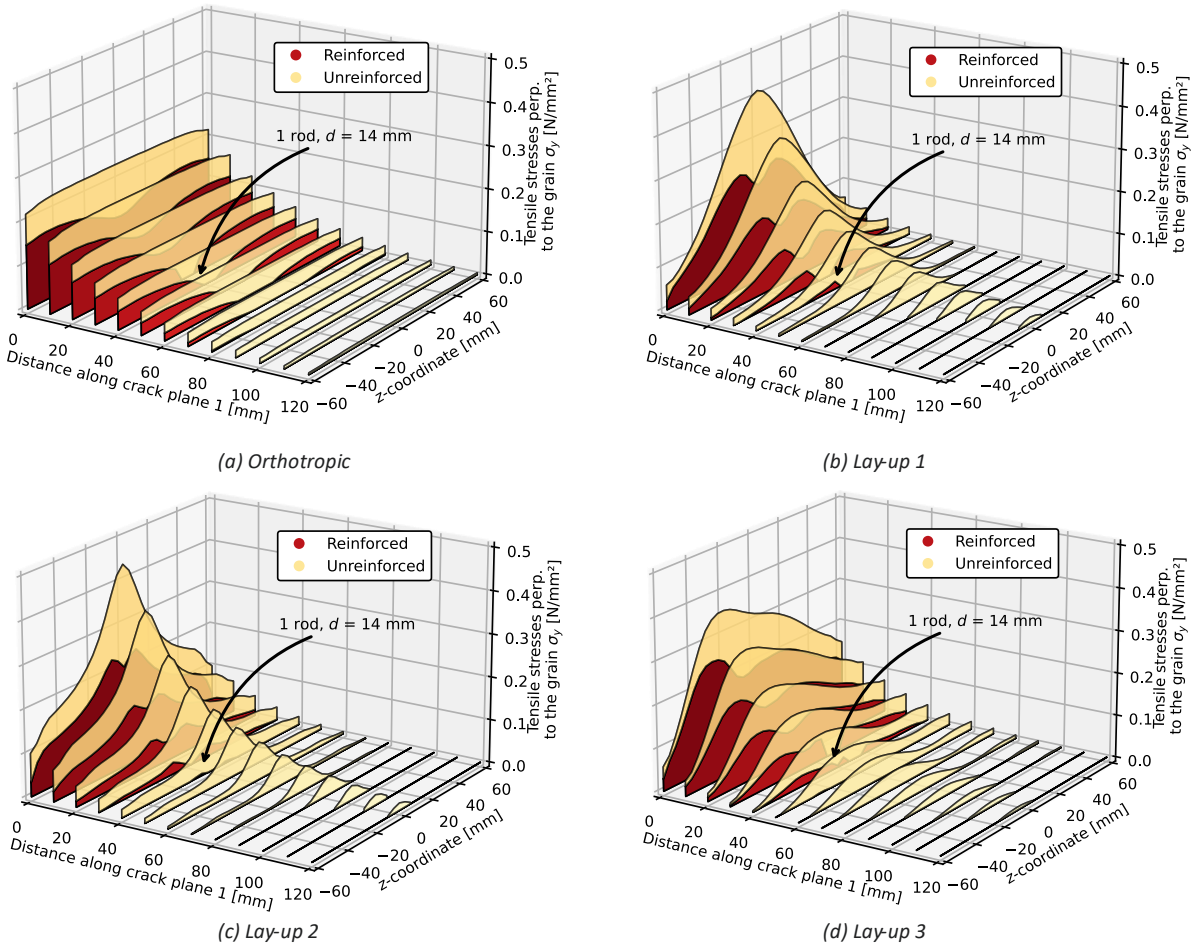

Figure 7-2: *The tensile stresses perp. to the grain along crack plane 1 at the same height as the maximum tensile stress at the periphery of the hole for the unreinforced and reinforced situation when 1 rod with an inclination of 45° is installed.*

In section 2.3, the concept of the fictive tensile force was introduced. The reinforcements must be designed for the full tensile force. Thus, no contribution from the glulam must be considered according to the approach by the second generation of Eurocode 5 [34]. This assumption is equivalent to a fully cracked cross-section. However, the rods and the glulam share this fictive tensile force in the undamaged state. Table 7-2 provides the fictive tensile forces in the glulam along crack plane 1 for the unreinforced and reinforced situation. The reduction and, thus, the part taken by the rods is the difference between the unreinforced and reinforced situations.

A more significant reduction of the fictive tensile force is obtained when 1 rod is employed for the three cylindrical anisotropic cases. In contrast, the orthotropic model achieves similar reductions for both scenarios. The difference between the reductions of one and two rods is up to 23% for the cylindrical anisotropic cases. Furthermore, the reductions obtained for lay-ups 1 and 2 are more pronounced than for lay-up 3. Thus, the effectiveness of the rods seems to be influenced by the eccentricity of the pith.

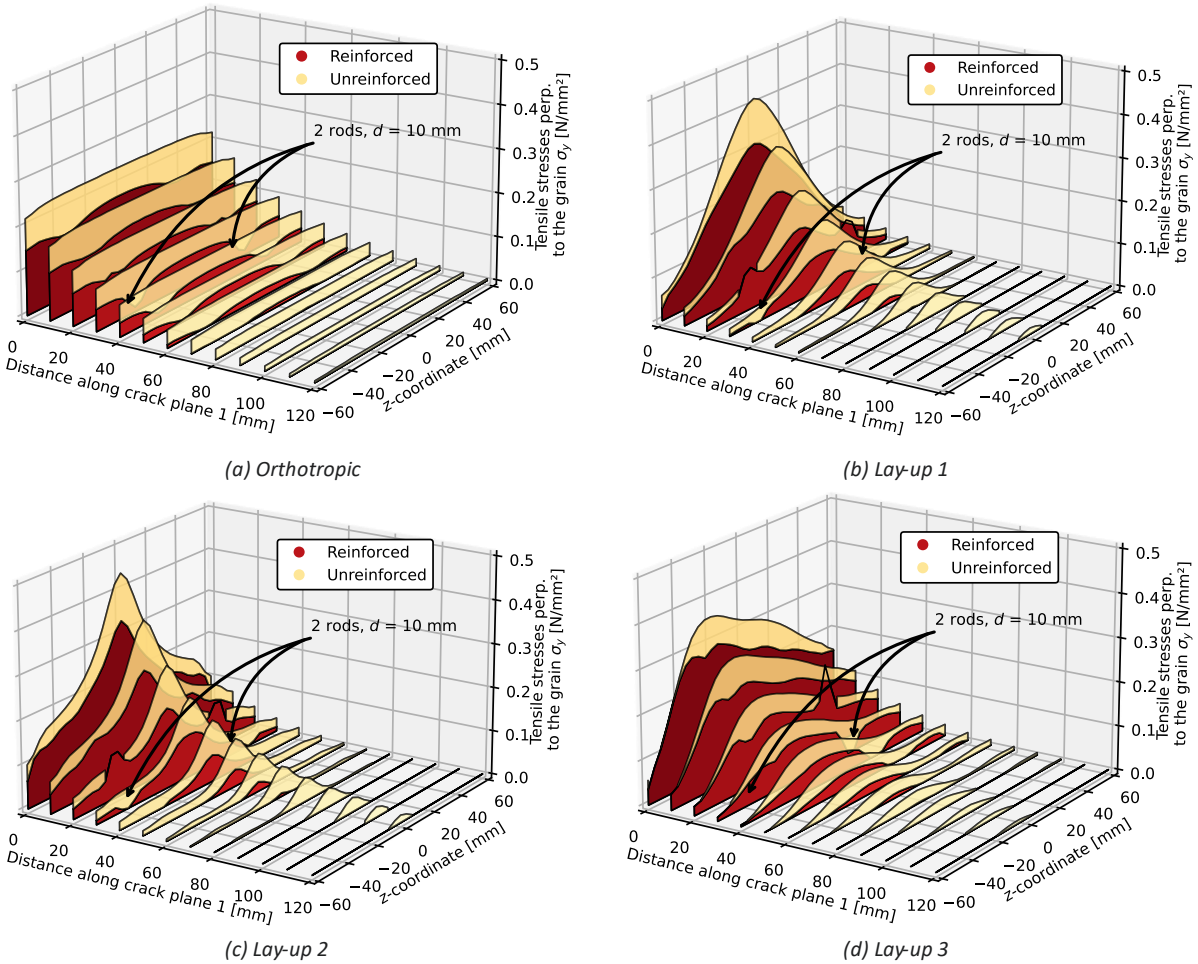

Figure 7-3: *The tensile stresses perp. to the grain along crack plane 1 at the same height as the maximum tensile stress at the periphery of the hole for the unreinforced and reinforced situation when 2 rods with an inclination of 45° are installed.*

Table 7-2: *Fictive tensile force $F_{t,90}$ in the glulam's unreinforced and reinforced state and the reduction obtained with the internal reinforcements*

	Orthotropic		Lay-up 1		Lay-up 2		Lay-up 3	
	(N)							
$F_{t,90,\ unreinf.}$	996		699		735		836	
$F_{t,90,\ reinf.}$	1 rod	2 rods	1 rod	2 rods	1 rod	2 rods	1 rod	2 rods
	451	453	256	377	230	397	358	546
Reduction	54,7%	54,5%	63,4%	46,1%	68,7%	46%	57,2%	34,7%

Figure 7-4 shows the effect of a single rod on the shear stresses along crack plane 1. The shear stresses demonstrate a similar reduction as the tensile stresses. A reduction of 36% is achieved for the orthotropic case, while a reduction of around 29% is obtained for the three cylindrical anisotropic cases. The shear stresses experience the most considerable reduction near the edge of the hole, where the stress pattern shows a more inhomogeneous distribution for the cylindrical anisotropic models.

The reduction, however, decreases as the plane moves a distance away from the hole. A somewhat evenly distributed reduction is observed for the orthotropic case. For all four cases, the position of the rod can be derived from the figure since the shear stresses show a noticeable dip at the location of the rod.

Figure 7-5 depicts the reduction of the shear stresses for the scenario where two rods are present. Again, the rods achieve a noteworthy reduction of the shear stresses. However, the reduction is less pronounced than when one rod is employed. The tensile stresses perp. to the grain exhibited similar behaviour. The reduction obtained by the two rods is 23% for the orthotropic case and 17% for the cylindrical anisotropic cases. Again, the orthotropic model slightly overestimates the reduction. This overestimation also becomes evident from the figure since a more pronounced reduction is noted at the edge of the hole for the orthotropic case. In contrast, lay-up 3 does not seem to experience a reduction at all at the face of the hole.

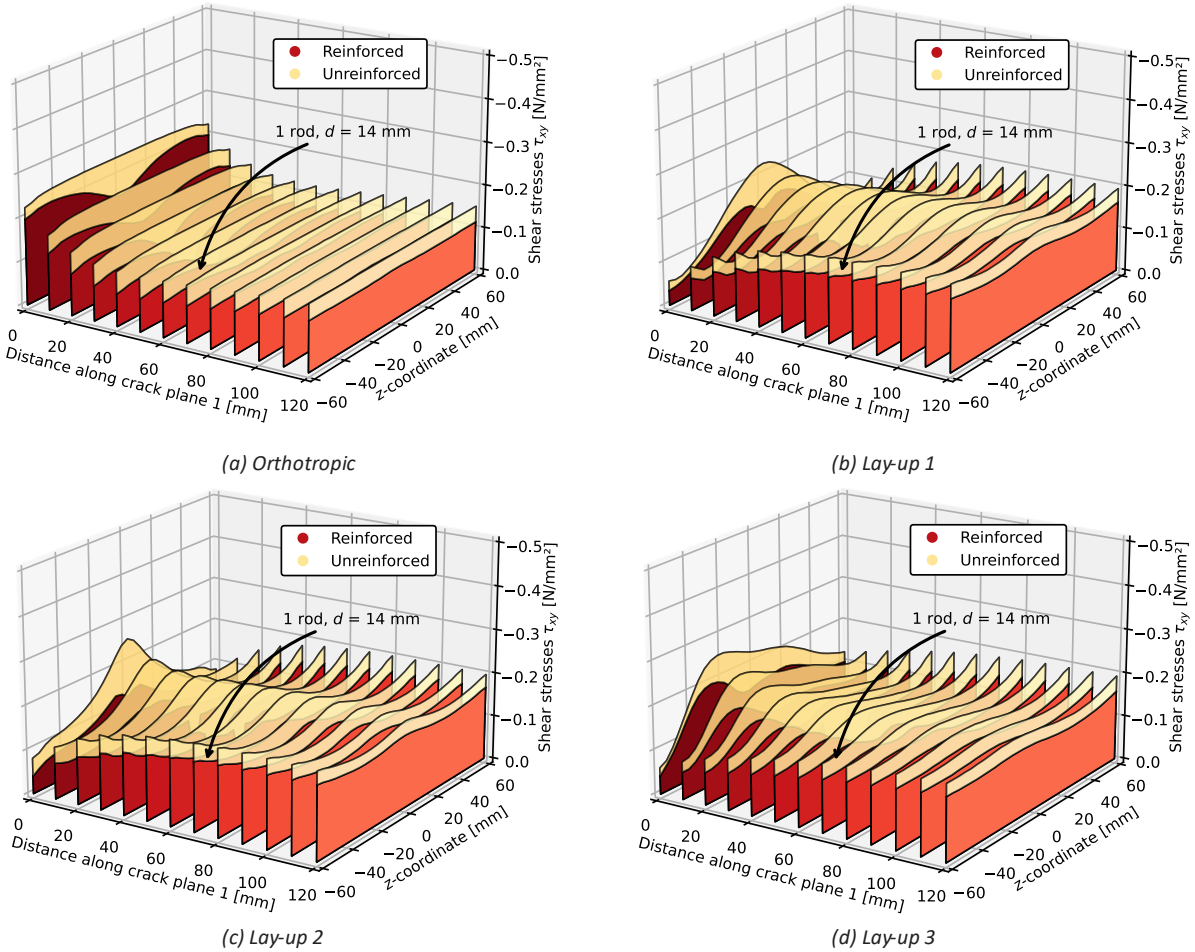

(a) Orthotropic *(b) Lay-up 1*

(c) Lay-up 2 *(d) Lay-up 3*

Figure 7-4: *The shear stresses along crack plane 1 at the same height as the maximum tensile stress at the periphery of the hole for the unreinforced and reinforced situation when 1 rod with an inclination of 45 degrees is installed.*

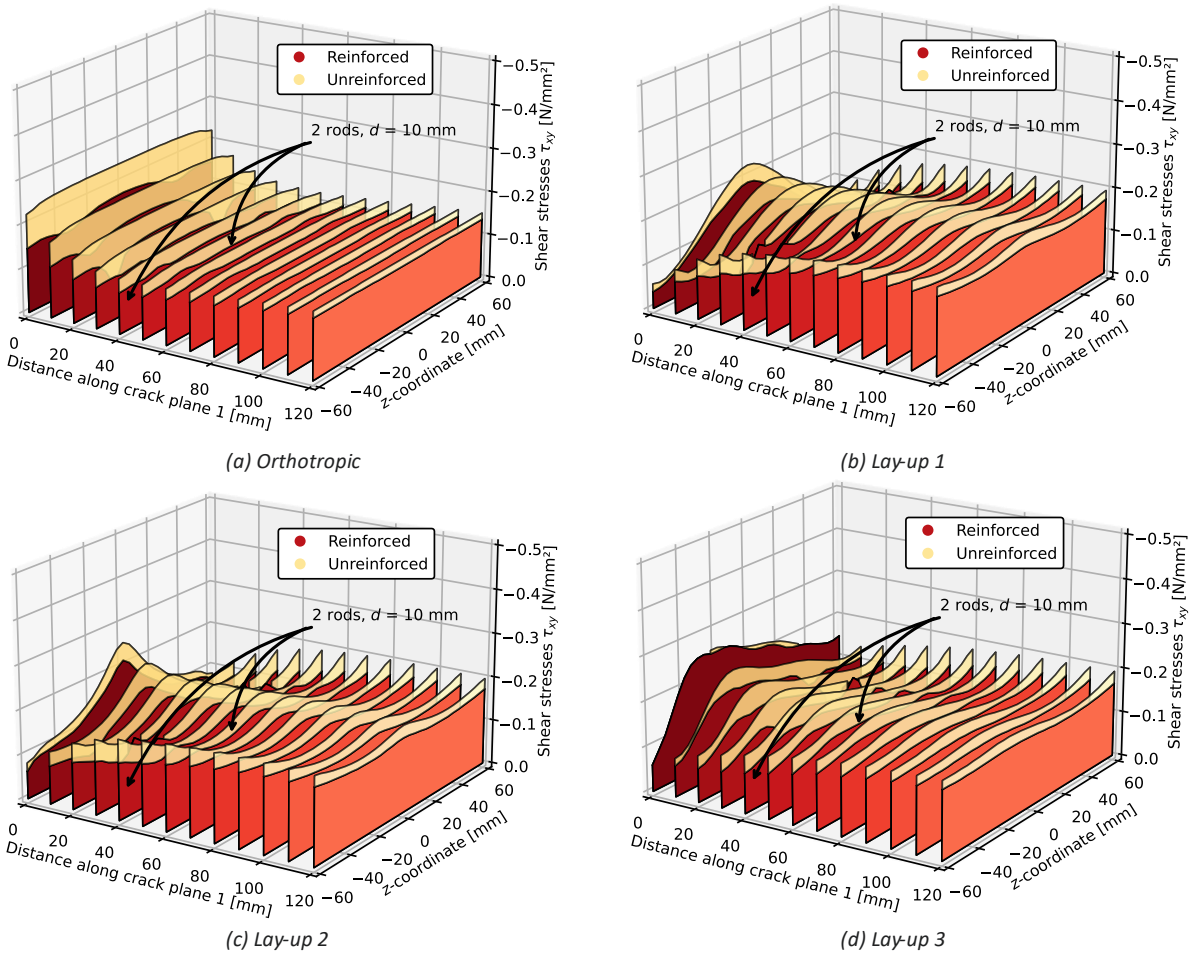

Figure 7-5: *The shear stresses along crack plane 1 at the same height as the maximum tensile stress at the periphery of the hole for the unreinforced and reinforced situation when 2 rods with an inclination of 45 degrees are installed.*

7.1.2 Parameter study

A parameter study has been performed to study the effect of an increasing diameter on reducing the maximum tensile stress perp. to the grain and the fictive tensile force. However, parametrizing the internal reinforced cylindrical anisotropic model proved very complex and time-consuming. As a result, manually creating individual models for each configuration in the parameter study was deemed impractical. Therefore, Young's modulus of the rod was scaled to an equivalent value corresponding to the specific rod configuration considered to overcome this problem. Therefore, only Young's modulus has to be adjusted for every model. The relation between Young's modulus of the reference rod and the considered rod is expressed in equation (7.1).

$$E_{eq} = \frac{A}{A_{ref}} E \tag{7.1}$$

In this equation, A is the area of the considered rod, and A_{ref} is the area of the reference rod. For the scenario where 1 rod is present, the area of the rod is equal to 153,9 mm^2. For the scenario where 2 rods are present, the area of the individual rods equals 78,5 mm^2. Furthermore, E is Young's modulus of steel. The results for rods with a diameter of 8 to 20 mm are shown in Table 7-3 for both scenarios.

Table 7-3: *Equivalent Young's modulus E_{eq} for the considered rods.*

Diameter (mm)	A (mm^2)	1 rod (N/mm^2)	2 rods (N/mm^2)
8	50,3	68.571	134.400
10	78,5	107.143	**210.000**
12	113,1	154.286	302.400
14	153,9	**210.000**	411.600
16	201,1	274.286	537.600
18	254,5	347.143	680.400
20	314,2	428.571	840.000

This approach should give an insight into the effect of increasing rod diameter on reducing the stress peak and fictive tensile force. However, there are some drawbacks to this approach. Namely, the distance between the periphery of the hole and the centre of the rod remains unchanged instead of depending on the requirement that this distance should be 2.5*d*. Furthermore, the discontinuity in the glulam due to the presence of the rod is also not considered accurately.

Figure 7-6 presents the results of the parameter study for the first scenario where only one rod is installed. It can be observed that the reduction gradually becomes less when the diameter increases for all four cases. The figure clearly shows that the reduction of the fictive tensile force is more pronounced than the reduction of the stress peak since the reductions are generally 20% higher. This reduction aligns with the fact that almost no tensile stresses remain once the crack plane precedes the rod. Furthermore, an increasing diameter does not resolve the observed lower reduction for lay-up 3 with a periodically varying eccentricity.

A similar parameter study was performed for scenario two with the two rods. Figure 7-7 depicts the results of this parameter study. In contrast to scenario 1, the range of the rods is decreased since the minimum spacing along the width of the cross-section should be met. Thus, only a rod with a diameter of 12 mm is allowed. The increase of the diameter from 8 mm to 12 mm results in a doubling of the reduction. Furthermore, the figure clearly illustrates that the orthotropic case overestimates the reduction for both the maximum tensile stress and the fictive tensile force.

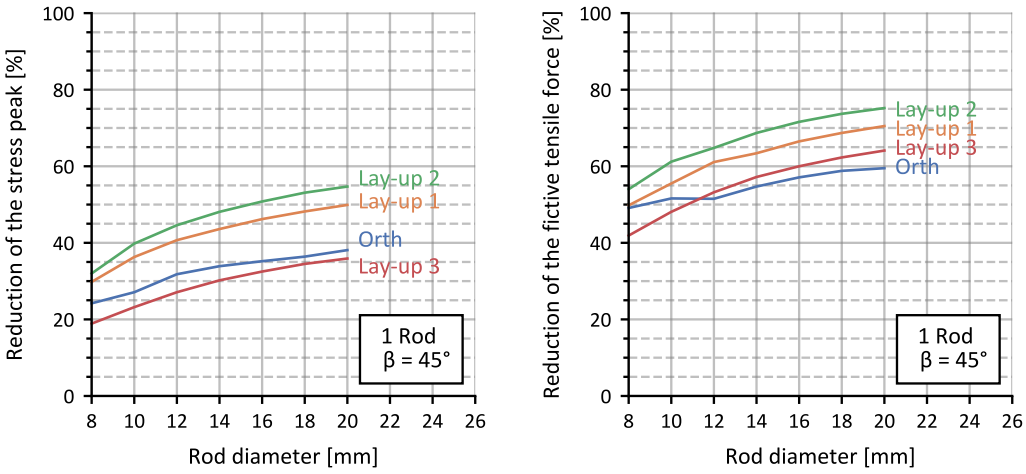

(a) Reduction stress peak *(b) Reduction fictive tensile force*

Figure 7-6: *Influence of the rod diameter on the reduction of the stress peak and fictive tensile force in the case of 1 rod.*

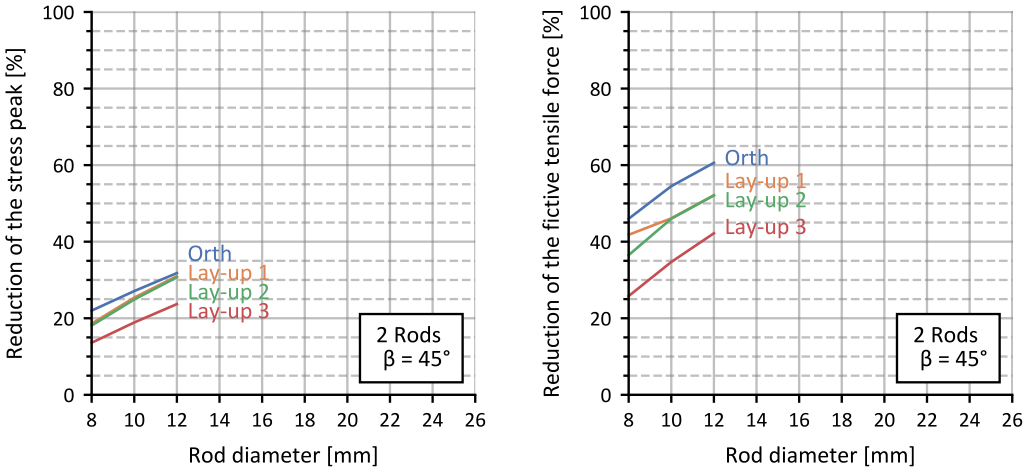

(a) Reduction stress peak *(b) Reduction fictive tensile force*

Figure 7-7: *Influence of the rod diameter on the reduction of the stress peak and fictive tensile force in the case of 2 rods.*

7.1.3 Discussion

This section discussed the effect of a rod on the reduction of the maximum tensile stress peak, the shear stresses, and the fictive tensile force for two scenarios: the first scenario considered a rod employed at the mid-width of the cross-section, while the second scenario considered two rods placed along the cross-sectional width. It was observed that the scenario with a single rod achieved the most pronounced reduction for the tensile stress peak, shear stresses and fictive tensile force for all four cases. However, the eccentricity of the pith strongly influences the effectiveness of the rods. Moreover, it appears that the orthotropic model underestimates the reductions.

A schematic representation of the region where most of the tensile stresses perp. to the grain are concentrated is illustrated in Figure 7-8. From this figure, it becomes evident that in the orthotropic case, the presence of either one or two rods does not have a significant impact, as both configurations are centred within the region containing the highest tensile stresses perp. to the grain. However, this changes when considering the cylindrical anisotropy of wood. In this case, the single rod is positioned

directly at the centre of these stresses, while the two rods are situated at the edges and thus not directly at the stress peak. Hence, this explains the observed differences between the orthotropic and the three cylindrical anisotropic cases.

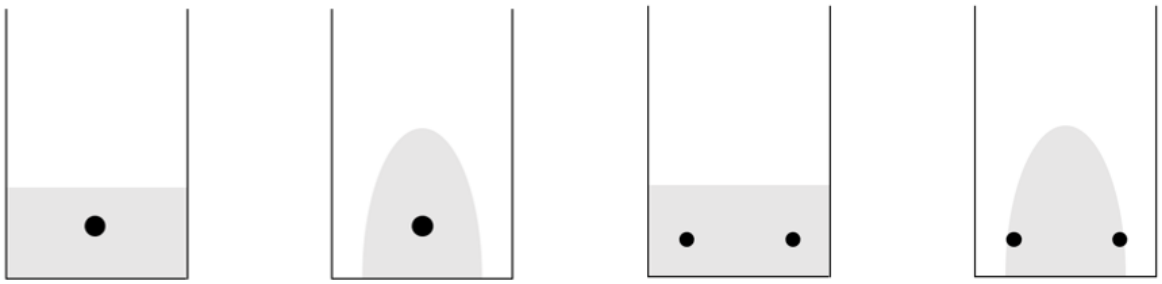

Figure 7-8: *Schematic representation of the positioning of the rods respective to the bulk of the tensile stresses perp. to the grain.*

Furthermore, it is important to note that shear stresses experience a notable reduction in both cases. From the literature, it became evident that a vertically placed rod does not contribute to reducing the shear stresses at all. However, placing the rods at an angle of 45° significantly increases their ability to reduce the shear stresses in the vicinity of the hole.

The evaluation of the damaged state using three distinct stationary cracks revealed that the presence of rods substantially mitigates the tensile stresses perp. to the grain within the remaining glulam area. The rods progressively take more of the fictive tensile force as the crack propagates. From these observations, it can be argued that the rods can halt the propagation of the crack once it has preceded the rod, as the rod already takes all the tensile stresses perp. to the grain in this region in the undamaged state.

7.2 External reinforcements

7.2.1 Stress distribution

The scripts for the external reinforced models were executed, and the results were processed. First, the tensile stresses perp. to the grain along the width of the cross-section at the height of the location of the maximum tensile stress are discussed. These tensile stresses along the width for both scenarios are presented in Figure 7-9 for the four considered cases.

The reduction of the tensile stresses perp. to the grain is situated near the mid-width of the cross-section for the three cylindrical anisotropic cases. Noteworthy is the increase of the tensile stresses perp. to the grain at the outer edges of the glulam. The plywood panels reduce the inhomogeneity observed along the width of the cross-section. Contrary to the cylindrical anisotropic models, the reductions are located near the edges of the cross-section, and the reduction achieved in the middle of the cross-section is less pronounced for the orthotropic case. This observation can be explained by the fact that the stresses in the orthotropic case are closer to the reinforcements than the cylindrical anisotropic models. However, this closer position does not seem to influence lay-up 3 with a periodically varying eccentricity of the pith. However, a somewhat more significant reduction was expected since the stress peak is closer to the panel than lay-ups 1 and 2.

The values of the tensile stress peaks for the unreinforced and reinforced situations are presented in Table 7-4. The reductions obtained by the plywood panels are also included. The table shows that the cylindrical anisotropic cases achieve a slightly more significant reduction than the orthotropic model. However, the difference between the three lay-ups is neglectable. Thus, a periodically varying eccentricity does not influence the effectiveness of the panels as was observed for the internal reinforcements.

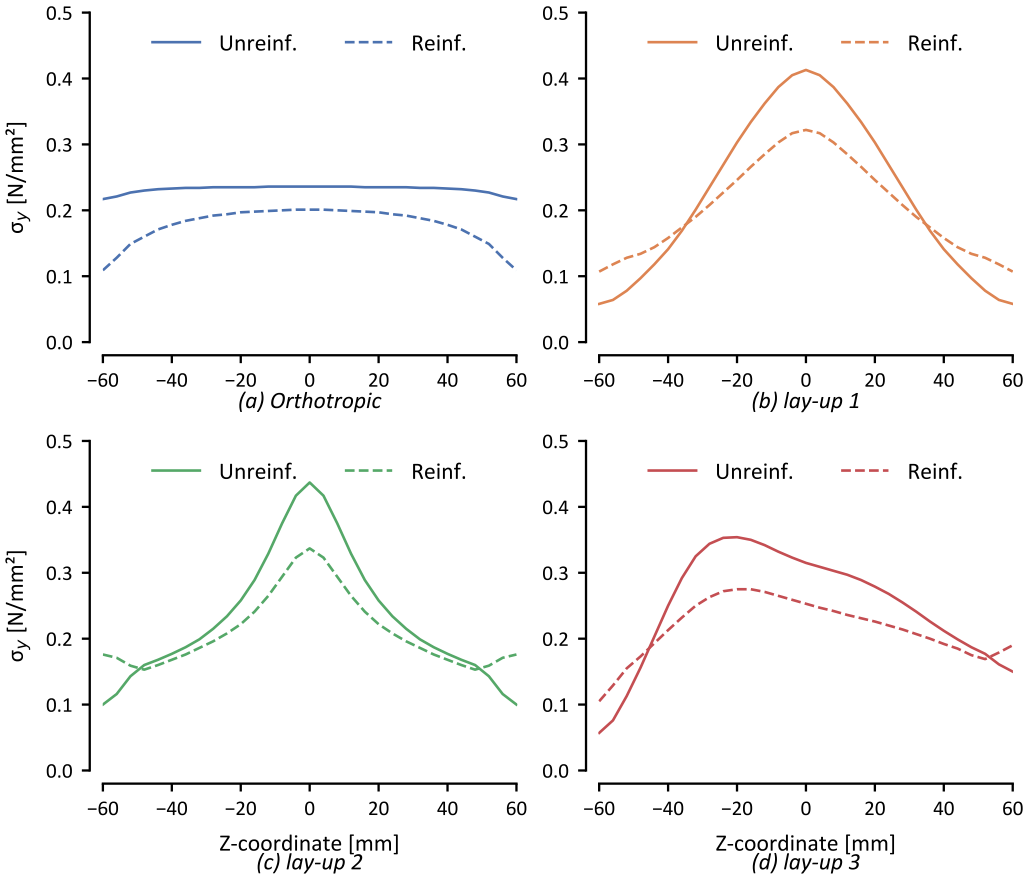

Figure 7-9: *Tensile stresses perp. to the grain along the width for the unreinforced and reinforced situations.*

Table 7-4: *The maximum tensile stress perp.to the grain for the unreinforced and reinforced case and the reduction obtained by the reinforcement.*

	Orthotropic	Lay-up 1	Lay-up 2	Lay-up 3
	(N/mm²)			
$\sigma_{y,\,max,\,unreinf.}$	0,236	0,413	0,437	0,354
$\sigma_{y,\,max,\,reinf.}$	0,201	0,322	0,337	0,275
Reduction	14,8%	22%	22,9%	22,3%

Figure 7-10 presents the influence of the plywood panels on the tensile stresses perp. to the grain along crack plane 1. The red area indicates the stresses perp. to the grain in the reinforced state, while the yellow area represents the reduction of the stresses obtained by the rod. The figure clearly illustrates the previously described pattern of the reductions for the cylindrical anisotropic models with an observed reduction near the mid-width of the cross-section and the orthotropic model with a pronounced reduction observed at the edges of the cross-section. Contrary to the rods, the reduction of the tensile stresses perp. to the grain does not become more pronounced as the crack plane moves away from the periphery of the hole. Instead, the reductions remain somewhat constant. Furthermore, the attentive reader will have noticed that the reduction is less significant than for the rods.

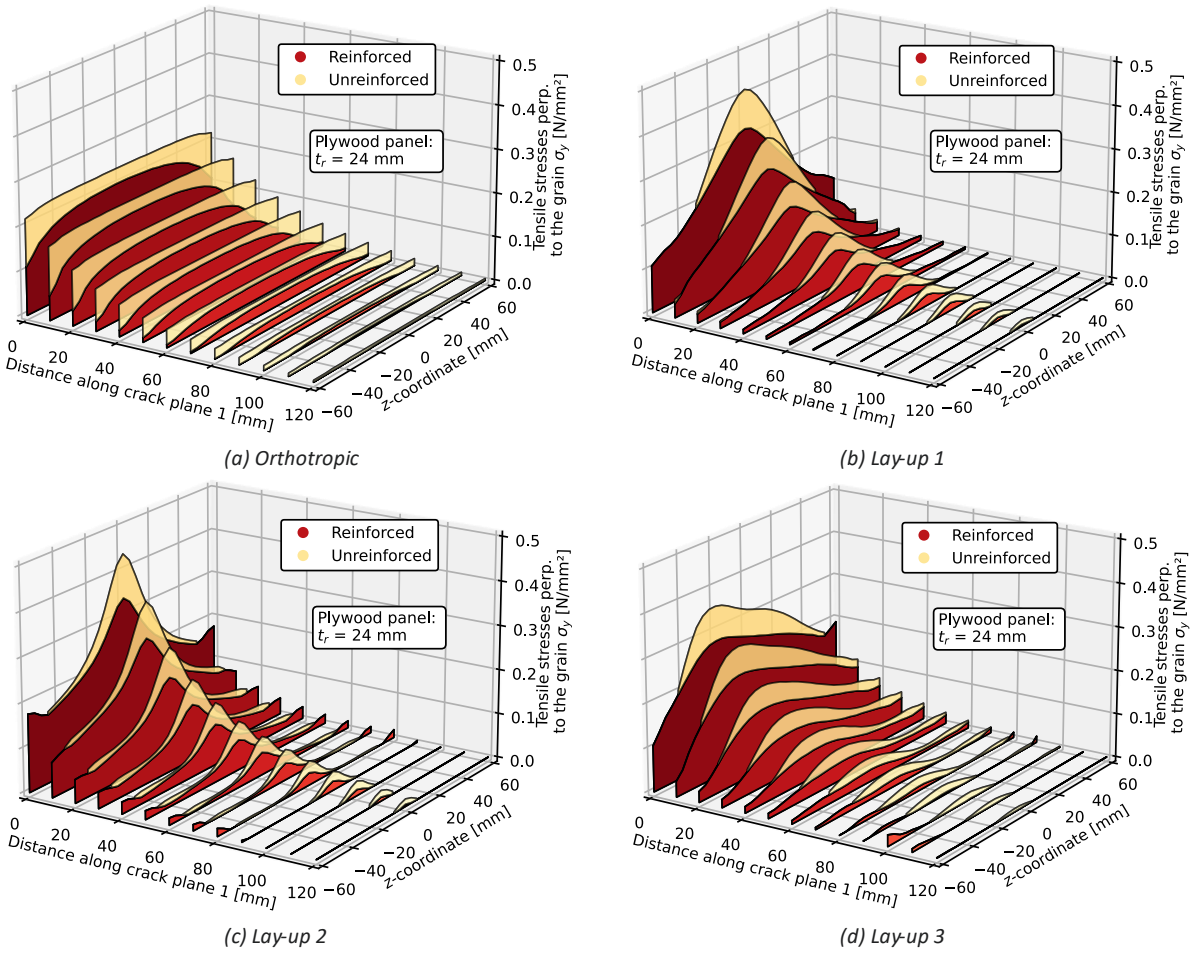

Figure 7-10: *The tensile stresses perp. to the grain along crack plane 1 at the same height as the maximum tensile stress at the periphery of the hole for the unreinforced and reinforced situation when plywood panels are employed.*

Table 7-5 presents the fictive tensile force in the glulam for the unreinforced and reinforced situation. The reduction and, thus, the part taken by the rods is the difference between the unreinforced and reinforced situations. The orthotropic model obtained a more significant reduction of the fictive tensile force than the cylindrical anisotropic models, which became evident from Figure 7-10. That the plywood panels are not so effective in reducing the fictive tensile force can also be explained by the fact that the tensile stresses even increase slightly at the end of the cross-section. These slight increases do not positively influence the integral that determines the value of the fictive tensile force.

Table 7-5: *Fictive tensile force in the glulam's unreinforced and reinforced state and the reduction obtained with the external reinforcements.*

	Orthotropic	Lay-up 1	Lay-up 2	Lay-up 3
	(N)			
$F_{t,90,\,unreinf.}$	996	699	735	836
$F_{t,90,\,reinf.}$	664	565	581	623
Reduction	34,4%	19,2%	21%	25,5%

Figure 7-11 shows the effect of the panels on the shear stresses along crack plane 1 for the four considered cases. The shear stresses demonstrate a similar pattern for the reduction as the tensile stresses perp. to the grain. The reduction of the shear stresses is uniform across all four cases, achieving a reduction of approximately 10%. This reduction is smaller than the reductions observed for the inclined rods. The reduction of the shear stresses decreases as the plane moves away from the hole. The shear stresses experience the most considerable reduction near the edge of the hole, where the stress pattern shows a more inhomogeneous distribution for the cylindrical anisotropic models. Another noteworthy characteristic of the shear stresses in the reinforced state is the minor peaks at the outer edges of the glulam. These peaks reach a maximum at approximately 90 mm away from the periphery of the hole. This maximum coincides with the location where the panel ends. Nevertheless, it is noteworthy that these observations contradict the prevailing preference for external reinforcements in mitigating shear stresses.

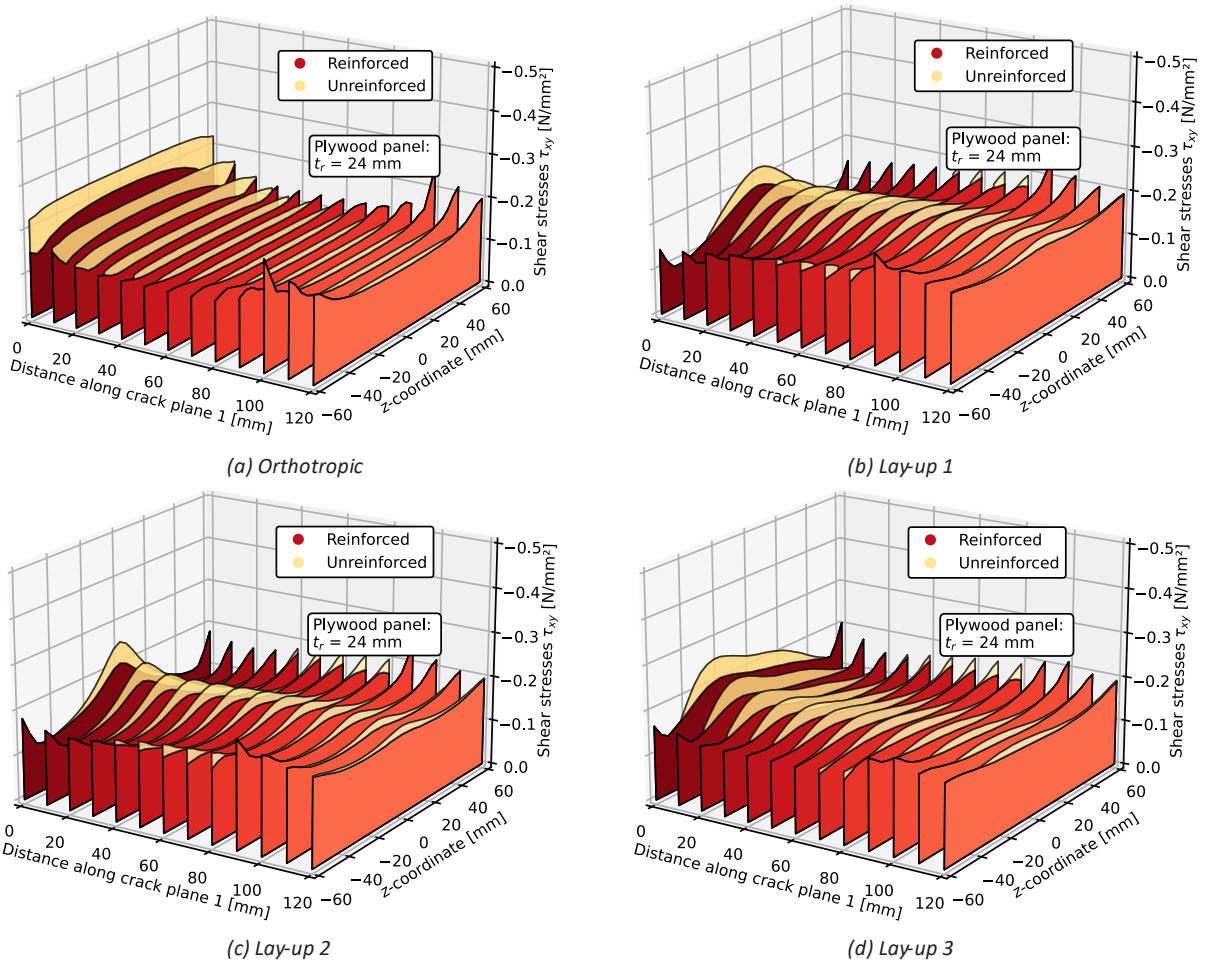

Figure 7-11: *The shear stresses along crack plane 1 at the same height as the maximum tensile stress at the periphery of the hole for the unreinforced and reinforced situation when plywood panels are employed.*

7.2.2 Parameter study

A parameter study has been performed to study the effect of the panel dimensions on the reduction of the tensile stress peak and the fictive tensile force. The parameters considered are the panel thickness t_r and the panel length h_{rp}.

The first parameter examined in this parameter study is the thickness of the reinforcement panels. The impact of panel thickness on reducing the stress peak $\sigma_{y,\,max}$ and the fictive tensile force $F_{t,90}$ is investigated. The panel thickness was varied for different ratios of reinforcement thickness vs beam

width, ranging from 0,1 to 0,6 with increments of 0,1. The results for the four considered cases are presented in Figure 7-12.

It is remarkable that increasing the panel thickness only yields a marginal improvement in reducing the stress peak and the fictive tensile force. The reduction of the stress peak does not explicitly depend on the considered lay-up, as all three lay-ups demonstrate similar levels of reduction. However, a more distinct difference is observed in the case of the fictive tensile force. With an increasing panel thickness, lay-up 3 exhibits greater reductions of this force, while the reductions for lay-ups 1 and 2 are nearly comparable.

Furthermore, it is noteworthy that the panels achieve a greater reduction of the fictive tensile force than the stress peak in the orthotropic case. Contrary, the three cylindrical anisotropic cases achieve a more significant reduction of the stress peak compared to the fictive tensile force.

In general, the increase in the reduction of the stress peak ranges from 8% ($2t_r/b$ = 0.1) to 12% ($2t_r/b$ = 0.6), while the increase in the reduction of the fictive tensile force ranges from 7% ($2t_r/b$ = 0.1) to 14% ($2t_r/b$ = 0.6). These incremental improvements are relatively modest, thus raising the question of whether a thicker panel is necessary to delay the crack initiation.

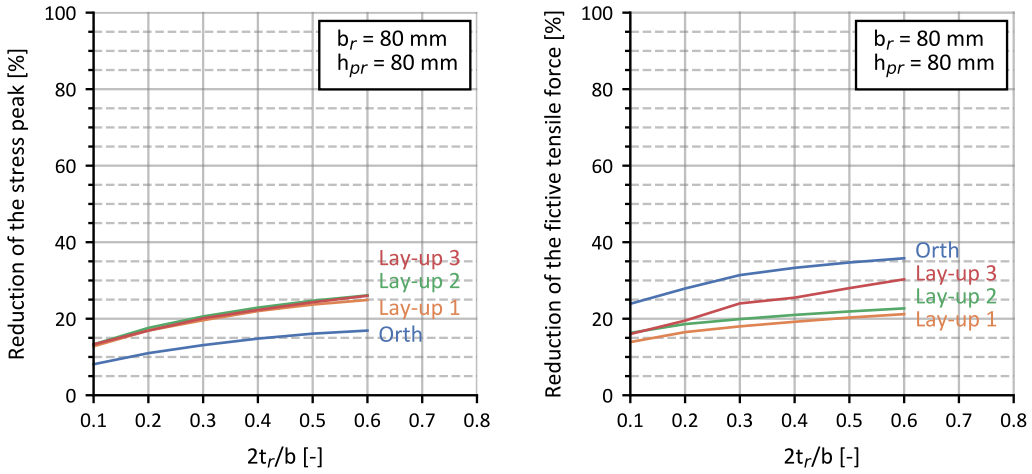

(a) Reduction stress peak

(b) Reduction fictive tensile force

Figure 7-12: *Influence of the panel thickness on reducing the stress peak and fictive tensile force.*

The second parameter examined in this parameter study is the length of the panel b_r. The panel length was systematically varied from 40 to 160 mm with increments of 40 mm, keeping the panel thickness t_r and height h_{pr} constant. The results are presented in Figure 7-13.

It can be observed that, similar to an increasing panel thickness, an increasing panel length does not substantially improve the reduction of the stress peaks and fictive tensile force. The reductions achieved are slightly lower, in the range of 7%. Consequently, the extension of the panel length does not result in a significantly greater reduction.

The objective of this parameter study was to study the reduction of the stress peak and fictive tensile force. However, it should be noted that the design standards primarily focus on ensuring that the reinforcement offers sufficient resistance against the full fictive tensile force. To fulfil this criterion, it may be necessary to increase the thickness or length of the panel to achieve a higher resistance. Nevertheless, this does not mean that this also results in lower stress peaks and, consequently, a delayed crack initiation.

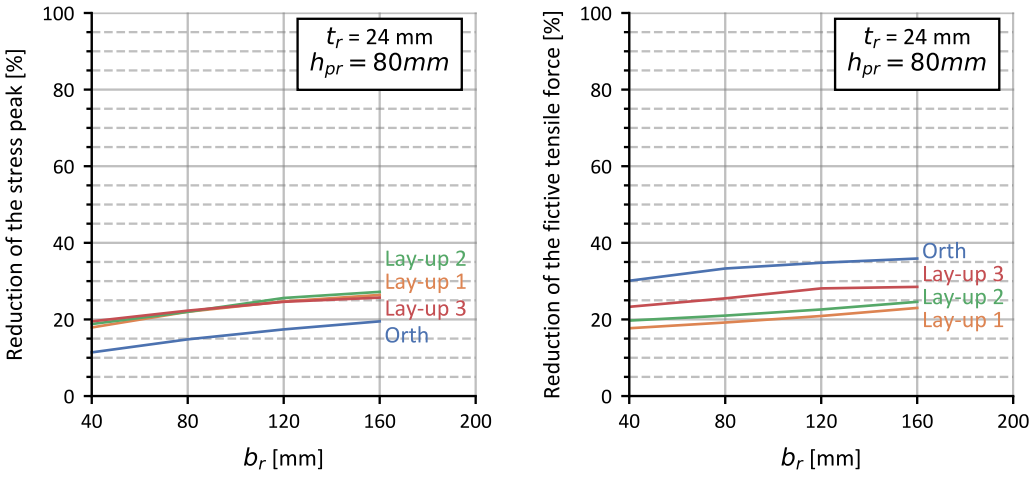

(a) Reduction stress peak *(b) Reduction fictive tensile force*

Figure 7-13: *Influence of the panel length b_r on reducing the stress peak and fictive tensile force.*

7.2.3 Discussion

This section discussed the effect of plywood panels made of birch on the reduction of the tensile stress peak, the shear stresses, and the fictive tensile force. It was observed that the reductions were not as pronounced as for the inclined rods. In general, the orthotropic model overestimated the reductions compared to the cylindrical anisotropic models. The periodically varying eccentricity had not such a pronounced influence as observed for the rods. Furthermore, the reduction of the shear stresses achieved by panels is insignificant. This is remarkable since external reinforcements are generally preferred due to their ability to reduce shear stresses. It was also shown that the panels are ineffective in the damaged state.

Although not explicitly investigated, it can be concluded that as the beam width increases, the efficiency of glued-on panels diminishes. This decrease in efficiency can be attributed to the fact that the panel will be situated further away from the stress peak near the mid-width of the cross-section for each increase in width. Consequently, there may come a point where the use of internal reinforcements becomes the only suitable option.

7.3 Discussion

This chapter investigated the effect of reinforcements on the structural behaviour of a glulam beam with a circular hole with a relative hole height of 0,3*h* along the neutral axis of the beam. Three specific scenarios were examined: the presence of one rod, two rods, and a plywood panel.

The orthotropic model underestimates the maximum tensile stress peak reduction for scenarios where a single rod is installed and plywood panels are glued to both sides of the cross-section compared to the cylindrical anisotropic cases. Contrary, the orthotropic model overestimates the reduction for the scenario where two rods are employed. However, in the case of the shear stresses, the orthotropic model overestimates the reduction for both scenarios where rods are used with 7% and 5%, respectively. The reduction of the shear stresses for the plywood panels is equal for all four cases.

The orthotropic case showed a different pattern for stress reduction for all three scenarios than the cylindrical anisotropic cases. Thus, the orthotropic model does not accurately describe the real influence of the reinforcements. Therefore, the cylindrical anisotropic models should be used to correctly assess the stresses in the vicinity of a hole.

When it is looked at the three cylindrical anisotropic cases, a pronounced influence of the periodically varying eccentricity *e* of the pith is observed. The reductions of the stress peak and fictive tensile force lay-ups 1 and 2 are in the same order of magnitude. In contrast, the reductions for lay-up 3 are either lower or higher depending on the considered reinforcement scenario. A slight increase is observed for the scenario where plywood panels are employed. Contrary, the periodically varying eccentricity reduced the effectivity of the rods considerably, where a more pronounced difference is observed for a single rod. The periodically varying eccentricity of the pith does not seem to influence the shear stresses since the reductions obtained are similar for all three considered lay-ups. Thus, the periodically varying eccentricity has a slight positive effect on the reductions for plywood panels and a marked negative influence for the rods. Furthermore, when the piths are aligned along the vertical axis (e = 0), more pronounced reductions are achieved for the rods compared to when a marked eccentricity ($e \neq 0$) of the pith is present.

In general, the implementation of rods exhibited better reductions for the stress peak, shear stresses and the fictive tensile force. Notably, the situation with a single rod yielded a greater reduction of these stresses than with 2 rods. Furthermore, the fictive tensile force reduction is generally more significant than the reduction of the tensile stress peak.

8

DAMAGED STATE

This chapter investigates the influence of stationary cracks on the stress distribution in the vicinity of a circular hole in an unreinforced and reinforced situation. First, the unreinforced situation is regarded, followed by the reinforced state. The scenario where a single rod is installed, as well as the scenario with the glued-on panels, will be discussed. Only lay-up 1 is discussed.

8.1 Damaged state in the unreinforced situation

This section describes the stress distribution in the damaged state of the glulam for the cylindrical anisotropic case taking lay-up 1 into account. Figure 8-1 depicts the tensile stresses perp. to the grain along a similar path as Figure 6-2. The undamaged state and crack stages 1 and 2 are shown. Crack stage 3 is not included since a fully developed crack along the width is considered, and thus the tensile stresses are zero in this stage. Comparing the entire state with crack stage 1 shows that once a crack has initiated, the stress peaks shift to the edges of the beam, however, with slightly lower values of the stress peaks. A larger difference is observed from crack stages 1 to 2, where the width of the crack increases from 20 to 40 mm. The stress peaks at the edge of the crack are reduced compared to crack stage 1 but are higher compared to the undamaged state at the same position. Based on this stress pattern, one would not expect the crack to extend sideways further.

Figure 8-2 depicts the redistribution of tensile stresses perp. to the grain for the cylindrical anisotropic model in undamaged (a) and damaged (b-d) states induced by the stationary cracks for the three stationary cracks examined. At crack stage 1, where a relatively small crack has formed, the stress peak at the crack tip increases slightly compared to the undamaged stage. Furthermore, the stress peak in the undamaged stage appears to have split at the edge of the hole for crack stage 1. This split means that the stresses are also pushed to the side of the crack. A similar pattern is observed as the crack develops, but the magnitude reduces. This reduction is because the tensile stresses appear to be transferred by a more extensive surface around the crack tip. The observed tensile stress distribution indicates that the assumption of a rounded crack surface was appropriate.

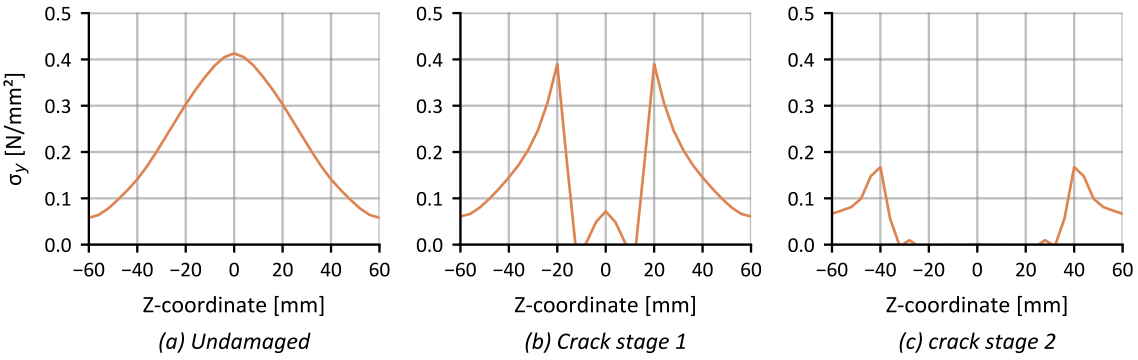

Figure 8-1: *Tensile stresses perp. to the grain at the face of the hole for the undamaged state and the first two crack stages.*

The influence of shear stresses on crack propagation was previously addressed. Figure 8-3 presents the shear stresses along crack plane 1 for the damaged state for crack state 3. The figure reveals that the crack does not explicitly influence the shear stresses. Although minor increases occur near the crack tip, they are less significant than the tensile stresses perp. to the grain. Hence, the shear stresses suffered minimal change from the presence of the crack. Nevertheless, examining what will happen when reinforcements are considered will be interesting.

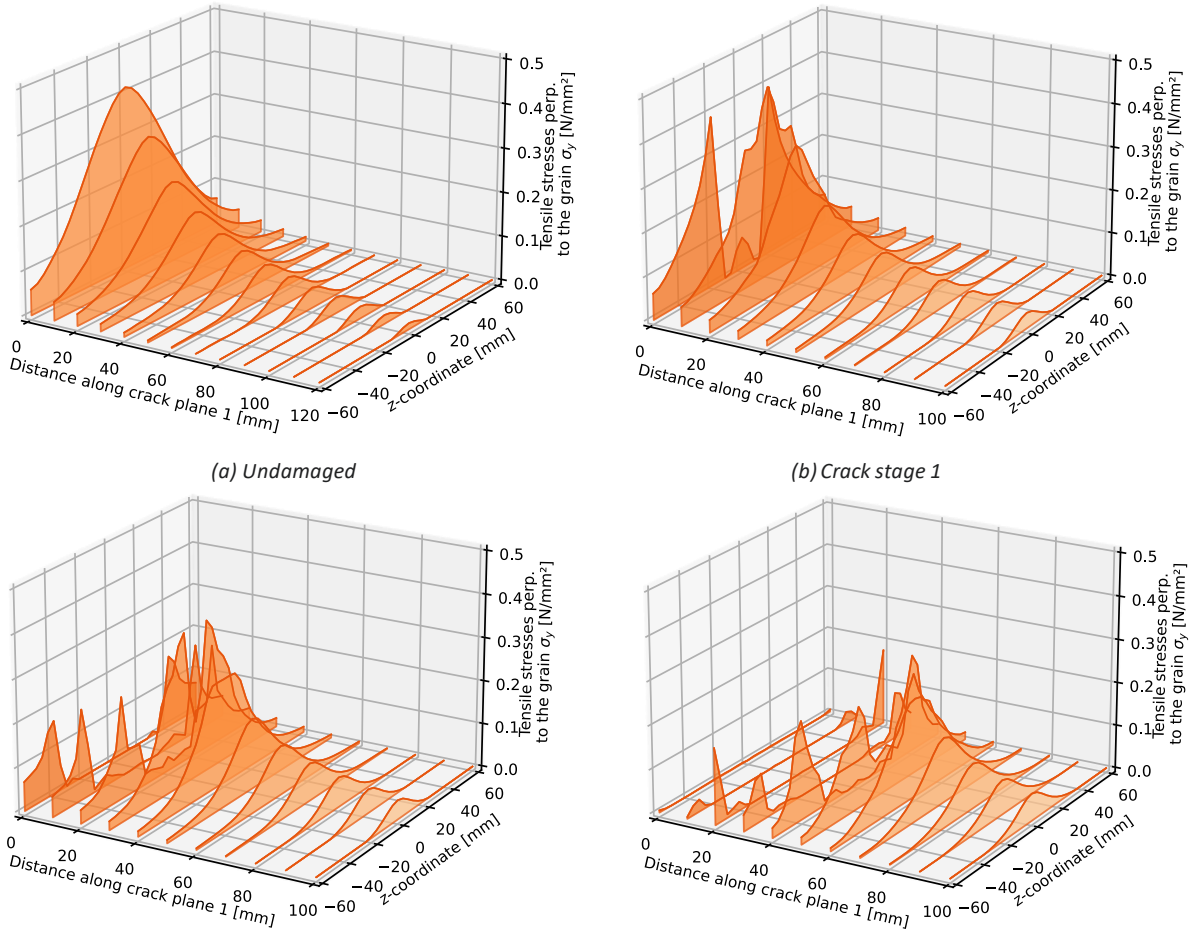

Figure 8-2: *Tensile stresses perp. to the grain along crack plane 1 for lay-up 1 in the undamaged stage(a) and the crack stages (b-d).*

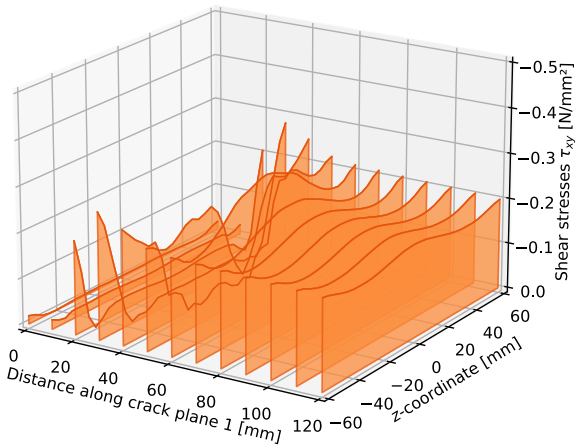

Figure 8-3: *Shear stresses along crack plane 1 for lay-up 1 in the damaged state for crack stage 3.*

8.2 Damaged state in the reinforced situation

8.2.1 Internal reinforcements

In section 2.4.1, it was discussed that internal reinforcements do not necessarily delay the initiation of cracks. Therefore, examining the stress distribution as soon as a crack has been initiated is interesting. The scenario where only one rod is installed is considered. The similar three crack stages as for the unreinforced state are used. Figure 8-1 illustrates the tensile stresses perp. to the grain along the width of the cross-section of the unreinforced and reinforced state. The undamaged stage is already discussed. A significant reduction of the stress peaks is observed in crack stage 1.

Table 8-1 presents the fictive tensile force for the three considered crack stages. The percentage taken by the rod slightly decreases once a crack has initiated but significantly increases once the crack propagates. Based on the observations, it can be carefully stated that if the crack has fully developed along the width until the rod, the fictive tensile force is entirely taken by the rod and thus, no tensile stresses remain at the side of the rod, which is the furthest away from the edge of the hole.

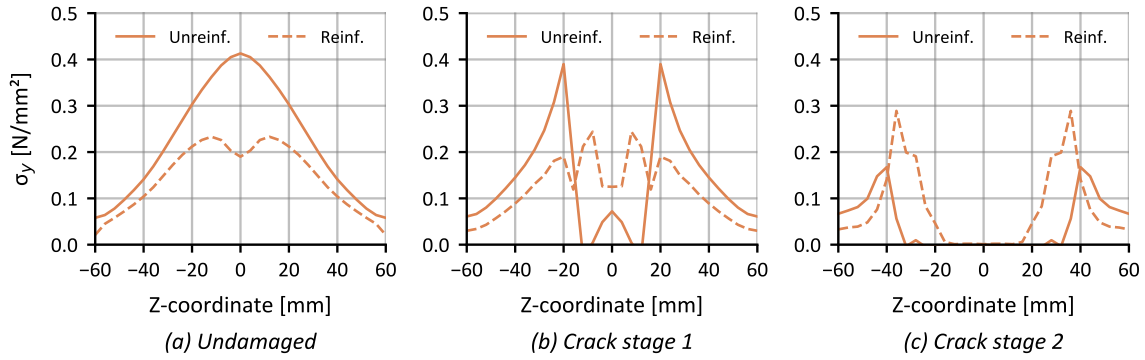

Figure 8-4: *Tensile stresses perp. to the grain at the face of the hole for the undamaged stage and the first two crack stages for the unreinforced and internal reinforced state.*

Table 8-1: *Fictive tensile force for the different crack stages for unreinforced and internal reinforced state*

	Undamaged state	Crack stage 1	Crack stage 2	Crack stage 3
	(N)			
$F_{t,90,\ unreinf.}$	699	768	702	581
$F_{t,90,\ reinf.}$	451	224	154	109
% Taken by reinforcement	35,5%	29,2%	78,1%	81,2%

Figure 8-5 depicts the redistribution of the tensile stresses perp. to the grain in the damaged situation induced by the three considered stationary cracks. Each figure compares the results obtained from the unreinforced (yellow area) and reinforced model (red area). The tensile stresses in the remaining undamaged part are reduced significantly but still show an occasionally high-stress peak at some locations. It can be observed that the tensile stresses perp. to the grain become gradually less as the crack propagates. The fictive tensile forces also observed this over the different crack stages. It can be concluded that implementing a rod can reduce the crack propagation once the crack has reached the rod since almost no tensile stresses perp. to the grain remain in the region preceding the rod.

Section 2.4.1 revealed that the presence of rods does not influence the shear stresses in the region preceding the rod. These stresses remained similar to those observed in the undamaged state. Consequently, when a has propagated until the rod, the shear stresses become the main reason for crack initiation. Therefore, it is interesting to examine if something similar occurs when considering the cylindrical anisotropy of wood. Figure 8-6 presents the shear stresses for the damaged state at crack stage 3 in the reinforced situation. The figure demonstrates that the shear stresses in the damaged state are practically identical to those in the undamaged state in the region preceding the rod. Consequently, based on this analysis, the shear stresses also become the main reason for crack propagation once the crack has propagated until the rod.

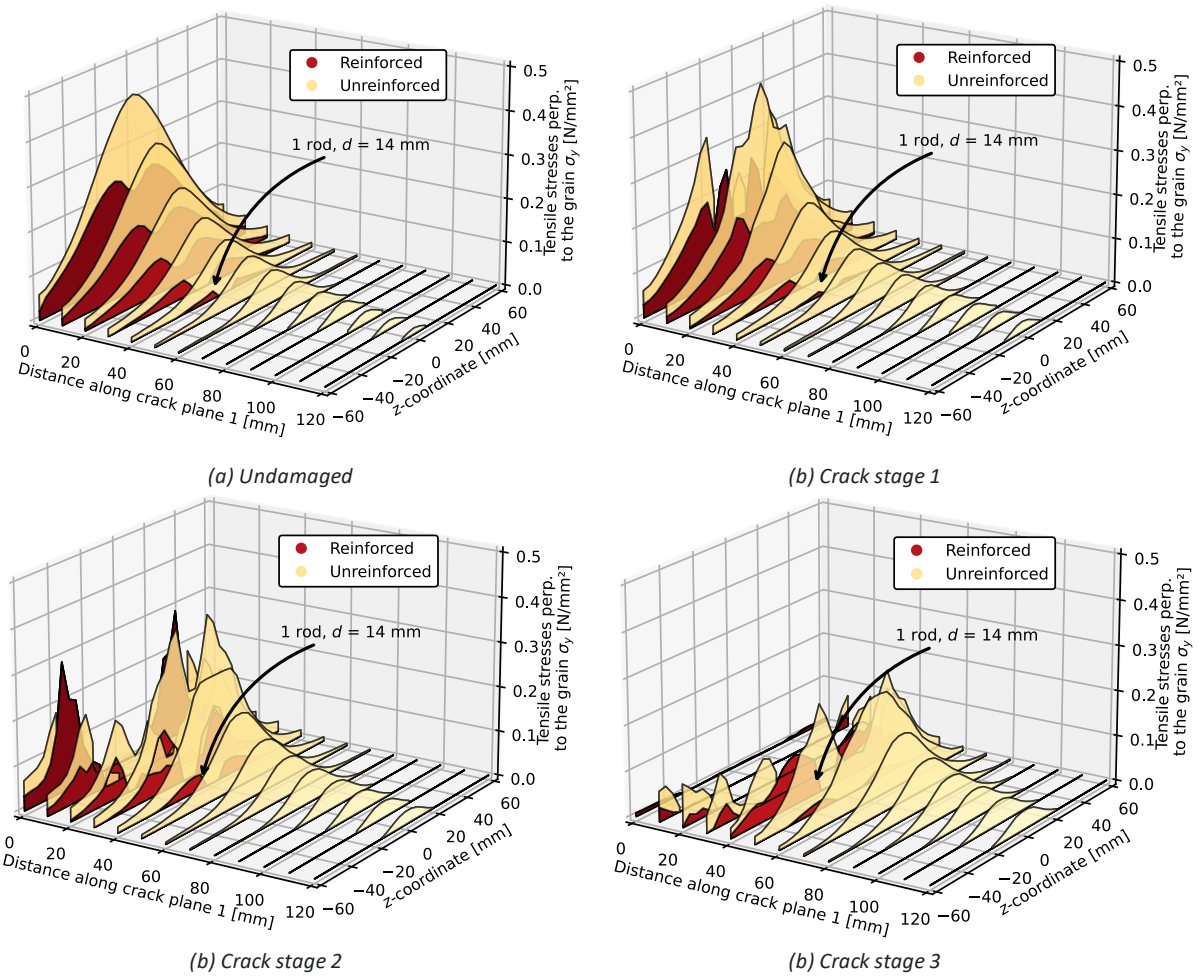

(a) Undamaged *(b) Crack stage 1*

(b) Crack stage 2 *(b) Crack stage 3*

Figure 8-5: *Tensile stresses perp. to the grain along crack plane 1 for lay-up 1 in the undamaged stage(a) and the crack stages (b-d) for the unreinforced and reinforced situation.*

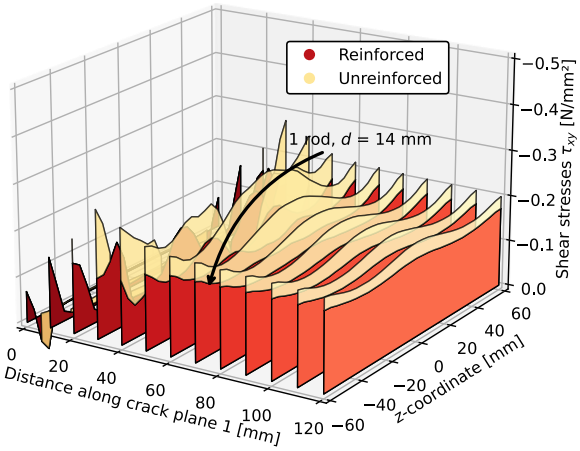

Figure 8-6: *Shear stresses along crack plane 1 for lay-up 1 in the damaged state for crack stage 3 for the unreinforced and reinforced situation.*

8.2.2 External reinforcements

The influence of the panel on the tensile stresses perp. to the grain in the case when a crack initiates and develops along the width of the beam was studied as well. Figure 8-7 illustrates the tensile stresses perp. to the grain along the width of the cross-section of the unreinforced and reinforced state. The

undamaged stage is already discussed. Noteworthy to mention is that when crack stage 1 is considered, the panels do not effectively reduce the tensile stresses. However, the peak moved closer to the outer edges. This can also be observed from crack stage 2. However, if the fictive tensile force is regarded, an increase in the reduction of the fictive tensile force in the glulam is observed as the crack propagates, as is presented in Table 8-2.

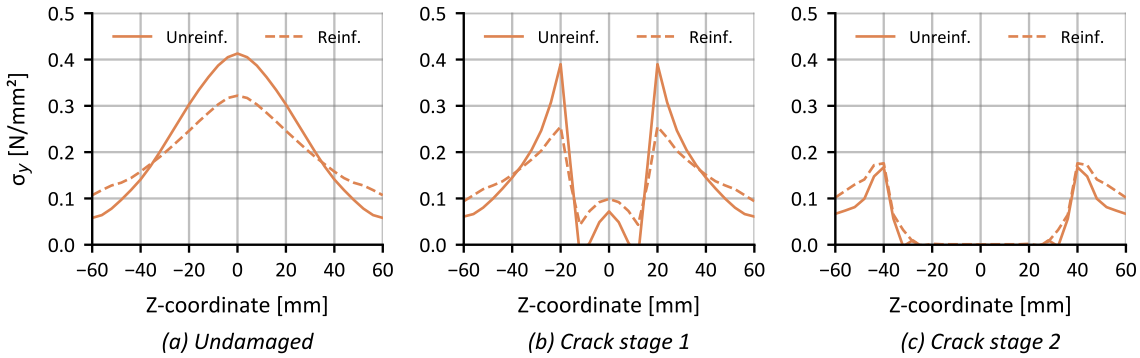

Figure 8-7: *Tensile stresses perp. to the grain at the face of the hole for the undamaged stage and the first two crack stages for the unreinforced and external reinforced state.*

Table 8-2: *Fictive tensile force for the different crack stages for the unreinforced and external reinforced state.*

	Undamaged state	Crack stage 1	Crack stage 2	Crack stage 3
	(N)			
$F_{t,90,\ unreinf.}$	699	768	702	581
$F_{t,90,\ reinf.}$	565	528	462	333
% Taken by reinforcement	19,2%	31,3%	34,2%	42,7%

Figure 8-8 depicts the redistribution of the tensile stresses perp. to the grain in the damaged situation induced by the three considered stationary cracks. Each figure compares the results obtained from the unreinforced (yellow area) and reinforced model (red area). It can be observed that the tensile stresses perp. to the grain become gradually less as the crack propagates. However, not as significant as was observed for the scenario with 1 rod. The tensile stresses in the remaining undamaged part are reduced slightly but may still be significant enough to drive crack propagation. Furthermore, it appears that most of the tensile stresses move along the crack tip as the crack develops. However, it reduces at every increment that the crack extends. The panel does not appear to be able to halt the propagation of the crack but only to slow it down to a certain extent.

Figure 8-9 presents the shear stresses in the reinforced situation for crack stage 3. The figure indicates that the presence of the panel does not affect the shear stresses in the region preceding the rod. The reduction observed is even less than that observed in the undamaged state. Hence, the panels are ineffective in preventing crack propagation caused by the shear stresses.

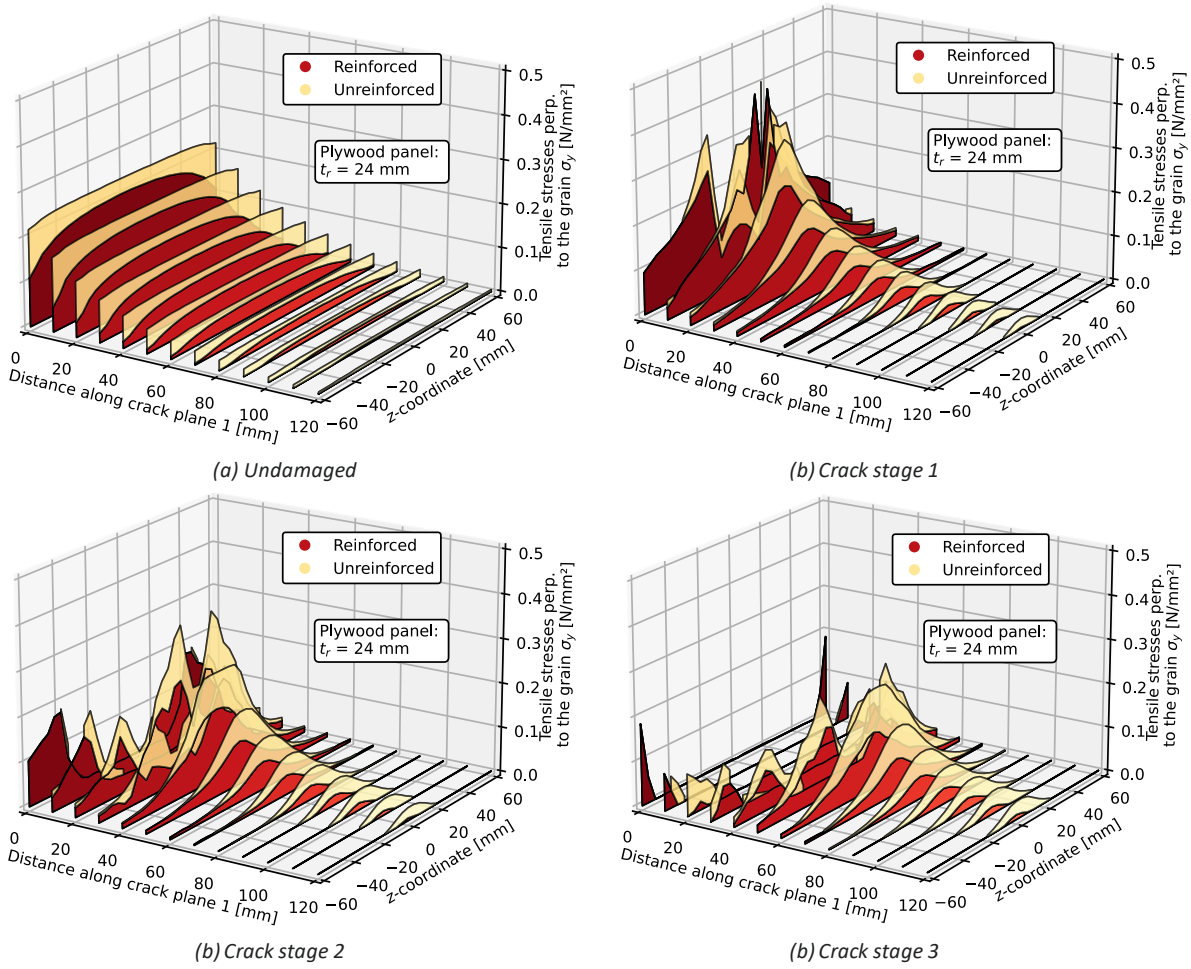

(a) Undamaged *(b) Crack stage 1*

(b) Crack stage 2 *(b) Crack stage 3*

Figure 8-8: *Tensile stresses perp. to the grain along crack plane 1 for lay-up 1 in the undamaged stage(a) and the crack stages (b-d) for the unreinforced and reinforced situation.*

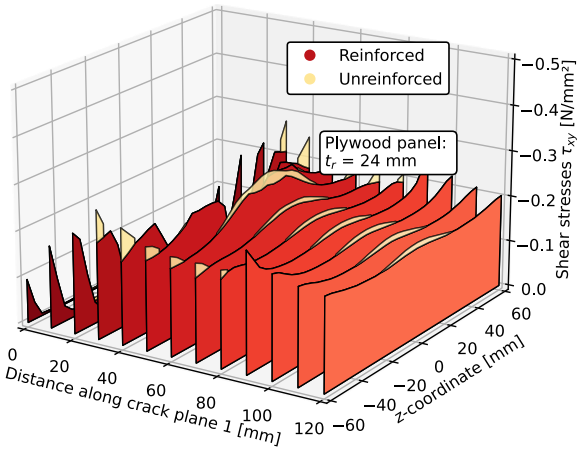

Figure 8-9: *Shear stresses along crack plane 1 for lay-up 1 in the damaged state for crack stage 3 for the unreinforced and reinforced situation.*

8.3 Discussion

The influence of crack propagation on the redistribution of tensile stresses perp. to the grain was examined. A pronounced influence of the rods on the reduction of the redistributed tensile stresses perp. to the grain was observed. As the crack propagates, the rod takes a gradually increasing

percentage of the fictive tensile force. It can even be argued that the rod can prevent crack propagation once it has reached the rod since no tensile stresses remain at the side further away from the hole. Contrary, the plywood panels do not seem to prevent the propagation of the cracks. The plywood panels did not reduce the redistributed tensile stresses perp. to the grain as effectively as the single rod. The panels appear unable to halt crack propagation but only to slow it down to a certain extent. Furthermore, neither reinforcement type significantly reduced the shear stresses, indicating that the primary action for crack propagation switches to the shear stresses at a certain point.

Both types of reinforcements can increase the ultimate load as some of the tensile stresses perp. to the grain are mitigated by the reinforcements if only the tensile stresses perp. to the grain are regarded. However, the rod seems to be the best option to increase the ultimate failure load. However, the stress concentrations are not the only factor determining the ultimate failure load of an internal reinforced rod. The influence of embedment and withdrawal stiffness is also important to consider. However, this is out of the scope of this thesis.

9

CONCLUSION & RECOMMENDATIONS

9.1 Conclusion

In this thesis, a numerical investigation explores how the cylindrical anisotropy of wood impacts stress distribution in the vicinity of a circular hole placed along the neutral axis of a glulam beam. The study compares an orthotropic reference case with three distinct lay-up patterns. The research investigates the unreinforced and reinforced scenarios, including the influence of stationary cracks. These investigations address the primary research question:

"What is the influence of the cylindrical anisotropy of wood on the stress distribution of a glulam beam with an unreinforced and reinforced hole?"

To answer the main research question, several sub-questions were addressed:

- *How does the cylindrical anisotropy of wood affect the stress distribution in the vicinity of an unreinforced hole?*

The numerical study found that the cylindrical anisotropy of wood leads to an uneven stress distribution for tensile stresses perp. to the grain and shear stresses along the cross-sectional width. The tensile stresses showed a prominent peak near mid-width, significantly higher than the orthotropic reference case. This aligns with experimental tests where crack initiation consistently occurred near the mid-width, explaining these observations. The magnitude of the peaks depends on the lay-up pattern. A periodically varying eccentricity positively influences the magnitude of the stress peak. Shear stresses displayed a similar pattern, but the peaks were of similar magnitude to the orthotropic reference model. Comparing the fictive tensile force between orthotropic and cylindrical anisotropic cases showed a smaller magnitude for the latter, depending on the lay-up pattern. Increasing the beam width did not result in a more prominent tensile stress peak.

- *How does the cylindrical anisotropy of wood affect the stress distribution in the vicinity of a reinforced hole?*

Three different reinforcement scenarios were examined: a single rod placed at the mid-width, two rods positioned along the width and plywood panels glued to both edges of the beam. The rods were placed at an angle of 45°. The comparison revealed that the scenario with a single rod placed at the mid-width of the cross-section was the most effective in reducing the tensile stresses perp. to the grain, shear stresses and fictive tensile force. However, introducing an eccentricity significantly influenced the effectiveness of internal reinforcements. Contrary to what seems to be generally believed, external reinforcements are ineffective in reducing any of the aforementioned criteria. The external reinforcements achieved the lowest reductions for the three cylindrical anisotropic cases and the orthotropic reference case.

- *What happens when stationary cracks are regarded to the stresses considering the cylindrical anisotropy of wood?*

Examining the influence of stationary cracks on the redistribution of tensile stresses perp. to the grain at three distinct stages has revealed that the pronounced stress peaks remain but follow the face of the crack tip. The damaged situation in the reinforced situation was also examined. Analogous to the undamaged state, the single rod exhibited the most effective reduction of the remaining tensile stresses in the glulam. As the crack propagates towards the rod, the magnitude of tensile stresses is gradually reduced. Consequently, it can be argued that rods can stop crack propagation when it reaches the rod since no tensile stresses remain in the region preceding the rod. Contrarily, the panels demonstrated a less effective reduction of the tensile stresses. The panels seem unable to halt the crack propagation but can slow down the crack propagation to a certain extent. Additionally, the analysis revealed that both reinforcement types cannot prevent crack initiation driven by shear stresses.

From this research, it can be concluded that the cylindrical anisotropy of wood significantly influences the stress distribution in the vicinity of an unreinforced and reinforced hole. Pronounced stress peaks are observed along the width of the beam in the unreinforced situation, which primarily contributes to the initiation of cracks near the mid-width of the cross-section. Therefore, neglecting the cylindrical anisotropy cannot be justified if one aims to achieve a structurally safer hole since it results in a different distribution of the stresses than the orthotropic model. Furthermore, the reduction patterns obtained by the reinforcements are different for the three cylindrical anisotropic cases and the orthotropic reference case. This difference misrepresents the reduction of the stresses, which might potentially lead to inaccurate conclusions. Overall, considering the cylindrical anisotropy of wood results in a more accurate representation of the stresses in the vicinity of an unreinforced and reinforced hole. However, the results strongly depend on the pith orientations employed for the relevant laminations.

The study found that a single rod placed at an angle of 45° was the most effective in reducing the tensile stress peak, shear stresses and fictive tensile force. Furthermore, the single rod is also the most effective in reducing the tensile stresses once a crack has been initiated. The single rod may even halt the crack propagation once the crack has reached the rod as long has the shear stresses remain under the shear strength of the glulam.

9.2 Recommendations

The following recommendations for further research are proposed:

- The thesis focussed on three specific lay-ups based on Aicher & Dill-Langer [10]. However, in practical applications, the orientations of the pith are more stochastic. Conducting simulations

with a more random orientation of the piths could lead to different conclusions and provide additional insights into the influence of cylindrical anisotropy on the structural behaviour of glulam beams with holes.

- The study did not consider the effects of local defects such as knots and resin pockets. These local defects have a significant impact on the structural behaviour. Therefore, investigating the effects of these local defects together with the cylindrical anisotropy of wood may result in more accurate representations of the stresses in the vicinity of the hole.
- One of the aims of this thesis was to examine the structural behaviour of holes in glulam beams by investigating the influence of various reinforcement methods. The thesis assumed a perfect bond between the rods and the timber, neglecting the embedment and withdrawal stiffness of the rods since this would further complicate the models for the internal reinforcements. These stiffnesses, however, also differ between screws and glued-in rods. For further research, examining the influence of embedment and withdrawal stiffness on reducing the tensile stresses perp. to the grain, shear stresses and fictive tensile force are recommended. Similarly, the bond between the panels and the timber was also assumed to be perfect.
- This research aimed at conventional stress analysis to quantify the stress distribution along the crack plane. However, a study from a fracture mechanics perspective, considering the cylindrical anisotropy, might be interesting to see the influence of this model on the ultimate failure load.

References

[1] L. Höfflin, “Runde Durchbrüche in Brettschichtholzträgern – Experimentelle und theoretische Untersuchungen,” 2005.

[2] S. Aicher and C. Tapia, “EVALUATION OF DESIGN CONCEPTS FOR HOLES IN GLULAM BEAMS—COMPARISON WITH TEST RESULTS,” *Otto-Graf-Journal,* vol. 18, pp. 329-344, 2019.

[3] S. Aicher and L. Höfflin, “Tragfähigkeit und Bemessung von Brettschichtholzträgern mit runden Durchbrüchen: sicherheitsrelevante Modifikationen der Bemessungsverfahren nach Eurocode 5 und DIN 1052,” 2006.

[4] H. Danielsson, “Strength of glulam beams with holes - Tests of quadratic holes and literature test result compilation,” *International Council for Research and Innovation in Building and Construction,* August 2008.

[5] M. Danzer, P. Dietsch and S. Winter, “Einfluss exzentrisch positionierter runder Einzeldurchbrücheche und Gruppen von Durchbrüchen auf die Tragfähigkeit von Brettschichtholzträgern,” Munich, 2017.

[6] S. Aicher and L. Höfflin, “Verifizierung versagensrelevanter Dehnungsverteilungen im Bereich runder Durchbrüche in Brettschichtholzträgern,” *Bautechnik,* vol. 80, no. 8, pp. 523-533, August 2003.

[7] S. Aicher and L. Höfflin, “Fracture behaviour and design of glulam beams with round holes,” in *Proceedings of the 10th World Conference on Timber Engineering*, 2008.

[8] S. Aicher, G. Dill-Langer and L. Höfflin, “Effect of Polar Anisotropy Loaded Perpendicular To Grain,” *Journal of Materials in Civil Engineering,* pp. 2-3, 2001.

[9] S. Aicher and G. Dill-Langer, “Influence of cylindrical anisotropy of wood and loading conditions on off-axis stiffness and stresses of a board in tension perpendicular to the grain,” *Otto Graf Journal,* vol. 7, 1996.

[10] S. Aicher and G. Dill-Langer, “Effect of lamination anisotropy and lay-up in glued-laminated timbers,” *Journal of Structural Engineering,* vol. 131, no. 7, pp. 1095-1103, July 2005.

[11] C. Tapia, “Internal and external reinforcements for holes in glued laminated beams,” Santiago, 2015.

[12] C. Tapia and S. Aicher, “Improved Design Equations for the Resultant Tensile Forces in Glulam Beams with Holes,” in *International Network on Timber Engineering Research*, 2017.

[13] S. Aicher and L. Höfflin, “Runde Durchbrüche in Biegeträgern aus Brettschichtholz. Teil 1: Berechnung,” *Bautechnik,* vol. 78, no. 10, pp. 706-715, October 2001.

[14] S. Aicher and L. Höfflin, “Design of rectangular holes in glulam beams,” *Otto-Graf Journal,* vol. 14, no. 211, 2003.

[15] M. Danzer, P. Dietsch and S. Winter, “Round holes in glulam beams arranged eccentrically or in groups,” *INTER International Network on Timber Engineering Research,* pp. 246-261, 2017.

[16] H. Blaß and I. Bejtka, “Querzugverstärkungen in gefährdeten Bereichen mit selbstbohrenden Holzschrauben,” 2003.

[17] S. Aicher and L. Höfflin, “Glulam beams with round holes - a comparison of different design approaches vs. test data,” in *CIB-W18 meeting 2002 (Vol. 35)*, Stuttgart, 2002.

[18] S. Aicher, “Glulam beams with holes reinforced by steel bars,” *Intl. Council for Research and Innovation in Building and Construction, Working Commission 18-Timber Structures,* 2009.

[19] S. Aicher, L. Höfflin and H. Reinhardt, “Verifizierung versagensrelevanter Dehnungsverteilungen im Bereich runder Durchbrüche in Brettschichtholzträgern,” *Bautechnik,* vol. 80, no. 8, pp. 523-533, August 2003.

[20] H. Danielsson, “The strength of glulam beams with holes; A probabilistic fracture mechanics method and experimental tests,” Lund, 2009.

[21] NEN-EN 1995-1-1:2005+A2:2014+NB:2013, “Eurocode 5 - Ontwerp en berekening van houtconstructies: Deel 1-1: Algemeen - Gemeenschappelijke regels en regels voor gebouwen”.

[22] DIN EN 1995-1-1/NA:2013, “Nationaler Anhang – National festgelegte Parameter – Eurocode 5: Bemessung und Konstruktion von Holzbauten – Teil 1-1: Allgemeines – Allgemeine Regeln und Regeln für den Hochbau”.

[23] ON B 1995-1-1:2015, “Bemessung und Konstruktion von Holzbauten – Teil 1-1: Allgemeines – Allgemeine Regeln und Regeln für den Hochbau”.

[24] H. Kolb and A. Epple, “Verstärkung von durchbrochenen Brettschichtbindern,” Stuttgart, 1985.

[25] S. Aicher and L. Höfflin, “A contribution to the analysis of glulam beams with round holes,” *Otto-Graf Journal,* vol. 11, p. 167, 2000.

[26] S. Aicher, “Glulam beams with internally and externally reinforced holes–Test, detailing and design,” in *Proceedings of the 44th CIB-W18 Meeting*, 2011.

[27] R. Jockwer, “Structural behaviour of glued laminated timber beams with unreinforced and reinforced notches,” Zurich, 2014.

[28] C. Tapia and S. Aicher, “Holes in glulam - Orientation and design of internal reinforcements,” *CDROM Proceedings of the World Conference on Timber Engineering (WCTE 2016),* p. 978, 2016.

[29] S. Aicher and C. Tapia, “Glulam with laterally reinforced rectangular holes,” in *World Conference on Timber Engineering*, Auckland, 2012.

[30] K. B. Dahl, “Mechanical properties of clear wood from Norway spruce,” Trondheim, 2009.

[31] H. Danielsson, “Perpendicular to grain fracture analysis of wooden structural elements - Models and applications,” Lund, 2013.

[32] DIN EN 14080:2013, “Holzbauwerke – Brettschichtholz und Balkenschichtholz – Anforderungen;”.

[33] P. Dietsch, “Reinforcement of timber structures–a new section for Eurocode 5,” in *Proceedings of the World Conference on Timber Engineering WCTE 2016*, Vienna, 2016.

[34] CEN/TC/SC 5, “CEN/TC/SC 5 "Eurocode 5: Design of timber structures",” 2021.

[35] Abaqus v2019, Dassault Systèmes Simulia Corp, Johnston, RI, USA, 2019.

[36] NEN-EN 14080, “Timber structures - Glued laminated timber and glued solid timber - Requirements,” 2013.

[37] H. Danielsson and P. J. Gustafsson, “Fracture analysis of glued laminated timber beams with a hole using a 3D cohesive zone model,” *Engineering Fracture Mechanics,* vol. 124, pp. 182-195, July 2014.

[38] NEN-EN 14080:2013, “Gelijmd gelamineerd hout en gelijmd massief hout”.

Appendix A

Example calculation second-generation Eurocode 5

An exemplary calculation of the fictive tensile force $F_{t,90}$ according to the consolidated draft version of the second-generation Eurocode 5 is shown in this appendix. The fictive tensile force at the right side of the hole is calculated for the analysed configuration described in section 5.1.

First, the internal forces are determined:

$$V_d = \frac{P}{2} = \frac{10.000}{2} = 5.000\ N$$

$$M_d = \frac{P}{2} * (\ell_v + \ell_h) = \frac{10.000}{2} * (740 + 120) = 4.300.000\ Nmm$$

Next, the calculation of the factor k_{diam}, the factor that accounts for the stress distribution and the location of crack onset, is performed:

$$k_{diam} = 1{,}1 + 1{,}3\left[\frac{d_{hole}}{h} - \left(\frac{d_{hole}}{h}\right)^2\right]$$

$$k_{diam} = 1{,}1 + 1{,}3\left[\frac{120}{400} - \left(\frac{120}{400}\right)^2\right]$$

$$k_{diam} = 1{,}373$$

d_{hole} is equal to 1,0 for circular holes. Thus, the shear component of the fictive tensile force can be calculated:

$$F_{t,90.V,Ed} = \frac{V \cdot 0{,}7 \cdot d_{hole}}{4 \cdot h} \cdot \left[3 - \left(\frac{0{,}7 \cdot d_{hole}}{h}\right)^2\right] \cdot k_{diam}$$

$$F_{t,90.V,Ed} = \frac{5.000 \cdot 0{,}7 \cdot 120}{4 \cdot 400} \cdot \left[3 - \left(\frac{0{,}7 \cdot 120}{400}\right)^2\right] \cdot k_{diam}$$

$$F_{t,90.V,Ed} = 1.065{,}3\ \mathrm{N}$$

The moment component can also be calculated:

$$F_{t,90.M,Ed} = 0{,}09 \cdot \frac{M_d}{h} \cdot \left(\frac{d_{hole}}{h}\right)^2$$

$$F_{t,90.\mathrm{M,Ed}} = 0{,}09 \cdot \frac{2.150.000}{400} \cdot \left(\frac{120}{400}\right)^2$$

$$F_{t,90.\mathrm{M,Ed}} = 87{,}1\ \mathrm{N}$$

Finally, the shear and moment components must be summed to obtain the fictive tensile force:

$$F_{t,90} = F_{t,90.\mathrm{V,Ed}} + F_{t,90.\mathrm{M,Ed}}$$

$$F_{t,90} = F_{t,90.\mathrm{V,Ed}} + F_{t,90.\mathrm{M,Ed}}$$

$$F_{t,90} = 1.152{,}4\ \mathrm{N}$$

Appendix B

Python scripts for the numerical models

This appendix shows the Python script for the external reinforced cylindrical anisotropic model.

B.1 Glulam class

The Glulam class creates a glulam beam with a hole object. This object is created later on in the script in the run_model function.

```
class Glulam(object):
    """
    Class to create glulam beam with hole
    """
    def __init__(self, model, name, hole_height, hole_geometry,
hole_length, posistion, sec_glulam):
        """
        Initializing
        """
        self._model = model
        self._name = name
        self._hole_height = hole_height
        self._hole_geometry = hole_geometry
        self._hole_length = hole_length
        self._posistion = posistion
        self._sec_glulam = sec_glulam

        # Hole variables
        x_hole = posistion[0]
        y_hole = posistion[1]

        n_laminations = glulam_height/lamel_thickness

        # Define pith orientation parameters
        pith_orientations = {
            1: (35, 35, 0, 0),
            2: (15, 60, 0, 0),
            3: (35, 35, -20, 20)
        }
        d1, d2, e1, e2 = pith_orientations.get(lay_up, (0, 0, 0, 0))

        assembly = model.rootAssembly

        # Create glulam
```

```
        glulam_sketch = model.ConstrainedSketch(name='__profile__',
sheetSize=200.0)
        glulam_sketch.rectangle(
            point1=(0.0, 0.0),
            point2=(glulam_length, glulam_height)
            )

        # Create hole geometry
        if hole_geometry == 'Square' or hole_geometry == 'Rectangular':
            glulam_sketch.rectangle(point1=(x_hole-0.5*hole_length,
y_hole-0.5*hole_height),
                                    point2=(x_hole+0.5*hole_length,
y_hole+0.5*hole_height))

            glulam_sketch.FilletByRadius(
                curve1=glulam_sketch.geometry[6],
                curve2=glulam_sketch.geometry[7],
                nearPoint1=(x_hole-0.5*hole_length, y_hole),
                nearPoint2=(x_hole, y_hole+0.5*hole_height),
                radius=radius)
            glulam_sketch.FilletByRadius(
                curve1=glulam_sketch.geometry[7],
                curve2=glulam_sketch.geometry[8],
                nearPoint1=(x_hole, y_hole+0.5*hole_height),
                nearPoint2=(x_hole+0.5*hole_length, y_hole),
                radius=radius)
            glulam_sketch.FilletByRadius(
                curve1=glulam_sketch.geometry[8],
                curve2=glulam_sketch.geometry[9],
                nearPoint1=(x_hole+0.5*hole_length, y_hole),
                nearPoint2=(x_hole+0.5*hole_length, y_hole-
0.5*hole_height),
                radius=radius)
            glulam_sketch.FilletByRadius(
                curve1=glulam_sketch.geometry[9],
                curve2=glulam_sketch.geometry[6],
                nearPoint1=(x_hole+0.5*hole_length, y_hole-
0.5*hole_height),
                nearPoint2=(x_hole-0.5*hole_length, y_hole),
                radius=radius)

        elif hole_geometry == 'Circular':
            glulam_sketch.CircleByCenterPerimeter(
                center=(x_hole, y_hole),
                point1=(x_hole-0.5*hole_length, y_hole))

        # Create Part
        part_glulam = model.Part(dimensionality=THREE_D, name=name,
type=DEFORMABLE_BODY)
        part_glulam.BaseSolidExtrude(depth=glulam_width/2,
sketch=glulam_sketch)
        del glulam_sketch

        # Partitioning of glulam
```

```
        datum_left_glulam =
part_glulam.DatumPlaneByPrincipalPlane(offset=x_hole-0.5*hole_length-
left_1, principalPlane=YZPLANE)
        datum_id_left_glulam = datum_left_glulam.id
        part_glulam.PartitionCellByDatumPlane(cells=part_glulam.cells,
datumPlane=part_glulam.datums[datum_id_left_glulam])

        datum_right_glulam =
part_glulam.DatumPlaneByPrincipalPlane(offset=x_hole+0.5*hole_length+righ
t_1, principalPlane=YZPLANE)
        datum_id_right_glulam = datum_right_glulam.id
        part_glulam.PartitionCellByDatumPlane(cells=part_glulam.cells,
datumPlane=part_glulam.datums[datum_id_right_glulam])

        # Create laminations with datum planes
        for n in range(1, n_laminations):
            datum_plane =
part_glulam.DatumPlaneByPrincipalPlane(offset=n*lamel_thickness,
principalPlane=XZPLANE)

part_glulam.PartitionCellByDatumPlane(datumPlane=part_glulam.datums[datum
_plane.id],
                cells=part_glulam.cells)

        # Create cylindrical coordinate systems and assign them to the
laminations
        for lamella in range(0, n_laminations):
            origin, point1, point2 = (0.0, 0.0, 0.0), (0.0, 0.0, 0.0),
(0.0, 0.0, 0.0)

            if lamella % 2 == 0:
                origin = (0.0, -d1+(lamel_thickness*lamella), e1)
                point1 = (0.0, -d1+(lamel_thickness*lamella+1), e1)
                point2 = (0.0, -
d1+(lamel_thickness*lamella)+lamel_thickness, -glulam_width)

            elif lamella % 2 != 0:
                origin = (0.0, -d2+(lamel_thickness*lamella), e2)
                point1 = (0.0, -d2+(lamel_thickness*lamella+1), e2)
                point2 = (0.0, -
d2+(lamel_thickness*lamella)+lamel_thickness, -glulam_width)

            pith_location = part_glulam.DatumCsysByThreePoints(
                coordSysType=CYLINDRICAL,
                name="lamel_{}".format(lamella+1),
                origin=origin,
                point1=point1,
                point2=point2,
            )

            lamel_cells = part_glulam.cells.getByBoundingBox(
                -1, -1+(lamel_thickness*lamella), -1, 1+glulam_length,
1+(lamel_thickness*(lamella+1)), 1+glulam_width
            )

            lamel_region = regionToolset.Region(cells=lamel_cells)
```

```
            part_glulam.MaterialOrientation(
                additionalRotationField='',
additionalRotationType=ROTATION_NONE,
                angle=0.0, axis=AXIS_3, fieldName='',
localCsys=part_glulam.datums[pith_location.id],
                region=lamel_region,
stackDirection=STACK_3,orientationType=SYSTEM
            )

        # Assign section
        cells_glulam = part_glulam.Set(name='Cells glulam',
cells=part_glulam.cells[:])
        part_glulam.SectionAssignment(
                region=cells_glulam,
                sectionName=sec_glulam.name)

        # Create instance
        instance_glulam = assembly.Instance(name='Instance
{n}'.format(n=name),
                part=part_glulam, dependent=True)

        # Selecting edges
        assembly.regenerate()

        # Select edges in z-direction for meshing beam width
        z_coords = [(0.0, glulam_width/4), (x_hole-0.5*hole_length-
left_1, glulam_width/4),
                (x_hole+0.5*hole_length+right_1, glulam_width/4),
(glulam_length, glulam_width/4),]
        z_edges_list = []
        for coord in z_coords:
            for z in range(0, glulam_height+1, lamel_thickness):
                z_edge = part_glulam.edges.findAt((coord[0], z,
coord[1]))
                z_edges_list.append(z_edge)

         # Select y edges (edges for lamel thickness)
        y_coords = [(0.0, 0.0), (0.0, glulam_width/2), (glulam_length,
0.0), (glulam_length, glulam_width/2),
            (x_hole-0.5*hole_length-left_1, 0.0), (x_hole-
0.5*hole_length-left_1, glulam_width/2), (x_hole+0.5*hole_length+right_1,
0.0),
            (x_hole+0.5*hole_length+right_1, 0.0),
(x_hole+0.5*hole_length+right_1, glulam_width/2)]
        y_edges_hole = []
        y_edges_middle = []
        y_edges_far = []
        for y_coord in y_coords:
            for y in range(-lamel_thickness/2, glulam_height+1,
lamel_thickness):
                if y >= y_hole-2*lamel_thickness and y <=
y_hole+2*lamel_thickness:
                    y_edge_hole = part_glulam.edges.findAt(((y_coord[0],
y, y_coord[1]),))
                    y_edges_hole.extend(y_edge_hole)
```

```
                elif y >= y_hole-3*lamel_thickness and y <=
y_hole+3*lamel_thickness:
                    y_edge_middle =
part_glulam.edges.findAt(((y_coord[0], y, y_coord[1]),))
                    y_edges_middle.extend(y_edge_middle)
                else:
                    y_edge_far = part_glulam.edges.findAt(((y_coord[0],
y, y_coord[1]),))
                    y_edges_far.extend(y_edge_far)

        # Edges in length direction beam inside hole area
        x_edges_middle_list = []
        x_coords_middle = [(x_hole-100, 0.0), (x_hole-0.5*hole_length-1,
glulam_width/2), (x_hole+100, 0.0), (x_hole+hole_length+1,
glulam_width/2)]
        for x_coord_middle in x_coords_middle:
            for x_middle in range(0, glulam_height+1, lamel_thickness):
                x_middle_edge =
part_glulam.edges.findAt(((x_coord_middle[0], x_middle,
x_coord_middle[1]),))
                x_edges_middle_list.extend(x_middle_edge)

        # Edges in length direction beam outside hole area
        x_edges_end1l_list = []
        x_coords = [(1, 0.0)]
        for x_coord in x_coords:
            for x in range(0, glulam_height+1, lamel_thickness):
                x_edge_end1l = part_glulam.edges.findAt(((x_coord[0], x,
x_coord[1]),))
                x_edges_end1l_list.extend(x_edge_end1l)

        x_edges_end2l_list = []
        x_coords = [(1, glulam_width/2)]
        for x_coord in x_coords:
            for x in range(0, glulam_height+1, lamel_thickness):
                x_edge_end2l = part_glulam.edges.findAt(((x_coord[0], x,
x_coord[1]),))
                x_edges_end2l_list.extend(x_edge_end2l)

        x_edges_end1r_list = []
        x_coords = [(glulam_length-1, 0.0)]
        for x_coord in x_coords:
            for x in range(0, glulam_height+1, lamel_thickness):
                x_edge_end1r = part_glulam.edges.findAt(((x_coord[0], x,
x_coord[1]),))
                x_edges_end1r_list.extend(x_edge_end1r)

        x_edges_end2r_list = []
        x_coords = [(glulam_length-1, glulam_width/2)]
        for x_coord in x_coords:
            for x in range(0, glulam_height+1, lamel_thickness):
                x_edge_end2r = part_glulam.edges.findAt(((x_coord[0], x,
x_coord[1]),))
                x_edges_end2r_list.extend(x_edge_end2r)

        # Select edges along the periphery of the hole
```

```
        edges_hole_1 = part_glulam.edges.getByBoundingBox(-1+x_hole-
0.5*hole_length, -1+y_hole-0.5*hole_height, -1,

1+x_hole+0.5*hole_length, 1.0+y_hole+0.5*hole_height, 1)
        edges_hole_2 = part_glulam.edges.getByBoundingBox(-1+x_hole-
0.5*hole_length, -1+y_hole-0.5*hole_height, -1+glulam_width/2,

1+x_hole+0.5*hole_length, 1+y_hole+0.5*hole_height, 1+glulam_width/2)
        edges_hole = edges_hole_1 + edges_hole_2

        edges_hole_middle_1 = part_glulam.edges.getByBoundingBox(-
1+x_hole-0.5*hole_length, y_hole-lamel_thickness-1, -1,

1+x_hole+0.5*hole_length, y_hole+lamel_thickness+1, 1)
        edges_hole_middle_2 = part_glulam.edges.getByBoundingBox(-
1+x_hole-0.5*hole_length, y_hole-lamel_thickness-1, -1+glulam_width/2,

1+x_hole+0.5*hole_length, y_hole+lamel_thickness+1, 1+glulam_width/2)
        edges_hole_middle = edges_hole_middle_1 + edges_hole_middle_2

        # Select cells for wedge elements
        wedge_cells = part_glulam.cells.findAt(
                ((x_hole-0.5*hole_length-1, y_hole-0.5*hole_height-1,
glulam_width/4), ),
                ((x_hole-0.5*hole_length-1, y_hole+0.5*hole_height+1,
glulam_width/4), ),
            )

        # Relevant edges:
        self.z_edges = z_edges_list
        self.y_edges_hole = y_edges_hole
        self.y_edges_middle = y_edges_middle
        self.y_edges_far = y_edges_far
        self.x_edges_middle_list = x_edges_middle_list
        self.edges_hole = edges_hole
        self.edges_hole_middle = edges_hole_middle
        self.x_edges_end1l = x_edges_end1l_list
        self.x_edges_end2l = x_edges_end2l_list
        self.x_edges_end1r = x_edges_end1r_list
        self.x_edges_end2r = x_edges_end2r_list

        # Relevant cells:
        self.wedge_cells = wedge_cells

        ############################################################
        self.instance_glulam = instance_glulam
        self.part_glulam = part_glulam
```

B.2 Panel class

Like the Glulam class, the Panel class creates a Panel object which is later created in the run_model function.

```
class Panel(object):
    """
    Class to create panel
    """
    def __init__(self, model, name, b_r, h_pr, panel_thickness,
sec_panel):
        """
        Initializing
        """
        self._model = model
        self._name = name
        self._b_r = b_r
        self._h_pr = h_pr
        self._panel_thickness = panel_thickness
        self._sec_glulam = sec_panel

        panel_length = hole_length + 2*b_r
        panel_height = hole_height + 2*h_pr

        assembly = model.rootAssembly

        # Create panel sketch
        panel_sketch = model.ConstrainedSketch(name='__profile__',
sheetSize=200.0)
        panel_sketch.rectangle(
            point1=(x_hole-0.5*panel_length, y_hole-0.5*panel_height),
            point2=(x_hole+0.5*panel_length, y_hole+0.5*panel_height))

        if hole_geometry == 'Square' or hole_geometry == 'Rectangular':
            panel_sketch.rectangle(point1=(x_hole-0.5*hole_length,
y_hole-0.5*hole_height),
                point2=(x_hole+0.5*hole_length, y_hole+0.5*hole_height))

            panel_sketch.FilletByRadius(
                curve1=panel_sketch.geometry[6],
                curve2=panel_sketch.geometry[7],
                nearPoint1=(x_hole-0.5*hole_length, y_hole),
                nearPoint2=(x_hole, y_hole+0.5*hole_height),
                radius=radius)
            panel_sketch.FilletByRadius(
                curve1=panel_sketch.geometry[7],
                curve2=panel_sketch.geometry[8],
                nearPoint1=(x_hole, y_hole+0.5*hole_height),
                nearPoint2=(x_hole+0.5*hole_length, y_hole),
                radius=radius)
            panel_sketch.FilletByRadius(
                curve1=panel_sketch.geometry[8],
                curve2=panel_sketch.geometry[9],
                nearPoint1=(x_hole+0.5*hole_length, y_hole),
                nearPoint2=(x_hole, y_hole-0.5*hole_height),
```

```
                radius=radius)
            panel_sketch.FilletByRadius(
                curve1=panel_sketch.geometry[9],
                curve2=panel_sketch.geometry[6],
                nearPoint1=(x_hole, y_hole-0.5*hole_height),
                nearPoint2=(x_hole-0.5*hole_length, y_hole),
                radius=radius)

        elif hole_geometry == 'Circular':
            panel_sketch.CircleByCenterPerimeter(
                center=(x_hole, y_hole),
                point1=(x_hole-0.5*hole_length, y_hole))

        # Create panel part
        part_panel = model.Part(dimensionality=THREE_D, name='Panel',
type=DEFORMABLE_BODY)
        part_panel.BaseSolidExtrude(depth=panel_thickness,
sketch=panel_sketch)
        del panel_sketch

        # Assign section panel
        cells_panel = part_panel.Set(name='Cells panel',
cells=part_panel.cells[:])
        part_panel.SectionAssignment(
                region=cells_panel,
                sectionName=sec_panel.name)

        # Assign material orientation to panel
        datum_system_panel =
part_panel.DatumCsysByThreePoints(name='Panel csys',
            coordSysType=CARTESIAN,
                origin=(0.0, 0.0, 0.0),
                point1=(0.0, panel_height, 0.0),
                point2=(panel_length/2, 0.0, 0.0))

part_panel.MaterialOrientation(regionToolset.Region(cells=part_panel.cell
s),
            orientationType=SYSTEM, axis=AXIS_3,
localCsys=part_panel.datums[datum_system_panel.id], fieldName='',
            additionalRotationType=ROTATION_NONE, angle=0.0,
            additionalRotationField='', stackDirection=STACK_3)

        # Create instance
        instance_panel = assembly.Instance(name='Instance
{n}'.format(n=name),
                part=part_panel, dependent=True)
        # Posistioning panels
        assembly.translate(instanceList=('Instance {n}'.format(n=name),
),
            vector=(0, 0, glulam_width/2))

        # Selecting edges
        assembly.regenerate()

        panel_z_edges = part_panel.edges.findAt(
```

```
            ((x_hole-0.5*panel_length, y_hole-0.5*panel_height,
panel_thickness/2),),
            ((x_hole-0.5*panel_length, y_hole+0.5*panel_height,
panel_thickness/2),),
            ((x_hole+0.5*panel_length, y_hole-0.5*panel_height,
panel_thickness/2),),
            ((x_hole+0.5*panel_length, y_hole+0.5*panel_height,
panel_thickness/2),),
        )

        # Select hole edges
        edges_hole_panel_1 = part_panel.edges.getByBoundingBox(-1+x_hole-
0.5*hole_length, -1+y_hole-0.5*hole_height, -1,

1+x_hole+0.5*hole_length, 1+y_hole+0.5*hole_height, 1)
        edges_hole_panel_2 = part_panel.edges.getByBoundingBox(-1+x_hole-
0.5*hole_length, -1+y_hole-0.5*hole_height, -1+panel_thickness,

1+x_hole+0.5*hole_length, 1+y_hole+0.5*hole_height, 1+panel_thickness)
        panel_hole_edges = edges_hole_panel_1 + edges_hole_panel_2

        # Relevant edges:
        self.panel_z_edges = panel_z_edges
        self.panel_hole_edges = panel_hole_edges


        ############################################################
        self.instance_panel = instance_panel
        self.part_panel = part_panel
```

B.3 Post-processing function

The post-processing function determines the location of the maximum tensile stress along the periphery of the hole, calculates the fictive tensile force and outputs the maximum tensile stress perp. to the grain along the width of the beam.

```
def post_processing(job_name, viewport):
    """
    Post processing:
    - Get Fictive tensile force for both regions
    - Get Maximum tensile stress for both regions
    - Save Shear and Tensile stresses for 3D plots
    - Save Tensile stresses along width
    - Save Tensile stresses along horizontal path
    """

    # Open Database (Odb)
    beam_odb =
visualization.openOdb(path='{name}.odb'.format(name=job_name),
readOnly=True)
    viewport.makeCurrent()
    viewport.setValues(displayedObject=beam_odb)
    viewport.odbDisplay.display.setValues(plotState=CONTOURS_ON_UNDEF)
```

```
    viewport.odbDisplay.commonOptions.setValues(renderStyle=FILLED)

    # Transformation from local to global coordinates

session.ScratchOdb(beam_odb).rootAssembly.DatumCsysByThreePoints(name='Gl
obal',
        coordSysType=CARTESIAN,
        origin=(0.0, 0.0, 0.0),
        point1=(10, 0.0, 0.0),
        point2=(5, 5, 0.0)
    )
    global_coordinate_system =
session.scratchOdbs["{}.odb".format(job_name)].rootAssembly.datumCsyses['
Global']
    viewport.odbDisplay.basicOptions.setValues(
        transformationType=USER_SPECIFIED,
datumCsys=global_coordinate_system)
    viewport.odbDisplay.setPrimaryVariable(
        variableLabel='S', outputPosition=INTEGRATION_POINT,
refinement=(COMPONENT, 'S22'), )
    viewport.odbDisplay.display.setValues(plotState=(CONTOURS_ON_UNDEF,
))

    # Only show glulam instance
    leaf = dgo.LeafFromPartInstance(partInstanceName=("Instance Glulam",
        ))
    viewport.odbDisplay.displayGroup.replace(leaf=leaf)

    # Set background color to white
    session.graphicsOptions.setValues(backgroundStyle=SOLID,
        backgroundColor='#FFFFFF')
    viewport.view.setProjection(projection=PARALLEL)

    # Import colormaps for contour plots
    colormaps = {'viridis': ['#440154', '#46317e', '#365c8d', '#277f8e',
'#1fa287', '#49c26d', '#a0da39', '#fee724'],
                 'Spectral': ['#9E0142', '#CB4F49', '#ED8E36', '#FDC862',
'#F0F098', '#B6E694', '#6DBDC1', '#2166AC'],
             }

    for name, colors in colormaps.items():
        session.Spectrum(name=name, colors=colors)
        session.Spectrum(name=name + 'R', colors=colors[::-1])

    ############################################################
    # Find location of maximum tensile stress along hole edge
    if hole_geometry == 'Circular':
        path_region_1 = session.Path(name='path_region_1',
            type=CIRCUMFERENTIAL,
            expression=((x_hole, y_hole, 0),
                        (x_hole, y_hole, 1),
                        (x_hole +1, y_hole, 0)),
            circleDefinition=ORIGIN_AXIS, numSegments=90,
            startAngle=0, endAngle=90, radius=hole_height/2)
        path_region_2 = session.Path(name='path_region_2',
            type=CIRCUMFERENTIAL,
```

```
            expression=((x_hole, y_hole, 0),
                        (x_hole, y_hole, 1),
                        (x_hole +1, y_hole, 0)),
            circleDefinition=ORIGIN_AXIS, numSegments=90,
            startAngle=180, endAngle=270, radius=hole_height/2)
    else:
        path_region_1 = session.Path(name='path_region_1',
            type=CIRCUMFERENTIAL,
            expression=((x_hole+0.5*hole_length - radius,
y_hole+0.5*hole_height-radius, 0),
                        (x_hole+0.5*hole_length - radius,
y_hole+0.5*hole_height-radius, 1),
                        (x_hole+0.5*hole_length - radius +1,
y_hole+0.5*hole_height-radius, 0)),
            circleDefinition=ORIGIN_AXIS, numSegments=90,
            startAngle=0, endAngle=90, radius=radius)
        path_region_2 = session.Path(name='path_region_2',
            type=CIRCUMFERENTIAL,
            expression=((x_hole-0.5*hole_length + radius, y_hole-
0.5*hole_height + radius, 0),
                        (x_hole-0.5*hole_length + radius, y_hole-
0.5*hole_height + radius, 1),
                        (x_hole-0.5*hole_length + radius +1, y_hole-
0.5*hole_height + radius, 0)),
            circleDefinition=ORIGIN_AXIS, numSegments=90,
            startAngle=180, endAngle=270, radius=radius)

    sy_arc_1 = xyPlot.XYDataFromPath(path=path_region_1,
name="XY_region_1",
        includeIntersections=True, projectOntoMesh=False,
        pathStyle=PATH_POINTS, projectionTolerance=0,
        shape=UNDEFORMED, labelType=TRUE_DISTANCE,
        removeDuplicateXYPairs=True,
        variable=('S',INTEGRATION_POINT, ((COMPONENT, 'S22' ), ), ))
    sy_arc_2 = xyPlot.XYDataFromPath(path=path_region_2,
name="XY_region_2",
        includeIntersections=True, projectOntoMesh=False,
        pathStyle=PATH_POINTS, projectionTolerance=0,
        shape=UNDEFORMED, labelType=TRUE_DISTANCE,
        removeDuplicateXYPairs=True,
        variable=('S',INTEGRATION_POINT, ((COMPONENT, 'S22' ), ), ))

    sy_arc_1 = [ix for iy, ix in sy_arc_1.data]
    sy_arc_2 = [ix for iy, ix in sy_arc_2.data]

    max_sy_1 = max(sy_arc_1)
    max_sy_2 = max(sy_arc_2)

    max_angle_1 = sy_arc_1.index(max_sy_1)*91/len(sy_arc_1)
    max_angle_2 = sy_arc_2.index(max_sy_2)*91/len(sy_arc_2)

    if hole_geometry == 'Circular':
        crack_plane_x1 = x_hole + 0.5*hole_length *
np.cos(max_angle_1*np.pi/180)
        crack_plane_y1 = y_hole + 0.5*hole_height *
np.sin(max_angle_1*np.pi/180)
```

```
        crack_plane_x2 = x_hole - 0.5*hole_length *
np.cos(max_angle_2*np.pi/180)
        crack_plane_y2 = y_hole - 0.5*hole_height *
np.sin(max_angle_2*np.pi/180)
    elif hole_geometry == 'Rectangular' or hole_geometry == 'Square':
        crack_plane_x1 = x_hole + 0.5*hole_length - radius + radius *
np.cos(max_angle_1*np.pi/180)
        crack_plane_y1 = y_hole + 0.5*hole_height - radius + radius *
np.sin(max_angle_1*np.pi/180)
        crack_plane_x2 = x_hole - 0.5*hole_length + radius - radius *
np.cos(max_angle_2*np.pi/180)
        crack_plane_y2 = y_hole - 0.5*hole_height + radius - radius *
np.sin(max_angle_2*np.pi/180)

    ############################################################
    # Results region 1

    # Fictive tensile force region 1
    path_start_1 = crack_plane_x1
    path_end_1 = crack_plane_x1 + 2*hole_height
    z_list = list(range(0, 1+glulam_width/2, z_edges_size))

    list_integrated_stresses_1 = []
    F_t90_1 = 0

    for curr_z in z_list:
        path_sy_1 = session.Path(name="sy_1_{}".format(curr_z),
type=POINT_LIST,
            expression=((path_start_1, crack_plane_y1, curr_z),
                        (path_end_1, crack_plane_y1, curr_z))
            )
        # Extract data along the path
        xy_sy_1 = xyPlot.XYDataFromPath(path=path_sy_1,
name="xy_hor_path_sy_1_{}".format(curr_z),
            includeIntersections=True, projectOntoMesh=False,
            pathStyle=PATH_POINTS, projectionTolerance=0,
            shape=UNDEFORMED, labelType=TRUE_DISTANCE,
            removeDuplicateXYPairs=True,
            variable=('S',INTEGRATION_POINT, ((COMPONENT, 'S22' ), ), ))
        # Create numpy array of data
        data_1 = np.array(xy_sy_1, dtype=[("x", np.float), ("s22",
np.float)])
        # Remove stresses bigger than zero from numpy array
        positive_s22_1 = data_1[data_1['s22'] > 0]
        # Integrate stresses
        integrated_stresses_1 = np.trapz(positive_s22_1['s22'],
positive_s22_1['x'])
        list_integrated_stresses_1.append(integrated_stresses_1)

    # Multiply integrated stresses with respective width
    list_integrated_forces_1 = []

    for j, integrated_stress_1 in enumerate(list_integrated_stresses_1):
        integrated_force_1 = z_edges_size * integrated_stress_1
        if j == 0 or j == len(list_integrated_stresses_1) - 1:
            integrated_force_1 *= 0.5
```

```
        list_integrated_forces_1.append(integrated_force_1)

    # Multiply force by 2 due to symmetry
    F_t90_1 = round(sum(2*list_integrated_forces_1), 0)
    # Print results to abaqus prompt
    print('Ft90 upper right corner for job {0} = {1} N'.format(job_name,
F_t90_1))

    # Shear stresses (Used to calculate the %reduction)
    path_start_1 = crack_plane_x1
    path_end_1 = crack_plane_x1 + 2*hole_height
    z_list = list(range(0, 1+glulam_width/2, z_edges_size))

    # --- Data stresses for 3D graphs
    x_list = np.arange(0, 121, 10)
    sy_1_total_list = []
    txy_1_total_list = []

    for curr_x in x_list:
        path_sy_1_3D = session.Path(
            name='sy_1_x{}'.format(curr_x),
            type=POINT_LIST,
            expression=((path_start_1 + curr_x, crack_plane_y1, 0),
                        (path_start_1 + curr_x, crack_plane_y1,
glulam_width/2)),
            )
        # Create data for tensile stresses S22
        xy_sy_1 = xyPlot.XYDataFromPath(
            path=path_sy_1_3D, includeIntersections=True,
shape=UNDEFORMED,
            pathStyle=UNIFORM_SPACING, numIntervals=15,
labelType=Z_COORDINATE, variable=(
                'S', INTEGRATION_POINT, ((COMPONENT, 'S22'), ), ))

        data_xy_sy_1 = np.array(xy_sy_1, dtype=[("z", np.float), ("s22",
np.float)])
        sy_1 =  data_xy_sy_1["s22"]
        sy_1_zeros = np.zeros(16)
        sy_1_reverse = sy_1[::-1].copy()
        sy_1_zeros[:len(sy_1_reverse)] = sy_1_reverse
        sy_1_new = sy_1_zeros[::-1].copy()
        sy_1_total = np.concatenate((sy_1_zeros, sy_1_new[1:16]), axis=0)
        sy_1_total_list.append(sy_1_total)

        # Create data for shear stresses S12
        xy_txy_1 = xyPlot.XYDataFromPath(
            path=path_sy_1_3D, includeIntersections=True,
shape=UNDEFORMED,
            pathStyle=UNIFORM_SPACING, numIntervals=15,
labelType=Z_COORDINATE, variable=(
                'S', INTEGRATION_POINT, ((COMPONENT, 'S12'), ), ))

        data_xy_txy_1 = np.array(xy_txy_1, dtype=[("z", np.float),
("s12", np.float)])
        txy_1 =  data_xy_txy_1["s12"]
        txy_1_zeros = np.zeros(16)
```

```
        txy_1_reverse = txy_1[::-1].copy()
        txy_1_zeros[:len(txy_1_reverse)] = txy_1_reverse
        txy_1_new = txy_1_zeros[::-1].copy()
        txy_1_total = np.concatenate((txy_1_zeros, txy_1_new[1:16]),
axis=0)
        txy_1_total_list.append(txy_1_total)

    # Create the directory if it doesn't exist
    directory = 'C:/temp/Numerical Models/Results/3D Cylindrical
Anisotropic External Reinforcements'
    if not os.path.exists(directory):
        os.makedirs(directory)

    # Print tensile stresses along horizontal path at z=0 and z=60
    sy_1_hor_0 = np.array([list_integrated_stresses_1[0]])
    sy_1_hor_60 = np.array([list_integrated_stresses_1[-1]])
    sy_1_hor_0_filename = os.path.join(directory,
'{}_Sy_1_hor_z=0.txt'.format(job_name))
    sy_1_hor_60_filename = os.path.join(directory,
'{}_Sy_1_hor_z=60.txt'.format(job_name))
    np.savetxt(sy_1_hor_0_filename, sy_1_hor_0, fmt="%.3f")
    np.savetxt(sy_1_hor_60_filename, sy_1_hor_60, fmt="%.3f")

    # Print tensile stresses S22 to txt file
    sy_1_total_array = np.column_stack(sy_1_total_list)
    sy_1_filename = os.path.join(directory,
'{}_Sy_1_3D.txt'.format(job_name))
    np.savetxt(sy_1_filename, sy_1_total_array, fmt="%.3f")

    # Print tensile stress along width at the face of the hole_center to
txt file
    sy_face_hole_1 = sy_1_total_array[:,0]
    sy_1_width_filename = os.path.join(directory,
'{}_Sy_1_Width.txt'.format(job_name))
    np.savetxt(sy_1_width_filename, sy_face_hole_1, fmt="%.3f")

    # Print maximum tensile strength along width to Abaqus prompt
    max_sy_1_width = round(np.max(sy_face_hole_1), 3)
    print('Sy,max for upper right corner for job {0} = {1}
N/mm2'.format(job_name, max_sy_1_width))

    # Print shear stresses S12 to txt file
    txy_1_total_array = np.column_stack(txy_1_total_list)
    txy_1_filename = os.path.join(directory,
'{}_Txy_1_3D.txt'.format(job_name))
    np.savetxt(txy_1_filename, txy_1_total_array, fmt="%.3f")

    ############################################################
    # Results region 2

    # Fictive tensile force region 2
    path_start_2 = crack_plane_x2
    path_end_2 = crack_plane_x2 - 2*hole_height
    z_list = list(range(0, 1+glulam_width/2, z_edges_size))

    list_integrated_stresses_2 = []
```

```
    F_t90_2 = 0

    for curr_z in z_list:
        path_sy_2 = session.Path(name="sy_2_{}".format(curr_z),
type=POINT_LIST,
            expression=((path_start_2, crack_plane_y2, curr_z),
                        (path_end_2, crack_plane_y2, curr_z))
            )
        # Extract data along the path
        xy_sy_2 = xyPlot.XYDataFromPath(path=path_sy_2,
name="xy_sy_2_{}".format(curr_z),
            includeIntersections=True, projectOntoMesh=False,
            pathStyle=PATH_POINTS, projectionTolerance=0,
            shape=UNDEFORMED, labelType=TRUE_DISTANCE,
            removeDuplicateXYPairs=True,
            variable=('S',INTEGRATION_POINT, ((COMPONENT, 'S22' ), ), ))
        # Create numpy array of data
        data_2 = np.array(xy_sy_2, dtype=[("x", np.float), ("s22",
np.float)])
        # Remove stresses bigger than zero from numpy array
        positive_s22_2 = data_2[data_2['s22'] > 0]
        # Integrate stresses
        integrated_stresses_2 = np.trapz(positive_s22_2['s22'],
positive_s22_2['x'])
        list_integrated_stresses_2.append(integrated_stresses_2)

    # Multiply integrated stresses with respective width
    list_integrated_forces_2 = []

    for j, integrated_stress_2 in enumerate(list_integrated_stresses_2):
        integrated_force_2 = z_edges_size * integrated_stress_2
        if j == 0 or j == len(list_integrated_stresses_2) - 1:
            integrated_force_2 *= 0.5
        list_integrated_forces_2.append(integrated_force_2)

    # Multiply force by 2 due to symmetry
    F_t90_2 = round(sum(2*list_integrated_forces_2), 0)
    # Print results to abaqus prompt
    print('Ft90 lower left corner for job {0} = {1} N'.format(job_name,
F_t90_2))


    # --- Data stresses for 3D graphs
    x_list = np.arange(0, 121, 10)
    sy_2_total_list = []
    txy_2_total_list = []

    for curr_x in x_list:
        path_sy_2_3D = session.Path(
            name='sy_2_x{x:3.0f}'.format(x=curr_x),
            type=POINT_LIST,
            expression=((path_start_2 - curr_x, crack_plane_y2, 0),
                        (path_start_2 - curr_x, crack_plane_y2,
glulam_width/2)),
        )
        # Create data for tensile stresses S22
```

```
        xy_sy_2 = xyPlot.XYDataFromPath(
            path=path_sy_2_3D, includeIntersections=True,
shape=UNDEFORMED,
            pathStyle=UNIFORM_SPACING, numIntervals=15,
labelType=Z_COORDINATE, variable=(
                'S', INTEGRATION_POINT, ((COMPONENT, 'S22'), ), ))

        data_xy_sy_2 = np.array(xy_sy_2, dtype=[("z", np.float), ("s22",
np.float)])
        sy_2 =  data_xy_sy_2["s22"]
        sy_2_zeros = np.zeros(16)
        sy_2_reverse = sy_2[::-1].copy()
        sy_2_zeros[:len(sy_2_reverse)] = sy_2_reverse
        sy_2_new = sy_2_zeros[::-1].copy()
        sy_2_total = np.concatenate((sy_2_zeros, sy_2_new[1:16]), axis=0)
        sy_2_total_list.append(sy_2_total)

        # Create data for shear stresses S12
        xy_txy_2 = xyPlot.XYDataFromPath(
            path=path_sy_2_3D, includeIntersections=True,
shape=UNDEFORMED,
            pathStyle=UNIFORM_SPACING, numIntervals=15,
labelType=Z_COORDINATE, variable=(
                'S', INTEGRATION_POINT, ((COMPONENT, 'S12'), ), ))

        data_xy_txy_2 = np.array(xy_txy_2, dtype=[("z", np.float),
("s12", np.float)])
        txy_2 =  data_xy_txy_2["s12"]
        txy_2_zeros = np.zeros(16)
        txy_2_reverse = txy_2[::-1].copy()
        txy_2_zeros[:len(txy_2_reverse)] = txy_2_reverse
        txy_2_new = txy_2_zeros[::-1].copy()
        txy_2_total = np.concatenate((txy_2_zeros, txy_2_new[1:16]),
axis=0)
        txy_2_total_list.append(txy_2_total)

    # Print tensile stresses along horizontal path at z=0 and z=60
    sy_2_hor_0 = np.array([list_integrated_stresses_1[0]])
    sy_2_hor_60 = np.array([list_integrated_stresses_1[-1]])
    sy_2_hor_0_filename = os.path.join(directory,
'{}_Sy_2_hor_z=0.txt'.format(job_name))
    sy_2_hor_60_filename = os.path.join(directory,
'{}_Sy_2_hor_z=60.txt'.format(job_name))
    np.savetxt(sy_2_hor_0_filename, sy_2_hor_0, fmt="%.3f")
    np.savetxt(sy_2_hor_60_filename, sy_2_hor_60, fmt="%.3f")

    # Print tensile stresses S22 to txt file
    sy_2_total_array = np.column_stack(sy_2_total_list)
    sy_2_filename = os.path.join(directory,
'{}_Sy_2_3D.txt'.format(job_name))
    np.savetxt(sy_2_filename, sy_2_total_array, fmt="%.3f")

    # Print tensile stress along width at the face of the hole_center to
txt file
    sy_face_hole_2 = sy_2_total_array[:, 0]
```

```
    sy_2_width_filename = os.path.join(directory,
'{}_Sy_2_Width.txt'.format(job_name))
    np.savetxt(sy_2_width_filename, sy_face_hole_2, fmt="%.3f")

    # Print maximum tensile strength along width to Abaqus prompt
    max_sy_2_width = round(np.max(sy_face_hole_2), 3)
    print('Sy,max for lower left corner for job {0} = {1}
N/mm2'.format(job_name, max_sy_2_width))

    # Print shear stresses S12 to txt file
    txy_2_total_array = np.column_stack(txy_2_total_list)
    txy_2_filename = os.path.join(directory,
'{}_Txy_2_3D.txt'.format(job_name))
    np.savetxt(txy_2_filename, txy_2_total_array, fmt="%.3f")

    # FICTIVE TENSILE FORCE IN PANEL
    #-------------------------------------------------------------------
----------------

    # Exclude the beam
    leaf_beam = dgo.LeafFromPartInstance(partInstanceName=("Instance
Panel", ))
    viewport.odbDisplay.displayGroup.replace(leaf=leaf_beam)

    z_edges_panel_size = float(panel_thickness)/panel_z_edges_number

    ############################################################
    # Find location of maximum tensile stress along hole edge
    if hole_geometry == 'Circular':
        path_region_1_panel = session.Path(name='path_region_1_panel',
            type=CIRCUMFERENTIAL,
            expression=((x_hole, y_hole, glulam_width/2),
                        (x_hole, y_hole, glulam_width/2 + 1),
                        (x_hole +1, y_hole, glulam_width/2)),
            circleDefinition=ORIGIN_AXIS, numSegments=90,
            startAngle=0, endAngle=90, radius=hole_height/2)
        path_region_2_panel = session.Path(name='path_region_2_panel',
            type=CIRCUMFERENTIAL,
            expression=((x_hole, y_hole, glulam_width/2),
                        (x_hole, y_hole, glulam_width/2 + 1),
                        (x_hole +1, y_hole, glulam_width/2)),
            circleDefinition=ORIGIN_AXIS, numSegments=90,
            startAngle=180, endAngle=270, radius=hole_height/2)
    else:
        path_region_1_panel = session.Path(name='path_region_1_panel',
            type=CIRCUMFERENTIAL,
            expression=((x_hole+0.5*hole_length - radius,
y_hole+0.5*hole_height-radius, glulam_width/2),
                        (x_hole+0.5*hole_length  - radius,
y_hole+0.5*hole_height-radius, glulam_width/2 + 1),
                        (x_hole+0.5*hole_length  - radius +1,
y_hole+0.5*hole_height-radius, glulam_width/2)),
            circleDefinition=ORIGIN_AXIS, numSegments=90,
            startAngle=0, endAngle=90, radius=radius)
        path_region_2_panel = session.Path(name='path_region_2_panel',
            type=CIRCUMFERENTIAL,
```

```
            expression=((x_hole-0.5*hole_length + radius, y_hole-
0.5*hole_height + radius, glulam_width/2),
                        (x_hole-0.5*hole_length + radius, y_hole-
0.5*hole_height + radius, glulam_width/2+1),
                        (x_hole-0.5*hole_length + radius +1, y_hole-
0.5*hole_height + radius, glulam_width/2)),
            circleDefinition=ORIGIN_AXIS, numSegments=90,
            startAngle=180, endAngle=270, radius=radius)

    panel_sy_arc_1 = xyPlot.XYDataFromPath(path=path_region_1_panel,
name="xy_region_1_panel",
        includeIntersections=True, projectOntoMesh=False,
        pathStyle=PATH_POINTS, projectionTolerance=0,
        shape=UNDEFORMED, labelType=TRUE_DISTANCE,
        removeDuplicateXYPairs=True,
        variable=('S',INTEGRATION_POINT, ((COMPONENT, 'S22' ), ), ))
    panel_sy_arc_2 = xyPlot.XYDataFromPath(path=path_region_2_panel,
name="xy_region_2_panel",
        includeIntersections=True, projectOntoMesh=False,
        pathStyle=PATH_POINTS, projectionTolerance=0,
        shape=UNDEFORMED, labelType=TRUE_DISTANCE,
        removeDuplicateXYPairs=True,
        variable=('S',INTEGRATION_POINT, ((COMPONENT, 'S22' ), ), ))

    panel_sy_arc_1 = [ix for iy, ix in panel_sy_arc_1.data]
    panel_sy_arc_2 = [ix for iy, ix in panel_sy_arc_2.data]

    panel_max_sy_1 = max(panel_sy_arc_1)
    panel_max_angle_1 =
panel_sy_arc_1.index(panel_max_sy_1)*91/len(panel_sy_arc_1)
    panel_max_sy_2 = max(panel_sy_arc_2)
    panel_max_angle_2 =
panel_sy_arc_2.index(panel_max_sy_2)*91/len(panel_sy_arc_2)

    if hole_geometry == 'Circular':
        crack_plane_x1 = x_hole + 0.5*hole_length *
np.cos(panel_max_angle_1*np.pi/180)
        crack_plane_y1 = y_hole + 0.5*hole_height *
np.sin(panel_max_angle_1*np.pi/180)
        crack_plane_x2 = x_hole - 0.5*hole_length *
np.cos(panel_max_angle_2*np.pi/180)
        crack_plane_y2 = y_hole - 0.5*hole_height *
np.sin(panel_max_angle_2*np.pi/180)
    else:
        crack_plane_x1 = x_hole +0.5*hole_length - radius + radius *
np.cos(panel_max_angle_1*np.pi/180)
        crack_plane_y1 = y_hole + 0.5*hole_height - radius + radius *
np.sin(panel_max_angle_1*np.pi/180)
        crack_plane_x2 = x_hole-0.5*hole_length + radius - radius *
np.cos(panel_max_angle_2*np.pi/180)
        crack_plane_y2 = y_hole - 0.5*hole_height + radius - radius *
np.sin(panel_max_angle_2*np.pi/180)

    # Fitive tensile force region 1
    path_start_1 = crack_plane_x1
    path_end_1 = crack_plane_x1 + 2*hole_height
```

```
    z_list = np.arange(glulam_width/2, panel_thickness+glulam_width/2,
z_edges_panel_size)
    list_integrated_stresses_1 = []

    for zi in z_list:
        path_sy_1 = session.Path(name="panel_xy_sy_1_"+str(zi),
type=POINT_LIST,
        expression=((path_start_1, crack_plane_y1, zi),
                    (path_end_1, crack_plane_y1, zi))
        )
        # Extract data along the path
        xy_sy_1_panel = xyPlot.XYDataFromPath(path=path_sy_1,
name="panel_xy_sy_1_"+str(zi),
            includeIntersections=True, projectOntoMesh=False,
            pathStyle=PATH_POINTS, projectionTolerance=0,
            shape=UNDEFORMED, labelType=TRUE_DISTANCE,
            removeDuplicateXYPairs=True,
            variable=('S',INTEGRATION_POINT, ((COMPONENT, 'S22' ), ), ))
        # Create numpy array of data
        data_1_panel = np.array(xy_sy_1_panel, dtype=[("x", np.float),
("s22", np.float)])
        # Remove stresses bigger than zero from numpy array
        positive_s22_1_panel = data_1_panel[data_1_panel['s22'] > 0]
        # Integrate stresses
        integrated_stresses_1 = np.trapz(positive_s22_1_panel['s22'],
positive_s22_1_panel['x'])
        list_integrated_stresses_1.append(integrated_stresses_1)

    # Multiply integrated stresses with respective width
    list_integrated_forces_1 = []

    for j, integrated_stress_1 in enumerate(list_integrated_stresses_1):
        integrated_force_1 = z_edges_panel_size * integrated_stress_1
        if j == 0 or j == len(list_integrated_stresses_1) - 1:
            integrated_force_1 *= 0.5
        list_integrated_forces_1.append(integrated_force_1)

    # Multiply by 2 because of 2 panels
    panel_F_t90_1 = round(sum(2*list_integrated_forces_1), 0)
    # Print results to abaqus prompt
    print('Ft90 upper right corner panel for job {0} = {1}
N'.format(job_name, panel_F_t90_1))

    # Fitive tensile force region 2
    path_start_2 = crack_plane_x2
    path_end_2 = crack_plane_x2 - 2*hole_height
    z_list = np.arange(glulam_width/2, panel_thickness+glulam_width/2,
z_edges_panel_size)

    list_integrated_stresses_2 = []

    # Calculate tensile force for lower left corner (front)
    for zi in z_list:
        path_sy_2 = session.Path(name="panel_xy_sy_2_"+str(zi),
type=POINT_LIST,
            expression=((path_start_2, crack_plane_y2, zi),
```

```
                        (path_end_2, crack_plane_y2, zi))
            )
        # Extract data along the path
        xy_sy_2_panel = xyPlot.XYDataFromPath(path=path_sy_2,
name="panel_xy_sy_2_"+str(zi),
            includeIntersections=True, projectOntoMesh=False,
            pathStyle=PATH_POINTS, projectionTolerance=0,
            shape=UNDEFORMED, labelType=TRUE_DISTANCE,
            removeDuplicateXYPairs=True,
            variable=('S',INTEGRATION_POINT, ((COMPONENT, 'S22' ), ), ))
        # Create numpy array of data
        data_2_panel = np.array(xy_sy_2_panel, dtype=[("x", np.float),
("s22", np.float)])
        # Remove stresses bigger than zero from numpy array
        positive_s22_2_panel = data_2_panel[data_2_panel['s22'] > 0]
        # Integrate stresses
        integrated_stresses_2 = np.trapz(positive_s22_2_panel['s22'],
positive_s22_2_panel['x'])
        list_integrated_stresses_2.append(integrated_stresses_2)

    # Multiply integrated stresses with respective width
    list_integrated_forces_2 = []

    for integrated_stress_2 in list_integrated_stresses_2:
        if integrated_stress_2 == list_integrated_stresses_2[0]:
            integrated_force_2 =
0.5*z_edges_panel_size*integrated_stress_2
            list_integrated_forces_2.append(integrated_force_2)
        if integrated_stress_2 == list_integrated_stresses_2[-1]:
            integrated_force_2 =
0.5*z_edges_panel_size*integrated_stress_2
            list_integrated_forces_2.append(integrated_force_2)
        else:
            integrated_force_2 = z_edges_panel_size*integrated_stress_2
            list_integrated_forces_2.append(integrated_force_2)

    # Multiply by 2 because of 2 panels
    panel_F_t90_2 = round(sum(2*list_integrated_forces_2), 0)
    # Print results to abaqus prompt
    print('Ft90 lower left corner panel for job {0} = {1}
N'.format(job_name, panel_F_t90_2))

    # SAVE FICTIVE TENSILE FORCE AND MAXIMUM STRESS PEAK TO TXT FILE
    #-------------------------------------------------------------------
----------------

    # Results Ft90
    results_file = 'C:/temp/Numerical Models/Results/3D Cylindrical
Anisotropic External Reinforcements/Results 3D Cylindrical Anisotropic
External Reinforcements.txt'

    with open(results_file, 'a') as f:
        f.write(str(job_name) + '\n')
        f.write('-----------------------------------------------------
--------' + '\n')
        f.write('Glulam:' + '\n')
```

```
        f.write('F_t90_1 \t max_sy_1_width \t F_t90_2 \t max_sy_2_width
\n')
        f.write("{}\t{}\t{}\t{} \n".format(F_t90_1, max_sy_1_width,
F_t90_2, max_sy_2_width))
        f.write('Panel:' + '\n')
        f.write('F_t90_1 \t F_t90_2 \n')
        f.write("{}\t{} \n\n".format(panel_F_t90_1, panel_F_t90_2))
```

B.4 Run_model function

The run_model function creates a model and a job of a specific iteration of the main function.

```
def run_model(model, viewport, job_name, solve):
    """
    Function to create a model
    """
    model = model
    assembly = model.rootAssembly
    viewport_1 = viewport
    viewport_1.restore()

    # Define material porperties
    mat_glulam = model.Material(
            name='glulam',
            description='material for the glulam'
            )
    mat_panel = model.Material(
            name='panel',
            description='material for the panel'
            )

    prop_glulam = (1065, 715, 11500, 0.3, 0.02, 0.02, 45, 715, 715)
    prop_panel = (9100, 8400, 370, 0.04, 0.4, 0.4, 620, 620, 50)

    mat_glulam.Elastic(
            table=(prop_glulam, ),
            type=ENGINEERING_CONSTANTS
            )
    mat_panel.Elastic(
            table=(prop_panel, ),
            type=ENGINEERING_CONSTANTS
            )

    # Create sections for the glulam and steel
    section_glulam = model.HomogeneousSolidSection(
            name='Section Glulam', material='glulam')
    section_panel = model.HomogeneousSolidSection(
            name='Section Panl', material='panel')

    # Create glulam beam
    glulam = Glulam(model=model, name='Glulam', hole_height=hole_height,
hole_geometry=hole_geometry,
```

```
                        hole_length=hole_length, posistion=pos_1,
sec_glulam=section_glulam)
    part_glulam = glulam.instance_glulam.part

    # Assign element types
    elemType1 = mesh.ElemType(elemCode=C3D8R, elemLibrary=STANDARD,
        secondOrderAccuracy=OFF, hourglassControl=DEFAULT,
        distortionControl=DEFAULT)

    set_cells_glulam = part_glulam.Set(name='all cells',
cells=part_glulam.cells[:])

    part_glulam.setElementType(regions=set_cells_glulam,
            elemTypes=(elemType1, ))

    # Assign wedge
    part_glulam.setMeshControls(elemShape=WEDGE, technique=SWEEP,
algorithm=MEDIAL_AXIS, regions=glulam.wedge_cells[:])

    # Seed Glulam
    part_glulam.seedEdgeBySize(deviationFactor=0.1, constraint=FINER,
edges=glulam.z_edges, size=z_edges_size)
    part_glulam.seedEdgeByNumber(constraint=FINER,
edges=glulam.y_edges_hole, number=20)
    part_glulam.seedEdgeByNumber(constraint=FINER,
edges=glulam.y_edges_middle, number=10)
    part_glulam.seedEdgeByNumber(constraint=FINER,
edges=glulam.y_edges_far, number=5)
    part_glulam.seedEdgeBySize(deviationFactor=0.1, constraint=FINER,
edges=glulam.x_edges_middle_list, size=5)
    part_glulam.seedEdgeBySize(edges=glulam.edges_hole, size=2.0,
deviationFactor=0.1, constraint=FINER)
    part_glulam.seedEdgeByNumber(constraint=FINER,
edges=glulam.edges_hole_middle, number=20)
    part_glulam.seedEdgeByBias(biasMethod=SINGLE,
end1Edges=(glulam.x_edges_end1l + glulam.x_edges_end2r),
        end2Edges=(glulam.x_edges_end2l + glulam.x_edges_end1r),
minSize=5.0, maxSize=20.0, constraint=FINER)

    flip_edges_1 = part_glulam.edges.findAt(
        ((1, 0, glulam_width/2), ),
        ((glulam_length-1, glulam_height, 0), ),
    )
    flip_edges_2 = part_glulam.edges.findAt(
        ((1, glulam_height, 0), ),
        ((glulam_length-1, 0, glulam_width/2), ),
    )

    part_glulam.seedEdgeByBias(biasMethod=SINGLE, end1Edges=flip_edges_1,
minSize=5.0,
        maxSize=20.0, constraint=FINER)
    part_glulam.seedEdgeByBias(biasMethod=SINGLE, end2Edges=flip_edges_2,
minSize=5.0,
        maxSize=20.0, constraint=FINER)

    part_glulam.generateMesh()
```

```
    # Create panel
    panel = Panel(model=model, name='Panel', b_r=b_r, h_pr=h_pr,
panel_thickness=panel_thickness,
                  sec_panel=section_panel)
    part_panel = panel.instance_panel.part

    # Assign element types panel
    set_cells_panel = part_panel.Set(name='all cells panel',
cells=part_panel.cells[:])
    part_panel.setElementType(regions=set_cells_panel,
            elemTypes=(elemType1, ))

    # Seed Panel
    part_panel.seedEdgeByNumber(edges=panel.panel_z_edges,
number=panel_z_edges_number, constraint=FINER)
    part_panel.seedEdgeBySize(deviationFactor=0.1, constraint=FINER,
edges=panel.panel_hole_edges, size=hole_edge_size )
    part_panel.seedPart(deviationFactor=0.1, minSizeFactor=0.1, size=5)
    part_panel.generateMesh()

    ############################################################
    # Create support and loading plate
    support = SteelPlate(name='support', model=model,
length=plate_length,
            height=plate_height, width=glulam_width/2., xyz=(0., -
plate_height, 0),
            RP=(plate_length/2., -plate_height, 0))

    load_plate = SteelPlate(name='load plate', model=model,
length=plate_length,
            height=plate_height, width=glulam_width/2.,
xyz=(glulam_length-glulam_height/2-plate_length/2, glulam_height, 0),
            RP=(glulam_length-glulam_height/2.,
glulam_height+plate_height, 0))

    # create step
    model.StaticStep(name='Load', previous='Initial', nlgeom=False,
            timePeriod=1.0, timeIncrementationMethod=AUTOMATIC,
maxNumInc=100)

    # Create interactions between glulam and steel plates
    face_glulam_bottom = glulam.instance_glulam.faces.findAt(
            ((10, 0, glulam_width/4), ),
            )
    surf_glulam_bottom = assembly.Surface(name='glulam bottom',
            side1Faces=face_glulam_bottom)

    face_glulam_top = glulam.instance_glulam.faces.findAt(
            ((glulam_length - 10, glulam_height, glulam_width/4.), ),
            )
    surf_glulam_top = assembly.Surface(name='glulam top',
            side1Faces=face_glulam_top)

    face_support_top = support.instance.faces.findAt(
            ((plate_length/2, 0, glulam_width/4), ),
```

```
            )
    surf_support_top = assembly.Surface(name='support top',
            side1Faces=face_support_top)

    face_load_bottom = load_plate.instance.faces.findAt(
            ((glulam_length - plate_length/2, glulam_height,
glulam_width/4), ),
            )
    surf_load_bottom = assembly.Surface(name='load plate top',
            side1Faces=face_load_bottom)

    # - create the interaction objects
    model.Tie(name='Tie support',
            master=surf_support_top, slave=surf_glulam_bottom,
            positionToleranceMethod=COMPUTED)
    model.Tie(name='Tie load plate',
            master=surf_load_bottom, slave=surf_glulam_top,
            positionToleranceMethod=COMPUTED)

    # Create interactions between glulam and panel
    face_glulam_panel = glulam.instance_glulam.faces.getByBoundingBox(
        x_hole-0.5*hole_length-left_1-1, -1, -1+glulam_width/2,
x_hole+0.5*hole_length+right_1+1, glulam_height+1, 1+glulam_width/2,
    )
    surf_glulam_panel = assembly.Surface(name='glulam panel face',
            side1Faces=face_glulam_panel)

    face_panel_glulam = panel.instance_panel.faces.findAt(
        ((x_hole-0.5*hole_length-1, y_hole, glulam_width/2), ),
    )
    surf_panel_glulam = assembly.Surface(name='panel gulam face',
            side1Faces=face_panel_glulam)

    # - create the interaction objects
    model.Tie(name='Tie panel-glulam',
            master=surf_panel_glulam, slave=surf_glulam_panel,
            positionToleranceMethod=COMPUTED)

    # Create boundary conditions
    #
    # - Symmetry in XY-plane#
    assembly.regenerate()

    nodes_glulam_symm_xy = glulam.instance_glulam.nodes.getByBoundingBox(
            -1, -1, -1, 1+glulam_length, 1+glulam_height, 1)

    set_nodes_symm_xy = assembly.Set(name='nodes symm xy',
            nodes=(nodes_glulam_symm_xy, ))

    model.DisplacementBC(name='XY symm', createStepName='Load',
            region=set_nodes_symm_xy, u3=0.)

    # - Symmetry in YZ-plane#
    assembly.regenerate()

    nodes_glulam_symm_yz = glulam.instance_glulam.nodes.getByBoundingBox(
```

```
            -1+glulam_length, -1, -1, 1+glulam_length, 1+glulam_height,
1+glulam_width)

    set_nodes_symm_yz = assembly.Set(name='nodes glulam symm yz',
            nodes=nodes_glulam_symm_yz)

    model.DisplacementBC(name='YZ symm', createStepName='Load',
            region=set_nodes_symm_yz, u1=0.)


######################################################################
    # Restrain DOFs in the support
    #
    ref_point_id = support.reference_point.id
    set_ref_point_support = assembly.Set(

referencePoints=(support.instance.referencePoints[ref_point_id],),
            name='Ref Point support')

    model.DisplacementBC(name='support', createStepName='Load',
            region=set_ref_point_support, u2=0.0, u3=0.0, ur1=0.0,
ur2=0.0)


######################################################################
    # Apply force and restrain DOFs from the loading plates
    #
    ref_point_id = load_plate.reference_point.id
    set_ref_point_loading = assembly.Set(

referencePoints=(load_plate.instance.referencePoints[ref_point_id],),
            name='Ref Point load')

    model.DisplacementBC(name='loading plate', createStepName='Load',
            region=set_ref_point_loading, u3=0.0, ur1=0.0, ur2=0.0)

    model.ConcentratedForce(name='Point load', createStepName='Load',
            region=set_ref_point_loading, cf2=-2500)

    viewport_1.setValues(displayedObject=assembly)
    viewport_1.maximize()
    cmap = viewport_1.colorMappings['Section']
    viewport_1.setColor(colorMapping=cmap)
    assembly.regenerate()


######################################################################
    # Create job
    my_job = mdb.Job(name=job_name, model=model.name,
            numCpus=10, numDomains=10, multiprocessingMode=MPI)

    if solve == True:
        import time
        start_time = time.time()
        local_t = time.localtime(start_time)
```

```
        print('\n***--- Start Time: {day}.{mon}.{y}
{h:02d}:{mm:02d}:{ss:02d} ---***'.format(
            day=local_t.tm_mday, mon=local_t.tm_mon, y=local_t.tm_year,
            h=local_t.tm_hour, mm=local_t.tm_min, ss=local_t.tm_sec))

        my_job.submit()
        my_job.waitForCompletion()
        elapsed_time = time.time() - start_time
        print('***--- Elapsed Time: {t:3.2f} min ---
***'.format(t=elapsed_time/60.))

        post_processing(job_name=job_name, viewport=viewport_1)
```

B.5 Main function

The main function creates the parameter study and submits the job for each configuration.

```
def main():
    """
    The parameter study is created here
    """
    global glulam_height
    global glulam_width
    global glulam_length
    global lamel_thickness
    global lay_up
    global hole_height
    global hole_geometry
    global hole_length
    global x_hole
    global y_hole
    global left_1
    global right_1
    global pos_1
    global radius
    global plate_length
    global plate_height
    global b_r
    global h_pr
    global panel_thickness

    global z_edges_size
    global hole_edge_size
    global panel_z_edges_number
    z_edges_size = 4 # mm
    hole_edge_size = 2 # mm
    panel_z_edges_number = 8

    # Steel plates
    plate_length = 250
    plate_height = 40

    # Glulam
```

```
    glulam_height = 400 # mm
    glulam_width = 120 # mm
    glulam_length = plate_length/2 + 4.5*glulam_height # mm
    lamel_thickness = 40 # mm
    lay_up = 2
    radius = 20 # mm acc. prEN1995-1-1:2021

    # Partitioning distances
    left_1 = 250
    right_1 = 250

    # Panel
    b_r = 80 # mm
    h_pr = 80 # mm
    panel_thickness = 24 # mm


    # Parameters parameterstudy
    hole_height = 120 # mm
    hole_geometry = "Circular"

    if hole_geometry == 'Rectangular':
        hole_length = 2.5*hole_height
    else:
        hole_length = hole_height

    x_hole = plate_length/2 + 2*glulam_height
    y_hole = glulam_height/2
    pos_1 = (x_hole, y_hole)

    lay_up_list = [1]
    b_r_list = [80]

    for curr_lay_up in lay_up_list:
        for curr_b_r in b_r_list:
            lay_up = curr_lay_up
            b_r = curr_b_r

            # Define file names
            name =
'Model_cyan_external_reinforced_{0}_{1}_{2}_{3}_{4}_{5}'.format(glulam_wi
dth, hole_geometry, hole_height, lay_up, panel_thickness, b_r)
            job_name = 'Job_{}'.format(name)

            # Create model
            model = mdb.Model(name=name)

            viewport_1 = session.Viewport(
                name='Viewport: 1', origin=(0,0), width=300,height=170)
            viewport_1.maximize()

            submit_job = False
            run_model(model=model, viewport=viewport_1,
job_name=job_name, solve=submit_job)
```